AN INVESTIGATION INTO THE USE OF THE VANADIUM REDOX FLOW ENERGY STORAGE SYSTEM FOR PEAK-SHAVING AND LOAD-LEVELING

by

Mpho Diko

Thesis presented in partial fulfilment of the requirements
for the Degree of Master of Engineering Sciences
at The University of Stellenbosch

Supervisor:

Professor R. Herman

April 2003

DECLARATION:

I, the undersigned, hereby declare that the work contained in this thesis is my own original work and has not been previously in its entirety or in part been submitted at any university for a degree.

M.Diko

2 December 2002

SYNOPSIS

This thesis investigates the credibility of the vanadium redox flow energy storage system, sometimes termed vanadium redox battery (VRB). The focus is on the use of this technology in peak-shaving and load-leveling applications. The initial problem is to find a suitable mathematical model for representing the daily load profile. A sinusoidal function is identified as an elementary approximation of the first order. Due to the periodicity characteristics that are inherent in a daily load profile, the Fast Fourier Transform (FFT) algorithm is identified as a mathematical model that closely resembles a load profile.

The main theme in this thesis is the determination of an optimal solution during the peak-shaving process. In this particular context, the optimal solution refers to the following: With the energy capacity of the VRB and the power rating of the entire system considered as the constraints, the interest is on (i) the constant power that the VRB can deliver in order to bring down the maximum demand quite significantly, (ii) and the time interval in which this constant power is delivered. Therefore, the VRB power delivered during peak-shaving (P_{VRB}) and the corresponding time interval are the main two parameters under consideration in the optimization process.

The mathematical algorithm that can be used to determine suitable values for these two parameters is developed. Maple® V 5.1 is used for determining the solution analytically. The obtained results are verified by simulation with Excel®. The investigation into the economic benefits that may be derived from the utilization of the vanadium energy storage device is also presented.

SINOPSIS

Hierdie tesis ondersoek die waarde en toepassing van die vadium "redox" vloei energie stoorstelsel (VRB). Die fokus is op die gebruik van hierdie tegnologie om pieklas te verminder en om laste meer egalig te maak. Die aanvanklike probleem is om 'n geskikte wiskundige model vir die daaglikse las-profiel te kry. Deur gebruik te maak van sinus-komponente en die toepassing van die Vinnige Fourier Transform (FFT) is hierdie probleem opgelos.

Die hooftema van hierdie werk is om 'n analitiese oplossing te vind vir die optimale toepassing van die konsep vir pieklas vermindering. In hierdie konteks verwys die optimale oplossing na die volgende: Met die gegewe vermoë van die VRB stelsel en drywingsvermoë van die kragelektronika is die vrae rondom (i) die konstante drywing wat die VRB kan lewer om die maksimum aanvraag van die las beduidend te verminder en (ii) die tydsduur waarin dit plaasvind. Dus is die twee veranderlikes waarvoor oplossings in die optimale proses gesoek word die drywing (P_{VRB}) en die tyd-interval daarvan.

Die wiskundige algoritme is met die hulp van Maple® V5.1 ontwikkel. Die resultate is daarna met behulp van simulasies in Excel® getoets. 'n Analise van die moontlike ekonomiese voordele is ook ondersoek.

ACKNOWLEDGEMENTS

I wish to record my sincere appreciation to:

- My supervisor, Prof. R. Herman for his help, patience, zealous determination and dedication.
- Mrs. Susan Locke for her wonderful and superb administrative work towards the success of my studies.
- NRF for the financial support.
- My family and friends, particularly my brother Mzimvubu and his wife Nocawe who have been always in the thick of things in my life.
- Mandisa Jojo, for her motivation, encouragement and guidance.
- My former lecturer at the University of Transkei, Mr. Joseph Kwame Okyere Bamfo, for being inspirational throughout my student life at Unitra.
- My Saviour Jesus Christ, for providing me with spiritual strength, knowledge and wisdom, (Proverbs 1:7).

LIST OF SYMBOLS AND ABBREVIATIONS USED

Chapter Two

CAES	Compressed air energy storage
SMES	Superconducting magnetic energy storage
E_p	Potential energy of the water stored in the upper reservoir
ρ	Density of the water
g	Acceleration due to gravity
h	Distance between the upper and the lowe reservoirs, or height of the rotor
E	Inductively (SMES) or electrically (capacitor) or mechanically (flywheel) stored energy
L	Inductance
I	DC current flowing through the coil
t	time
P	Rate at which energy is transferred
V	Voltage across the coil (flywheel) or between the two plates (capacitor)
q	Electrically stores charge
C	Capacitance
ε	Permittivity of the dielectric
A	Area of the plates
d	Distance between the plates
ω	Rotating velocity of the flywheel
r	Radius of the rotor
m	Mass of the rotor
I	Moment of inertia
Pb/H^+	Lead-acid battery
e^-	Electron

H_2SO_4	Sulphuric acid
X	Anode (reducing agent)
n	Number of electrons donated or gained
X^{n+}	Anodic ion
n +	Oxidation state
Y	Cathode (oxidizing agent)
Y^{n+}	Cathodic ion
PbO_2	Lead dioxide
DC	Direct current
BOP	Balance of plant
USA	United states of america
VRB	Vanadium redox battery
V^{n+}	Vanadium ion
UNSW	University of New South Wales

Chapter Three

S	Apparent power (demand measured in kVA)
S_{max}	Maximum peak
S_c	Maximum peak after peak-shaving
t	Time (measured in hours or minutes or radians)
t_s , t_f	Starting and finishing points battery discharge
Δt	Discharge interval
t_m	Time at which the demand is maximum
ε	One minute
P_a	Difference between the maximum peak and the mean
P_{VRB}	Constant power released by the Vanadium battery over Δt
ω	Angular velocity

μ	Mean value of power (in kVA or kW) under consideration
A_0	Amplitude of the DC component in a fourier series
A_n	Amplitudes of the sine harmonics
B_n	Amplitudes of the cosine harmonics
α_n , β_n	Phase angles of sine and cosine harmonics
∞	Infinity
$h_2 , h_3 , \ldots h_n$	Sum of two, sum of three or sum of n harmonics

Chapter Four

FFT	Fast Fourier Transform
N	Number of discrete points
dt	Sampling period
L_s	Sample length
f_s	Sampling frequency
f_r	Spectral resolution
f_N	Nyquist frequency
φ	Row matrix with 48 entries of power values in kVA
φ^*	Row matrix with 64 entries of power values in kVA
t^*	Time interval with a length of 22.5 minutes
t^{**}	Time interval with a length of 90 minutes
X	Row vector with 64 points used in a matlab code
$\mathrm{fft}(X)$	Fast fourier transform of vector X
h	Frequency component displayed on the frequency spectrum
ω_0	Fundamental frequency

Chapter Five

ESKOM	Electricity supply commission (South Africa)
UPS	Uninterrupted power supply
VESS	Vanadium energy storage system
VRB	Vanadium redox battery
DPQC	Dynamic power quality compansator
SS	Static switch
Z_L	Impedance of the line
Z_{load}	Impedance of the load
M	Molarity (concentration of the solution)

Chapter Six

E_c	Energy cost
E_R	Total energy for one day (or area enclosed by fft power signal and total length of one-minute intervals)
E_D	Total energy for one day (area enclosed by power signal with 48 points and total length of 30-minute intervals
P	Average real power (in kW) over a specified time interval
Δt	Time interval in which a meter averages the power supply
h	hour
N	Number of days in a month
M	Number of minutes in one day
TOU	Time of use
η_c, η_B	Conversion and battery efficiencies
x	Number of years
x_0	Number of years for a break-even point

F_c	Capital cost of the VRB installation
T_{CB}	Total cost for power before using the VRB
T_{CA}	Total cost for power after the use of VRB
G_1	Total cost for power per year before VRB
G_2	Total cost for power after VRB
X	Money value at present
P	Present worth factor

This thesis is dedicated to my family members,

Fezekile, Mzimvubu, Nocawe,

Kwanda, Sinabo, Zintle and Aphile.

LIST OF FIGURES

LIST OF TABLES

CONTENTS

Chapter One

1 INTRODUCTION

1.1 GENERAL PERSPECTIVE ON ELECTRICITY SUPPLY AND ENEGY STORAGE

Electrical generating utilities and other local authorities that supply electric power are faced with a paradoxical scenario. On the one hand, they are faced with projected increases in electrical demand, and on the other, there is always a possibility that their electrical power generating units (electrical plants) may be operating at less than capacity. The most important point is that these utilities always try their best to ensure that the power supply is continuous throughout the year for 365 days. The unfortunate part, which is always a point of concern in this whole issue, is that a certain amount of the generated power is not always sold to the customers, particularly during the off-peak hours when the demand is low. Utilities regard this unused electricity as a waste. These problems together with those that are not mentioned led to a serious consideration of energy storage strategies. This can be achieved by storing energy during the off-peak demand and then releasing it when the demand is high.

In any given area it is always common to find customers (residential, commercial or industrial) that depend solely on the utility grid for their power supply. On the other hand it is also possible to find customers depending only on distributed generation (DG) units such as diesel generators, or renewable energy technologies such as wind turbines. Also, customers may use both the DG unit and the grid. Whichever method is employed to generate power, the bottom line is that customers are entitled to a more reliable and cost-effective electricity, whereas utilities are obligated to meet the demands of the customers.

In the light of the above discussion it transpires that a utility plant or a DG unit is hardly 100% effective. Peak demands are undesirable because they can cause voltage sags and may contribute to outages. In certain industrial processes (e.g. steel manufacturing) an interruption in power supply can cause damage that may result in substantial economic losses. In order to overcome problems of this nature, electric power sources need to be augmented by energy storage devices. Some of the available energy storage technologies have a capability to provide "ride-through" for momentary outages, and extended protection from longer outages [2,27,36].

Energy storage devices are imperative in load-leveling and peak-shaving applications. Load-leveling and peak-shaving are cost-reduction applications, and they are normally found at the power supply level or consumer side or both. A perfectly flexible load leveling system can improve a utility's effective generating capacity by a reasonable percentage of about 40 % [19].

1.2 DESCRIPTION OF THE PROBLEM

The demand for electrical power (expressed in kVA or kW) at any given point in time is recorded by a demand meter. Amongst other reasons for using this meter is to enable the supplier and the customer to track the power consumption over a specified period. The reason for recording the flow of power supply is that the supplier wants to identify the greatest of all the peaks (maximum demand) that has occurred within a specified time interval. In most two-part tariffs this maximum demand component often comprises half of the total electricity bill. Employing a peak-shaving strategy can reduce the costs associated with the maximum demand. As already said in the previous section, peak-shaving is achieved by utilizing an energy storage device. Some of the storage devices that are suitable for this kind of application are discussed in chapter two. However, the researchers are particularly interested in the vanadium redox energy storage

device, sometimes called vanadium redox battery (VRB). The reason for choosing the VRB is that it is a promising newly developed storage device and therefore its technical and economic feasibility for commercialization need to be investigated.

Like any other storage device, VRB has limitations in as far as the energy capacity is concerned. For example, the energy capacity and the power rating of the VRB system installed at the University of Stellenbosch for evaluation are 520 kWh and 250 kVA respectively [17, 39]. The main task is to know how much power in kVA or kW this particular VRB can deliver and for how long when shaving the maximum demand. The investigations suggest that this problem can be solved by first developing a mathematical model that closely resembles a daily load profile, such as the one given below:

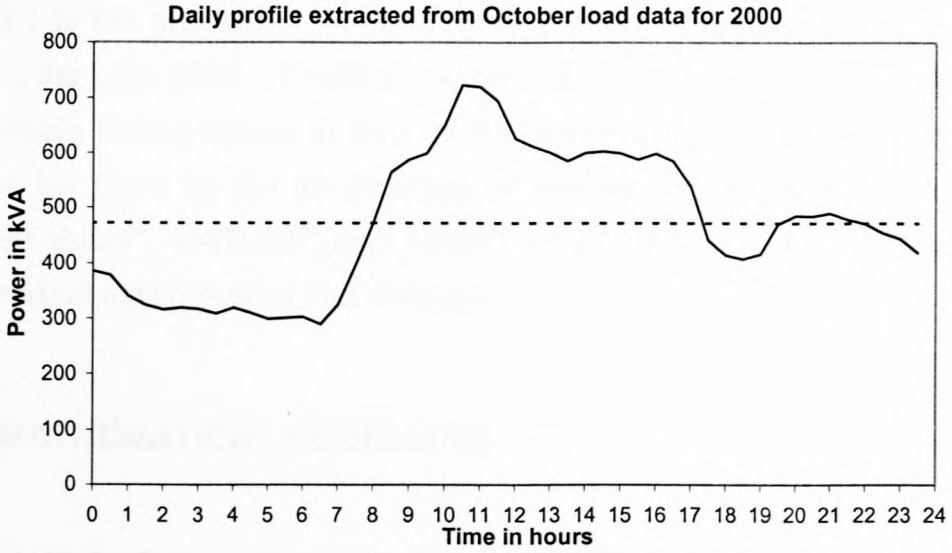

Figure 1.1 Daily load profile of 2 October 2000

The only difference between the profile in figure 1.1 and other daily load profiles is that the maximum daily peaks are not necessarily the same. Also, the duration and positions on the time domain of the daily peaks are not the same. Apart from these differences, the investigations show that all the profiles exhibit similar

characteristics. Hence, a mathematical model that serves as a representative of all the daily load profiles is required so that the developed optimization technique of the VRB can be employed directly on the profile. Suitable values for the VRB power and the time interval (mentioned in the foregoing paragraph) can be determined through the developed mathematical model.

1.3 RESEARCH METHODOLOGY

1.3.1 LOAD DATA ANALYSIS

Statistical load data for the year 2000 is analyzed in order to investigate the general trends and characteristics that are inherent in daily load profiles. The statistical analysis of the load data suggests that the maximum peak shown in figure 1.1 is the greatest of all the 365 daily maximum peaks recorded by the meter in the year 2000. Therefore, in order to keep consistency and avoiding any possible biased results in favor of the customer, the profile in figure 1.1 is used as the basis for the development of models and optimization strategies. Microsoft Excel®, MATLAB® and Maple® V 5.1 are used for statistical and mathematical manipulations and simulations.

1.3.2 MATHEMATICAL MODELLING

The initial problem is to represent a daily load profile with a suitable mathematical function whose period is 24 hours. The investigation suggests that a sinusoidal function is an elementary approximation of the first order that can be used to model a load profile. A sinusoidal function is generally expressed as follows:

$$S(t) = P_a \sin(\omega t - \alpha) + \mu \qquad \ldots (1.1)$$

A full description of the quantities in equation (1.1) is presented in chapter three. The optimization algorithm is derived from equation (1.1). The sinusoidal function is arbitrarily decomposed into a series of harmonics, and again the optimization is employed on the sum of a certain number of these harmonics.

In chapter four the Fast Fourier Transform (FFT) algorithm is identified as the best model that closely resembles the load profile. The results obtained in chapter three are now verified with FFT algorithm.

The results obtained in chapter four are used in chapter six for the economic investigation on the benefits that the VRB can offer when used in peak-shaving application. The figures (money) used in the economic analysis are the estimated values.

Chapter two

2 OVERVIEW OF ELECTRICITY STORAGE TECHNOLOGIES

2.1 INTRODUCTION

The accomplishment of tasks by residential, commercial and industrial customers[1] depends largely on the electricity supply. The high level of competition amongst customers and the rapid growth of electronic loads make the quality and reliability of power supply a critical issue. The electrification of rural areas, in South Africa for instance, adds more challenges to the utilities such as Eskom[2]. One of the factors causing these challenges is the inadequacy of power generation to meet the demands of the customer. Furthermore, the utilities are also concerned with the cyclic disparities between on-peak and off-peak electricity demands (refer to figure 3.1 for the on-peak and off-peak disparity). Hence, a suitable energy storage device is required in order to address problems of this kind in a more cost-effective manner.

This chapter discusses the development of the vanadium energy storage system. An overview of some of the commercial energy storage technologies is also presented. The focal point in this chapter is on the load-leveling and peak shaving applications. The comparison (in terms of commercial status) among the energy storage technologies will be presented later in this chapter.

The selection of the energy storage technologies that are discussed in this chapter is not meant to underestimate whatsoever the credibility of those that are

[1] Customers: Individuals or group of individuals who use electricity and pay for it.
[2] Eskom: National electricity utility based in South Africa.

not mentioned. The selection is based mainly on the commercial competitiveness and their capabilities for load-leveling application.

2.2 SOME COMMON STORAGE DEVICES

A number of energy storage technologies have been developed and some are still under development for numerous applications. The focus will be on the following technologies:

- Pumped hydropower
- Compressed air energy storage (CAES)
- Superconducting magnetic energy storage (SMES)
- Advanced Electrochemical Capacitors
- Flywheels
- Batteries

The discussion under each storage device will include the historical background, technical considerations, economic implications, advantages and potential drawbacks.

2.3 OVERVIEW OF PUMPED HYDROPOWER

It is argued that a pumped hydro technology is the oldest of all the energy storage technologies. Since the beginning of the twentieth century people have been using pumped hydro, and the research has proven that until 1970 it was the only commercially available storage option for generation application [26, 32].

A pumped hydro facility is designed in such a way that it comprises two large reservoirs, which are located at different levels (one being at the upper level and

the other one being at the lower or base level). The process of storing energy in this technology is mechanical in the sense that water is pumped into the upper reservoir. By the principle of conservation of energy, the water at the upper level is stored as potential energy. Mathematically,

$$E_p = \rho \times g \times h \qquad \ldots (2.1)$$

where

E_p = potential energy of the water stored in the upper reservoir

ρ = density of the water

g = acceleration due to gravity

h = distance between the upper reservoir and the lower reservoir.

During the demand periods, the stored water is released back into the lower reservoir, passing through hydraulic turbines and in the process a huge amount of electric power is being generated. Values of 1000 MW generated by this technology are reported [26, 32, 33].

Pumped hydro technologies are suitable for energy management applications (load-leveling), particularly on the generation side. However, they are not feasible for peak-shaving on the customer side (University of Stellenbosch) due to geographic and environmental constraints. The key point here is that they require large construction site. Hence, other energy storage technologies need to be evaluated for the purposes of peak-shaving on the customer side - the main focus in this thesis.

2.4 COMPRESSED AIR ENERGY STORAGE (CAES)

The design of this system is in such a way that an off-peak energy is used to compress air. The compressed air is stored in an air-tight underground storage cavern. Upon demand, stored air is released from the cavern, at the same time the air is being heated and expanded through a combustion turbine to create electrical energy. It is reported that CAES facilities with power ratings ranging from 5 to 350 MW have been developed [32, 33]. Once again, the geographic concerns make this system less favorable for the load-leveling application at the consumer side.

2.5 SUPERCONDUCTING MAGNETIC ENERGY STORAGE

A SMES system stores energy in the magnetic field created by the flow of direct current in a coil of superconducting material. The coil is usually immersed in a liquefied inert gas such as helium, which is contained in a vacuum-insulated cryostat[3]. The immersion is done in order to maintain the coil in its superconducting state. The energy, which is stored inductively and the rated power are commonly given specifications for SMES technologies, and they can be respectively expressed as follows [32]:

$$E = \frac{1}{2} L \times I^2 \times t \qquad \ldots (2.2)$$

$$\mathrm{P} = \frac{dE}{dt} \qquad \ldots (2.3)$$

Substituting equation (2.2) into equation (2.3) yields

[3] Cryostat: An apparatus used to maintain constant low temperature.

$$\mathrm{P} = L \times I \frac{dI}{dt} \quad \ldots (2.4)$$

Simplifying,

$$\mathrm{P} = V \times I \quad \ldots (2.5)$$

where

L = inductance of the coil

I = dc current flowing through the coil

V = voltage across the coil

t = time

Some of the advantages associated with a SMES system are as follows [26, 32]:

- The energy output is less dependent on the discharge rate.
- Good efficiency and fast response capability.
- It can store huge amounts of energy – on the order of 10 GWh.

Some of the potential disadvantages of a SMES technology are as follows [26]:

- A SMES technology requires compressors and sometimes pumps in order to keep the liquefied gas cool. These components normally occupy a large space.
- Construction of the site for a SMES unit involves a substantial investment.
- Finally, the maintenance of the technology also involves higher costs due its sophisticated design.

In the light of the above it is evident that a SMES technology is not economically viable. This argument is based upon the fact that load-leveling and peak-shaving are used primarily for cost reduction.

2.6 ADVANCED ELECTROCHEMICAL CAPACITORS

Capacitors are designed in such a way that an electrical field is induced between two electrically conducting plates separated by an insulating dielectric. The relationship between the stored charge and the voltage between the plates is mathematically expressed as follows:

$$q = C \times V \qquad \ldots (2.6)$$

and

$$C = \frac{\varepsilon \times A}{d} \qquad \ldots (2.7)$$

where

q = stored charge
C = capacitance
V = voltage between the two plates
ε = permittivity of the dielectric
A = area of the plates
d = distance between the plates

Therefore, from equations (2.6) and (2.7) the expression for the amount of energy a capacitor is capable of storing is expressed as follows [11, 32]:

$$E = \frac{1}{2} \times C \times V^2 \qquad \ldots (2.8)$$

These capacitors are widely used in many applications; for instance, in power distribution they are used as power factor correction devices. Capacitors are generally characterized by a strong capability to release energy instantly and also by a quick recharge.

On the negative side, these capacitors are not utilized in high-energy applications due to the fact that they release energy only for a short while regardless of the amount of stored energy [32].

2.7 FLYWHEELS

A Flywheel is used to store mechanical energy when it is coupled to an electric machine. A power converter is also used to drive the electric machine to provide a wider operating range [26, 32]. The operation of flywheel technology depends on two quantities. One is the moment of inertia (I) of the rotor and the square of the rotational velocity (ω) of the flywheel. The moment of inertia depends on the radius, mass and height of the rotor. Energy is transferred to the flywheel when the electric machine operates as a motor (the flywheel accelerates), charging the energy storage device. The flywheel is discharged when the electric machine regenerates through the drive (slowing the flywheel) [32]. The mathematical equations describing the relationships between the quantities are as follows [26,32]:

$$E = \frac{1}{2} \times \mathrm{I} \times \omega^2 \qquad \ldots (2.9)$$

and for a flat circular disc, of radius r

$$\mathrm{I} = \frac{r^2 \times m \times h}{2} \qquad \ldots (2.10)$$

where

E = stored energy

I = moment of inertia

ω = rotating velocity of the flywheel

r = radius of the rotor

m = mass of the rotor

h = height of the rotor

The research about flywheel technologies has shown that high-speed flywheels (the ones with small radii) are more favored than low-speed flywheels (big radii) [26]. Two major disadvantages of a flywheel have been identified. Firstly, they are unable to give up the stored energy rapidly. Secondly, as it is observed from equations (2.9) and (2.10) that the amount of energy stored is proportional to the mass of the rotor, meaning that flywheels are not environmental friendly in the sense that they require a bigger space in order to store sufficient amounts of energy. These drawbacks make them not seriously considered for the load-leveling application. Hence, a rigorous research on other alternatives such as batteries is inevitable.

2.8 BATTERIES

In recent years, much of the focus in the development of electricity storage devices has been centered on batteries. There are currently a wide variety of batteries available commercially and many more in the design phase. It is

argued that batteries are the most cost-effective energy storage technologies available in the market [3, 10, 20, 32]. Batteries are generally categorized into primary batteries (non-rechargeable) and secondary batteries (rechargeable). Most importantly, secondary batteries are characterized by chemical redox mechanisms. The discussion in this section focuses on a comparison of lead-acid (Pb/H^+) and vanadium flow batteries. The reason for choosing these batteries is that the first one represents an established, mature technology [3, 15, 20], whereas a vanadium flow battery is regarded as the most promising technology that can be used for a variety of applications with load-leveling being the center of attraction [1, 8, 17, 39].

The discussion will commence with the fundamental principles and descriptions of a redox reaction, and then followed by a full discussion on lead-acid batteries and vanadium redox flow batteries. The discussion will end with a performance and commercial comparison among various batteries.

2.8.1 SCHEMATIC REPRESENTATION OF A SECONDARY BATTERY

By definition, a battery is a DC power generative device, which is able to convert the chemically stored energy into work of an electrical nature. The figure given below shows a simple representation of a secondary battery:

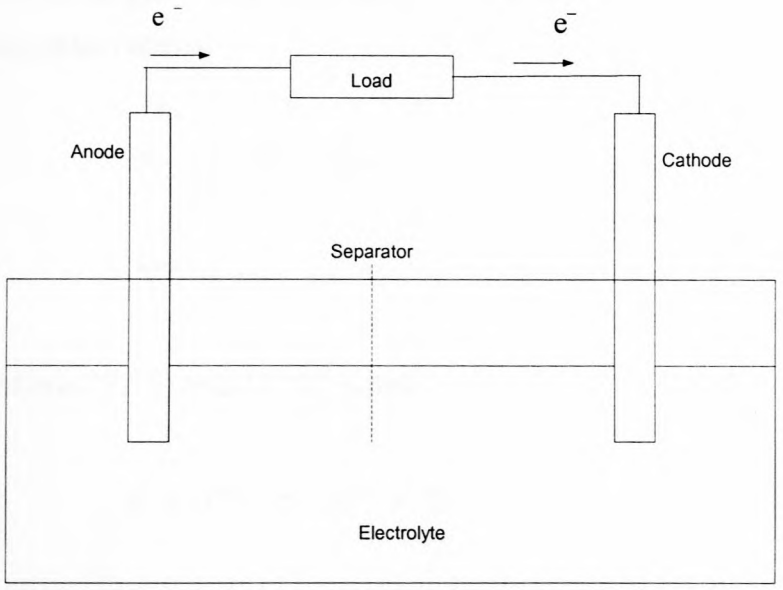

Figure 2.1 Schematic representation of a battery [40]

The two electrodes (anode and cathode) are immersed in an ionic solution of specified concentration. Sulphuric acid solution (H_2SO_4) is the one, which is normally used as an electrolyte in battery manufacturing. The electrolyte is in the form of free positively charged ions (cations) and negatively charged ions (anions). On the other hand, the anode and cathode are in excess and deficiency of electrons (e^-) respectively. The anode releases electrons towards the cathode and becomes positively charged. The process of releasing electrons is called the oxidation half reaction. The cathode accepts electrons and becomes negatively charged. The process of accepting electrons is called the reduction half reaction. The combination of the two half reactions is called the redox reaction. The separator (sometimes called salt bridge) allows the exchange of ions between the two half reactions. The battery is said to be discharging whenever the oxidation half reaction takes place. An external source (e.g. grid) is required to take the electricity back into the battery via the conducting wire; in this case the battery is said to be recharging. The redox reaction is regarded as the process of converting the chemically stored energy

into electrical energy. The chemical equations given below represent the reactions discussed above:

$$X \Leftrightarrow X^{n+} + ne- \quad \ldots (2.11)$$

$$Y^{n+} + ne^{-} \Leftrightarrow Y \quad \ldots (2.12)$$

adding equations (2.11) and (2.12) yields

$$X + Y^{n+} \Leftrightarrow X^{n+} + Y \quad \ldots (2.13)$$

where

X = reducing agent (anode)
Y = oxidizing agent (cathode)
n = number of electrons

Equations (2.11), (2.12) and (2.13) represent an oxidation half reaction, reduction half reaction and a redox reaction respectively. A battery system is made up of a set of low-voltage/power modules connected in series and parallel to achieve a desired electrical characteristic. A battery is charged when it undergoes an internal chemical redox reaction under a potential applied to the electrodes. It delivers the absorbed energy (discharges) when the chemical reaction is reversed. The discharge-charge process is best represented by equations (2.11), (2.12) and (2.13).

2.8.2 TECHNOLOGY OF LEAD-ACID BATTERY

Studies of quantum theory have proven that Lead is one of the strongest reducing agents. The electrons that occupy d-orbitals[3] in the highest energy level are readily released to the external circuit due to the amount of ionization[4] energy available at all the time. This quantum phenomenon is amongst factors, which facilitated the development of lead-acid $\left(Pb/H^{+}\right)$ battery for a variety of applications.

Sponge lead (Pb) and lead dioxide (PbO_2) have been identified as suitable reducing and oxidizing agents respectively for the manufacturing of a lead-acid battery. The chemical mechanisms described in section 2.8.1 apply perfectly well to the discharge-charge cycles of the (Pb/H^{+}) battery. The research on the development of batteries has identified three designs of a lead-acid battery, and the batteries are [3,20]:

- Flooded electrolyte
- Starved electrolyte
- Gelled electrolyte

A detailed discussion on the chemical manufacturing of each of the above designs is omitted. However, the performances, ratings and specifications will be summarized later in this section.

A lead-acid battery is a DC source and for that reason it has to interface with the electric utility through the power converter[5]. The interface is accomplished by integrating three well-defined, sized and specified subsystems. This integration

[3] Orbital: It is a region in space around the nucleous and it describes the probability of finding an electron.
[4] Ionization energy: It is the energy required to strip one electron from a neutral gaseous atom.
[5] Converter: It is a power electronic device, which rectifies ac to dc when the battery is charged and later converts dc to ac when the battery discharges.

is done in order to get a reliable energy storage system. The three subsystems are as follows [2,3]:

- Battery subsystem
- Power converter
- Balance of plant

The three subsystems given above are developed and manufactured independently by different suppliers. Each subsystem is designed for specific purposes, which are briefly described as follows:

- The battery subsystem is designed in such a way that it satisfies the energy (in kWh) required by the customer peak load for the duration of the peak load.
- The power converter is designed specifically to satisfy the peak power (kW) requirement of the load, which corresponds to the peak discharge rate of the battery.
- The balance of plant (BOP) is designed to provide environmentally sound housing for the battery and converter subsystems. This subsystem normally includes heating, air conditioning, controls, etc.

Several lead-acid batteries have been used to provide solutions (economically) to both the utility and the customer. In most instances, economic benefits are achieved through the peak-shaving and load-leveling strategies. It is necessary to compare the performance of a lead-acid battery with the performances of other batteries that are already in the market. However, the description of some of the terms, which are used in the battery industry, is also necessary. Jerry Mader defines the terms as follows [20]:

- *Specific energy*: the ratio of energy delivered by the battery to the weight of the battery, measured in watt hours per kilogram (Wh/kg) or (kWh/ft^3)

usually taken at a three-hour discharge rate. It is a quantifiable indicator of the range a battery will deliver under specified conditions.

- *Specific power*: the ratio of the power delivered by the battery to the weight of the battery, measured in watts per kilogram (w/kg) or (kW/ft^3) usually taken as the maximum delivered over 30 seconds. It is a quantifiable indicator of the acceleration a battery will provide.

- *Cycle life*: the number of charge/discharge cycles that a battery ca withstand before it fails. End of life is usually defined by reaching a level of degradation as a percent of capacity.

- *Battery life*: the time until a battery reaches the end of criterion (unable to recharge).

The performance comparison of at least five available batteries is given in the following table [26]:

Table 2.1 Battery systems for electric Power Storage

Battery system	Specific Energy (kWh/ft^3)	Specific Power (kW/ft^3)	Efficiency (% over 24 hours)	Life, deep cycles	Cost per kWh
Lead-Acid	2	3	92	400	$125
Nickel Metal Hydride	5	6	92	800	$375
Lithium Polymer	6	11	88	600	$550
Sodium Sulfur	7	15	88	1000	$350
Sodium Salt	5	15	87	800	$300

It is evident from table 2.1 that cost makes the lead-acid battery more attractive. In actual fact, cost and reliability are the ones that determine the commercial feasibility of any energy storage device. It is argued that the materials that are involved in the design of lead-acid batteries are not expensive [3], and this is proved by a relatively low cost shown in table 2.1 However, it should be noted that the comparison in table 2.1 is for batteries only, meaning that views about the viability of lead-acid batteries might be different when compared with other storage devices.

It is necessary to present some of the potential drawbacks associated with lead-acid batteries [3,10,26].

- Lead-acid batteries have low energy and power densities than any other commercial storage technology.
- In comparison with other batteries it is said that lead-acid batteries require more room and they have more weight for any application, typically about

5 square feet of floor space per kilowatt output if used for anything beyond energy stabilization.

- ❖ Unless properly handled, lead-acid batteries are mildly toxic.
- ❖ The performance of lead-acid batteries degrades with ambient temperature: at 0°C many lead-acid batteries produce only half the power they can at 40°C.

Somewhere in the foregoing paragraphs three different designs of lead-acid batteries were mentioned. Now, the essential features of these designs operating in the United States of America for load-leveling and peak-shaving are summarized in the following table:

Table 2.2 Peak-shaving and Load-leveling Lead-Acid Battery Technologies in USA [3]

Power (kW)	Energy (kWh)	Batteries in system	System Voltage (V)	Battery type	Floor space (m^2)
10 000	40 00	8256	2000	Flooded	4496
300	600	300	600	Flooded	186
300	580	192	384	Gelled	45
300	600	1200	600	Flooded	213
500	500	324	648	Flooded	52

Table 2.2 confirms that many lead-acid batteries need to be stacked in order to produce more energy and power. Furthermore, the argument that the system requires more space is also confirmed in the table.

In the light of the above discussions it is evident that in as much as lead-acid batteries relish much of the utilization for many applications, other energy storage developments are required. Hence, section 2.9 will be focusing on a newly

developed energy storage technology called Vanadium Energy Storage Technology, alternatively termed Vanadim Redox Battery.

2.9 DEVELOPMENT OF THE VANADIUM ENERGY STORAGE TECHNOLOGY

Electricity is different from other commodities in the sense that it is difficult to store. As a result of this, utilities such as Eskom have to devise means so that the electricity production matches the customer peak demand. Although the demand for electricity fluctuates widely from season-to-season and throughout the day, the electricity supply systems must still be able to deliver power over short duration peak periods. Consequently, in the absence of energy storage devices the supply systems are required to generate more power than is normally required. Now, if this extra capacity is not used or cannot be stored, then it is wasted. Both the power supplier and the customer do not desire this kind of a situation. Furthermore, constant uninterrupted power is of particular importance.

The discussion on various storage technologies was surveyed in the previous sections. It was revealed that each of the existing technologies suffers drawbacks that limit their commercial use. As a reminder, it was mentioned that pumped storage for instance, requires a big site because of the two reservoirs. Flywheels suffer from technical and cost weaknesses. Lead-acid batteries on the other hand also raise various environmental and maintenance issues. Hence, an energy storage system, which is viable economically and technically and is durable, is required to address the problems, particularly peak-shaving and load-leveling. Now, this section discusses the development of the Vanadium Redox Flow Energy Storage System (VRB) and focuses on the 1 kW and 200 kW VRB prototypes that were developed in Australia and Japan respectively.

The 250 kVA VRB, which was installed at the University of Stellenbosch for experimental purposes will be fully discussed in chapter five.

2.9.1 OVERVIEW OF THE DISCOVERY OF VANADIUM

Vanadium element (V) was discovered in 1801[1,7]. The element of vanadium exists in two forms. One form of the element called the pure vanadium appears as a silver gray metal, soft and ductile in nature. The other form of the element is a chemical element extracted from vanadiferous magnetite ore as a natural by-product in iron production. Vanadium is not a heavy metal and is not considered environmentally hazardous. At present, vanadium has a wide industrial usage including steel applications. Studies in the field of quantum theory and electrochemistry confirmed that vanadium is one of the best reducing agents in redox processes. The combination of these attributes facilitated the research on the usage of vanadium and hence the development of vanadium batteries. The research about redox reactions using vanadium couples as the electrodes started at the University of New South Wales in 1984 [29]. Further developments were carried out by the Kashima-Kita electricity utility of Japan in 1997 [1]. At present, a vigorous research on the technical and economic viability of the vanadium storage systems for commercial purposes is underway.

2.9.2 PRINCIPLE OF VANADIUM BATTERY

Energy in the vanadium storage technology (VRB) is stored chemically in two forms of ionic vanadium in acidic liquid electrolyte. The battery comprises of two electrolyte-storing tanks that store anodic and cathodic electrolytes separately. Both electrolytes are sulphuric acid solutions (H_2SO_4) of vanadium. The VRB also comprises of a number of flow cells, which are bound together forming what

is known as stacks. The electrolyte is pumped from separate storage tanks into each of the flow cells.

The two different forms of the electrolyte (i.e. anodic and cathodic) remain separated by a Proton Exchange Membrane. When the ion exchange takes place through the proton membrane one ionic form of vanadium is oxidized and the other form is reduced. During this chemical process, a current is generated and collected by electrodes, and consequently made available to the external circuit.

The electrochemical reaction is reversible so that the VRB can be charged and discharged with electrical energy being converted to chemical energy and vice-versa. The VRB operates on the $V^{4+}/V^{5+}//V^{3+}/V^{2+}$ redox couples and produces a nominal cell potential of approximately 1.25 V, depending on the concentration of the vanadium [1,7,8,17,29,39]. A useful terminal voltage can be achieved by a series connection of many cells into the stack. The amount of power available is related to the stack voltage and the current density established in the membrane. On the other hand the energy available depends only on the supply of the discharged electrolyte to the stack. The chemical half-reactions are represented by the following chemical equations:

$$V^{2+} \Leftrightarrow V^{3+} + e^{-} \quad \ldots (2.14)$$

$$V^{5+} + e^{-} \Leftrightarrow V^{4+} \quad \ldots (2.15)$$

And

$$V^{2+}/V^{3+} // V^{4+}/V^{5+} \quad \ldots (2.16)$$

Reactions (2.14), (2.15) and (2.16) are oxidation half-reaction, reduction-half reaction and redox reaction respectively. The Discharging of the VRB is indicated by the forward reactions (releasing of an electron or a charge), whereas the recharging is indicated by the reverse reactions (acceptance of an electron or a charge). Like any other flow battery, the reverse reaction in a VRB is possible only when it is connected to the ac source (usually the grid).

2.9.3 PERFORMANCE OF 1 kW VANADIUM REDOX BATTERY

This VRB was developed at the University of New South Wales (UNSW) as a prototype for experimental purposes [29]. The reason behind the development of this battery was based on the considerations of a reliable storage device that would effectively store the energy generated by renewable energy systems (e.g. photovoltaic and wind turbines). The success of the 1 kW UNSW VRB attracted the attention of many power system engineers since one of their concerns is peak-shaving and load-leveling strategies. This section presents the specifications and performance of the first ever developed VRB.

Table 2.3 Specifications for 1 kW Vanadium Battery [29]

Parameter	Specification
Electrode (felt) area (cm^2)	1500
Number of cells	10
Membrane material	Selemium CMV
Average cell cavity thickness (mm)	6.1
Felt thickness (mm)	0.3
Pressure drop through stack (kPa)	80
Electrolyte flow rate (litre/min)	6
Charging current (A)	20 - 60
Discharging current (A)	20 - 120
Nominal power at 75 A and 50% SOC (W)	940
Peak power at 120 A and 100% SOC (kW)	1.58
Electrolyte	1.5 M vanadium sulphate in 2.6 M H_2SO_4
Electrolyte volume per half-cell (l)	12
Upper voltage limit, charge (V)	17.00
Lower voltage limit, discharge (V)	8.00

It is reported that the battery was subjected to a large number of charge/discharge cycles, and the performance of the battery is summarized in the following table:

Table 2.4 Performance of 1 kW Redox Battery [29]

Charge current (A)	Discharge current (A)	Average power (kW)	Coulombic efficiency (%)	Voltage efficiency (%)	Energy efficiency (%)	Discharge capacity (A h)
20	20	0.28	92.6	95.0	88.0	-
30	30	0.41	97.8	91.6	89.6	40
45	45	0.59	99.0	85.1	84.3	42
60	60	0.77	98.4	82.5	81.1	41
45	75	0.94	95.2	81.9	78.0	40
45	91	1.10	97.0	80.1	77.7	41
45	106	1.23	97.5	76.4	74.5	41
45	120	1.33	98.2	73.2	71.9	41

In section 2.9.2 it was stated that pumping of the electrolyte from the storage tanks into the stacks is a basic operation of the VRB. Now, it is natural that a certain percentage would always account for the energy losses, and unfortunately table 2.4 does not give such an indication. However, under normal circumstances the pumping energy losses would account for up to 2-3% [8]. For instance, at a current of 30 A the energy efficiency would be plus or minus 88%. Comparing this figure with the ones presented in table 2.1, it is evident that efficiency wise VRB is virtually the same as other batteries, perhaps with Lead-Acid and Nickel Metal Hydride batteries emerging a little bit. However, the combination of this VRB efficiency with other potential advantages attached to it attracted the international community, and Japan was not an exception. Hence, the following section will be discussing further developments on the vanadium storage battery that took place in Japan.

2.9.4 DEVELOPMENT OF 200 kW – 4hr VANADIUM BATTERY

This battery was developed in 1997 by Kashima-Kita (one of the biggest private electricity utilities in Japan) following the success of UNSW prototype [1, 7]. The principles of the battery are exactly the same as those already discussed for a redox flow battery. This section presents only the specifications and target results of the battery.

Table 2.5 Specifications of 200 kW Vanadium Battery [1]

Parameter	Specification
Current density	80 – 100 A/cm^3
Out power	200 kW – 4hours
Module	8 stacks
Stack	2 substacks
Substack	21 cells
Electrode area	400 cm^2
Output power of stack	25 kW
Volume	22 m^3 each
Concentration	1.8 mol/L

The performance target and operational results of the VRB unit with the specifications given in table 2.5 are summarized as follows:

Table 2.6 Development target and operational results for the 200 kW battery

Parameter	Target	Results
Output power	200 kW	Achieved
Current density	80 mA/cm^2	Achieved
Current efficiency	95 %	93 %
Power efficiency	80 %	80 %
Voltage efficiency	84 %	86 %
Charge and discharge cycle	1500 cycle	650 cycle
Operational style	Automatic continuous operation	Achieved

The success of the Kashima-Kita project made the VRB a promising technology in the field of energy storage. It is shown in table 2.6 that unlike other battery systems VRB does not suffer from degradation with time. It is reported that the charge and discharge cycles that the Kashima-Kita battery underwent were deep[6] cycles.

2.9.5 INSTALLATION OF 250-kVA VANADIUM ENERGY STORAGE SYSTEM IN SOUTH AFRICA

This technology was installed at the University of Stellenbosch (South Africa) for experimental purposes, and now it is known as the Stellenbosch VESS Trial [17,39]. The trial is an international effort in the sense that it involved Vanteck[7] Technology Corporation (from Canada), Highveld[8] Vanadium and steel

[6] Deep cycle: When a battery is completely discharged and fully recharged.
[7] Vanteck: They have rights to the VRB technology for the continent of Africa.
[8] Highveld: Producers of vanadium electrolyte.

Corporation (South Africa) and Eskom (South Africa). The trial was established to show the versatile configuration and operation of the battery. The primary aim of the trial was to demonstrate applications ranging from sub-second uninterruptible power supply ride-through capabilities through to power quality and emergency power back up. A detailed discussion on this trial is presented in chapter five.

2.9.6 ADVANTAGES OF THE VANADIUM REDOX BATTERY

There are a number of advantages that make the VRB a promising storage device for commercialization. Some of the potential advantages include:

- The VRB has a lower environmental impact during its life cycle due to the kind materials used in its construction.
- The solutions have an indefinite life, so only the mechanical components need replacement at the end of their life.
- VRB technologies have no life degradation from repeated deep discharge and recharge cycles. Standard lead-acid batteries are capable of 300-to-1, 500 cycles with strict charge and discharge parameters [3,8,25]. On the other side VRBs are capable of over 10,000 plus cycles [8].
- The system volume can be increased by increasing the volume of the solution [1,8,17,29,39].
- The VRB can be charged and discharged simultaneously and can be charged or discharged at any voltage level. Overcharging is also possible without any loss of performance or damage [29,39].
- The VRB is capable of rapid charge both electrically and hydraulically. This means that the discharged vanadium electrolyte can be pumped out and immediately replaced with a charged solution, or even adding more electrolyte [1,29,39].

- The power rating dictated by the stacks is independent of the energy capacity, which is dictated by the volume of the electrolyte.
- The VRB remains undamaged even if the power demand is fluctuating.

2.9.7 DISADVANTAGES OF THE VANADIUM REDOX BATTERY

Like any other redox flow battery, the main disadvantage of the vanadium redox battery is a low energy density in comparison with the more usual secondary battery systems.

2.9.8 COMPARISON OF ENERGY STORAGE TECHNOLOGIES

It has been observed that each storage device has some inherent limitations that make it practical or economical for only a limited range of applications. The capability of each technology for high power and high energy applications are indicated by the following symbols:

♦ Fully capable and reasonable

⌀ Reasonable for this application

◊ Feasible but not quite practical or economical

None Not feasible or economical

The following table was published on the website – www.electricitystorage.org/tech/technologies_comparisons.htm on the 06 February 2003.

Table 2.7 Technology comparisons

Storage technology	Main advantage	Disadvantage (relative)	Power application	Energy application
Pumped storage	High capacity, low cost	Special site requirement		♦
CAES	High capacity, low cost	Special site requirement, Need gas fuel		♦
Flow battries: PSB VRB ZnBr	High capacity, independent power and energy ratings	Low energy density	∅	♦
Metal-Air	Very high energy density	Electric charging is difficult		♦
NaS	High power & energy densities, High efficiency	Production cost, Safety concerns (addressed in design)	♦	♦
Li-ion	High power & energy densities, High efficiency	High production cost, Requires special charging circuit	♦	◊
Ni-Cd	High power & energy densities, Efficiency		♦	∅
Other advanced batteries	High power & energy densities, High efficiency	High production cost	♦	◊
Lead-Acid	Low capital cost	Limited cycle life when deeply discharged	♦	◊
Flywheels	High power	Low energy density	♦	◊
SMES, DSMES	High power	Low energy density, High production cost	♦	
E.C. Capacitors	Low cycle life, High efficiency	Low energy density	♦	∅

2.10 SUMMARY

Peak-shaving and load-leveling applications are employed to reduce costs that customers incur as a result of their high load demands. Utilities on the other hand are faced with a serious challenge of generating extra power that is not used during the off-peak hours. Energy storage is one technique that can be employed to address all of these problems quite effectively.

A number of energy storage technologies have been discussed, particularly their commercial viability as well as their potential drawbacks. However, the viability of any energy storage device, either technically or economically, has to be investigated before commercialization. This kind of investigation is usually tackled by employing suitable models. Now, out of all the storage devices that have been mentioned in this chapter, the vanadium energy storage system is the only one that is still under development, and for that reason the commercial status of the technology is on the spotlight. Hence, a mathematical model for the 250 kVA VRB installed at the University of Stellenbosch is developed in chapters three and four.

Chapter Three

3 MATHEMATICAL MODELLING OF A DAILY LOAD PROFILE

3.1 INTRODUCTION

This chapter presents the derivation of a mathematical optimization technique that may be applied to a daily load profile. Peak shaving and load leveling when an energy storage device is utilized are the applications in which this optimization technique could be used. It should be emphasized though that in order to achieve the desired goal, a suitable mathematical function that resembles a profile is required.

It is necessary to present an illustration of a typical load profile before going into the derivation process. A weekly load profile as it is shown in the following figure will suffice the illustration.

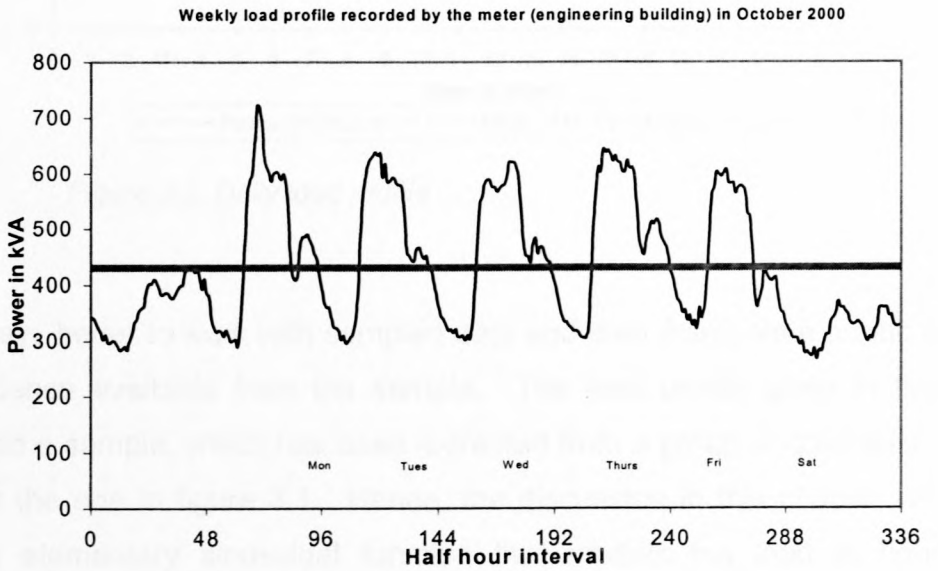

Figure 3.1 Weekly load profile extracted from October

It is observed in figure 3.1 that the load profile fluctuates about the mean and in every 24 hours the profile repeats itself. If the individual daily load profiles as shown in figure 3.1 had been put in juxtaposition, then one would have noticed only two discrepancies. Firstly, the maximum daily peaks are not the same in terms of height, and secondly, the position with respect to time domain at which these maximum peaks occur is not fixed. Apart from these two differences, the daily load profiles look virtually the same. A magnified picture of a single daily load profile, which occurred on Monday according to figure 3.1 is given below:

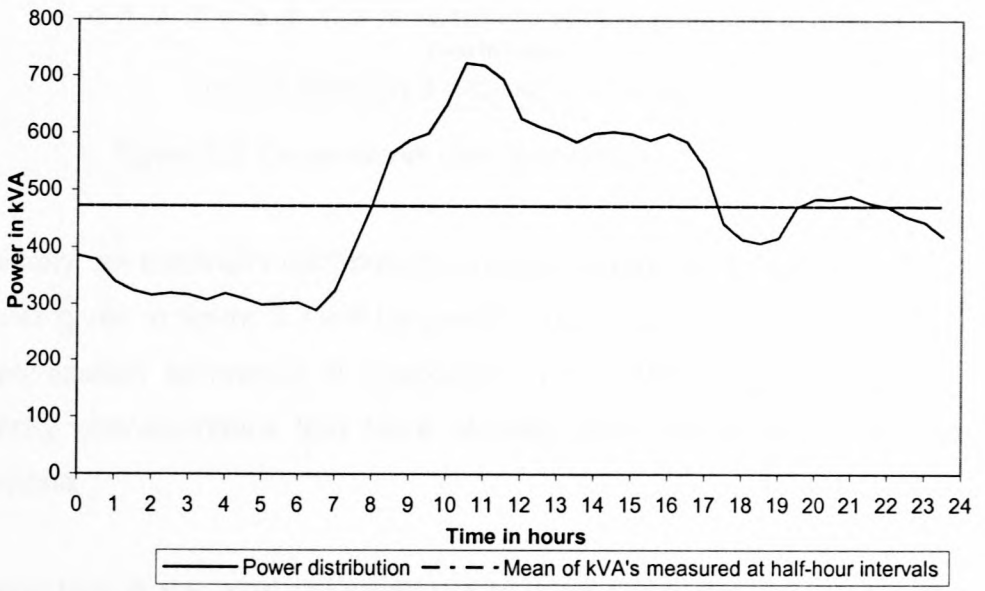

Figure 3.2 Daily load profile

It is always better to work with sampled data and then extrapolate on the basis of the evidence available from the sample. The load profile given in figure 3.2 serves as a sample, which has been extracted from a group of daily load profiles such as the one in figure 3.1. Hence, the discussion in this chapter will begin with an elementary sinusoidal function that models the load in figure 3.2. Conventionally, a daily distribution of electricity through the meter is usually illustrated with a figure similar to the one given below [28]:

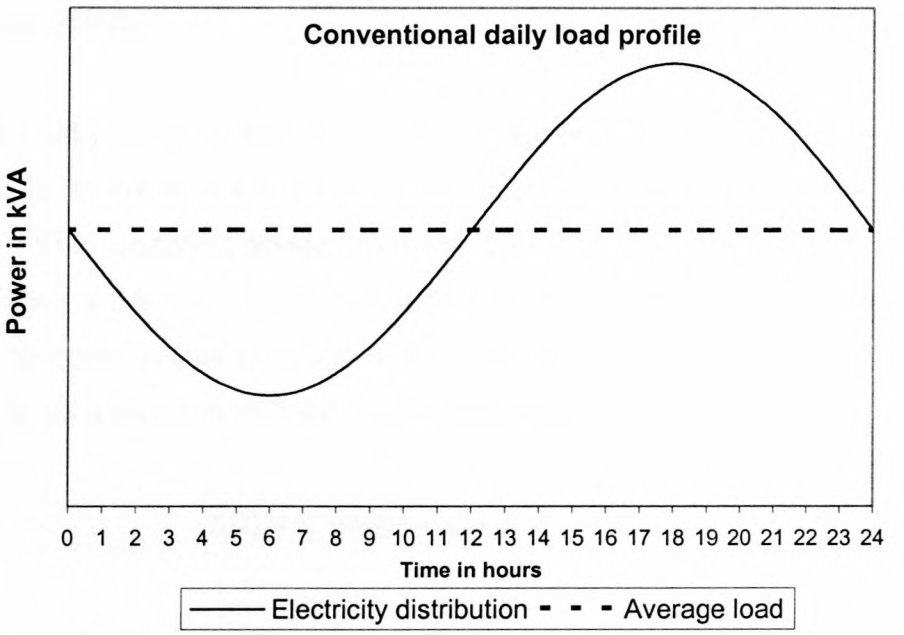

Figure 3.3 Conventional daily load profile

Technically, an electricity distribution through a meter is not sinusoidal, however, the curve given in figure 3.3 will be used in this chapter as a building block when the optimization technique is rigorously investigated. This is based on the periodicity characteristics that have already been mentioned in the foregoing paragraphs.

The main task in this kind of exercise is to bring down significantly the maximum peak of a load profile in cost-effective manner. In order to accomplish the task, an energy storage device is required. Although the investigation is meant for a variety of energy storage technologies, the VRB technology whose energy capacity is 500 kVA is the one, which was available for the researchers. This means that the derivation of the mathematical equations will be subjected to certain constraints, of which one of them is the energy capacity of the VRB system.

3.2 THE USE OF AN ENERGY STORGE DEVICE FOR PEAK SHAVING

Given a load profile as the one shown in figure 3.3, perhaps the first important question is to know if the peak at 18 hours can be reduced to a reasonable amount. This question arises from the fact that the highest peak at particular point in time is the one, which accounts for the maximum demand cost. The first attempt to address this question is to consider a load profile such as the one in figure 3.3, as a function defined by the following equation:

$$S(t) = P_a \sin(\omega t - \alpha) + \mu \qquad \ldots(3.1)$$

Where

$S(t)$ = Apparent power

t = Time in hours

μ = Mean (average of the kVA values recorded over half hour intervals)

α = Phase angle (time at which the curve starts crossing the mean

P_a = $S_{\max} - \mu$, where $|P_a|$ = amplitude

ω = Angular frequency in radians

The work is begun by first extracting all the useful information from figure 3.2 and substituting into equation (3.1). For the time being, zero will be assigned to α, but this is done without the loss of generality.

Thus, equation 3.1 and figure 3.2 provide the following information:

S_{max} = 725 kVA

μ = 472 kVA

$P_a =$ = 253 kVA

α = 0

Substituting these values into equation (3.1) results into the following sinusoidal function:

$$S(t) = -253 \sin(\omega t) + 472 \quad \ldots (3.2)$$

The negative value for P_a in the above equation is just meant for conformity with the conventional principle already discussed in section 3.1. Unless otherwise specified, throughout this chapter and other subsequent chapters the following tabulated time-radian conversion will be used.

Table 3.1 Time-Radians Conversion

Time	Radians
12:00 a.m.	0
12:00 p.m. = 720 minutes	π
1 minute	$\frac{\pi}{720}$
1 hour	$\frac{\pi}{12}$

The graph of the function defined by equation (3.2) is shown in the following figure:

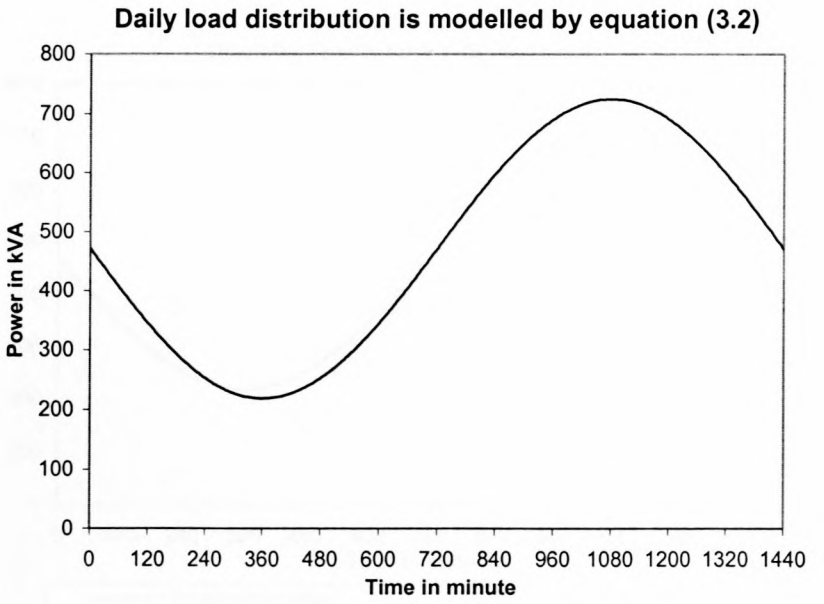

Figure 3.4 Modelling a daily load profile with a sinusoidal wave

The problem that we want to solve is to shave the maximum peak, which happens to be 725 kVA according to figure 3.4. The VRB technology with an energy capacity of 500 kWh is used with an attempt to address the problem of peak shaving. A simulation with Microsoft Excel is used to investigate an impact caused by the change in Δt.

As it was stated before, in this investigation the assumption is that the maximum peak occurs at $t = 1080\,\text{min} = \frac{3\pi}{2}$. Furthermore, for any given period of time the power released by the VRB is assumed to be constant. The discharge period is denoted by $\Delta t = t_f - t_s$, where t_s and t_f are the starting and finishing points of discharge respectively. The power released by the VRB is denoted by P_{VRB}. On

the same system of axis, an investigation when $\Delta t = 2hrs$ and $P_{VRB} = 250\ kVA$ as well as when $\Delta t = 4\ hrs$ and $P_{VRB} = 125\ kVA$ is made.

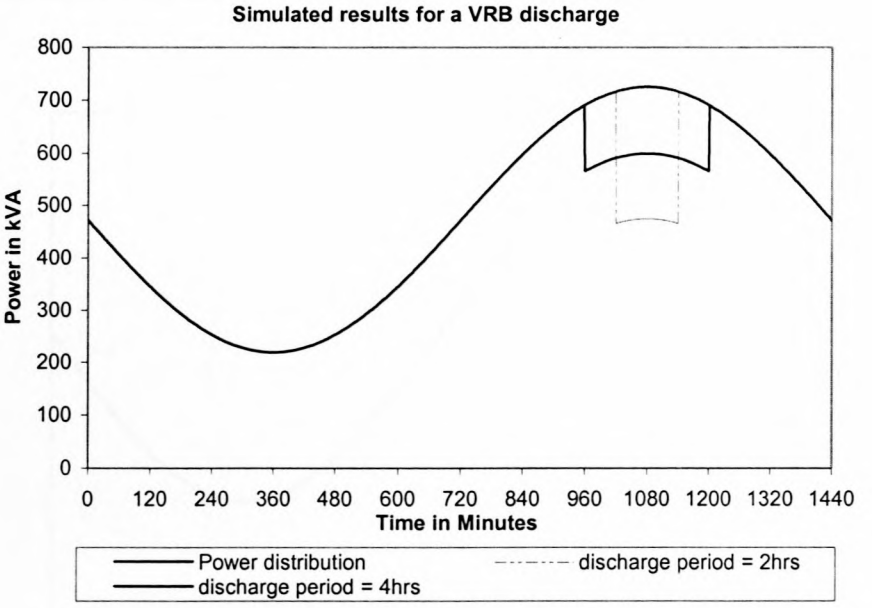

Figure 3.5 Simulated results when the discharge period is 2hrs and 4hrs

The first revelation that we see in figure 3.4 is that any attempt at allowing the VRB to release a huge chunk of 250 kVA for 2 hours or 124 kVA for 4 hours with the aim of shaving the maximum peak would not be cost-effective. The reason is that although the original peak is successfully cut off and dropped down to a smaller amount, but there is a kVA value at exactly one minute before t_s, which remains conspicuous and completely exposed to the meter. In the case of a two-hour discharge for instance, the value, which is at 1 minute before t_s is almost the same as the original peak. Pertaining to what has been discussed it transpires that a suitable optimizing strategy is required. A condition for an optimal solution is derived in the following section.

3.3 CONDITION FOR AN OPTIMAL SOLUTION

We begin our discussion in this section by first depicting some useful quantities in symbolic form on the curve.

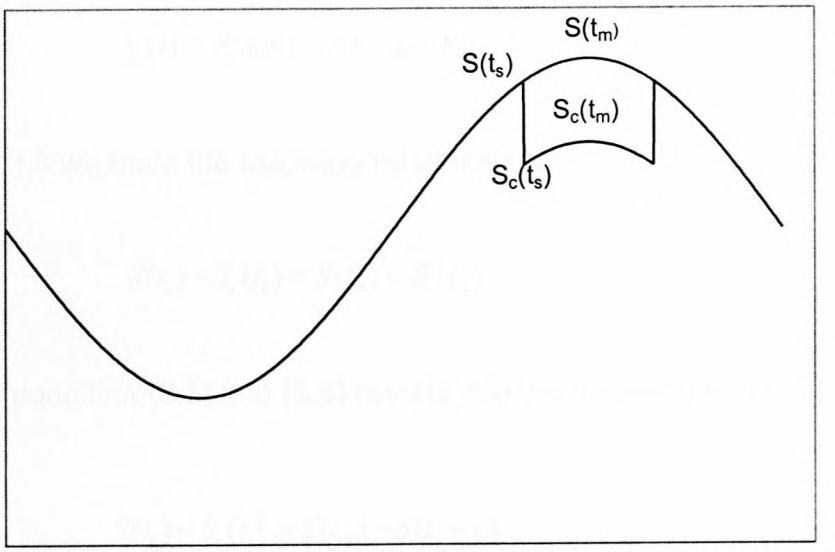

Figure 3.6 Deriving a condition for an optimal solution

The quantities represented by symbols in figure 3.5 are defined as follows:

$t_m \in \Delta t = t_f - t_s$ = Time such that $S(t_m)$ = maximum peak

$S_c = S(t_m) - \mathrm{P}_{VRB}$

ε = 1 minute interval

Hypothetically, an optimal solution occurs when

$$S(t_s - \varepsilon) = S_c(t_m) \quad \ldots (3.3)$$

In the foregoing sections a daily load profile has already been represented by a sinusoidal function defined by equation (3.1). If a constant VRB power is subtracted from equation (3.1), then the following equation is obtained:

$$S_c(t) = P_a \sin(t - \alpha) + \mu - \mathrm{P}_{VRB} \quad \ldots (3.4)$$

From figure 3.5 we have the following relationship:

$$S(t_s) - S_c(t_s) = S(t_m) - S_c(t_m) \quad \ldots (3.5)$$

Substituting condition (3.3) into (3.5) results into the following equation:

$$S(t_s) - S_c(t_s) = S(t_m) - S(t_s - \varepsilon) \quad \ldots (3.6)$$

Further substitution into equation (3.6) yields the following intermediate steps, which are intentionally not labeled:

$$P_a \sin(t_s - \alpha) - \left[P_a \sin(t_s - \alpha) - \mathrm{P}_{VRB}\right] = P_a \sin(t_m - \alpha) - P_a \sin\left((t_s - \varepsilon) - \alpha\right)$$

Simplifying on the left,

$$\mathrm{P}_{VRB} = P_a \sin(t_m - \alpha) - P_a \sin\left((t_s - \varepsilon) - \alpha\right)$$

Transposing all the terms into the left hand side yields the following labeled equation:

$$P_a[\sin((t_s-\varepsilon)-\alpha)-\sin(t_m-\alpha)]+\mathrm{P}_{VRB}=0 \qquad \ldots (3.7)$$

It is necessary to explain how equation (3.7) is solved when the appropriate numerical values are assigned to P_a, α, ε and t_m. As a reminder, it is important to recall that all mathematical computations and software simulations are done with the assumption that there is a certainty about the existence as well as the position of t_m. A software package such as Maple® V 5.1 can be used for the determination of the solution of equation (3.7). Since the interest and focus is on the value of t_s, then any arbitrary value may be assigned to P_{VRB}. By taking an advantage of the fact that our sinusoidal function is symmetrical about t_m, then the value of t_f may be calculated from the following equation:

$$\frac{t_s+t_f}{2}=t_m \qquad \ldots (3.8)$$

One should be cautious about the choice of the arbitrary value for P_{VRB}. The reason is that the product of Δt and P_{VRB} should not exceed the energy capacity of the VRB system. This energy capacity serves as a constraint in the mathematical and software calculations. At this stage it is essential to write the constraint in mathematical form.

$$\mathrm{P}_{VRB}\times(t_f-t_s)\le 500\ kWh \qquad \ldots (3.9)$$

In the calculations, P_{VRB} and Δt are expressed in kW and radians respectively, hence, the conversion given in table 3.1 is used in order to rewrite equation (3.9).

$$\mathrm{P}_{VRB}\times(t_f-t_s)\le\frac{500\pi}{12} \qquad \ldots (3.10)$$

Furthermore, it is sufficient to calculate the value of t_s since the curve is symmetrical. Equation (3.8) and equation (3.10) are combined to yield the following equation:

$$P_{VRB} \times (t_m - t_s) \leq \frac{250\pi}{12} \quad \ldots (3.11)$$

Once again, in equation (3.11) P_{VRB} and t_s are the only two unknowns. This suggests that equation (3.7) and equation (3.11) may be solved simultaneously. However, the solution is best found with Maple® V 5.1 when an equal sign is considered in equation (3.11). It should be noted that equation (3.7) is a non-linear equation, and Maple® normally considers the variables as global variables. This means that there is a possibility of getting an infinite number of solutions. Hence, the solutions need to be tested so that the constraint in equation (3.9) is satisfied.

3.4 VERIFYING EQUATION (3.7) WITH MAPLE® AND EXCEL®

It is necessary to verify the validity of equation (3.7) before going to a more generalized situation. The calculation is going to be done by considering the function in equation (3.2). The numerical values assigned to the constants and variables in equation (3.7) are as follows: $P_a = -253$, $\alpha = 0$, $\varepsilon = \frac{\pi}{720}$, $t_m = \frac{3\pi}{2}$ and the output variables are t_s and P_{VRB}. Maple® gives 3.9795 rad. and 65.7248 kVA as the output values for t_s and P_{VRB} respectively. Equation (3.8) is used to calculate the value of t_f and it is found to be 5.4454 rad. The next step is to test if the condition in equation (3.9) is satisfied. The difference between t_f and t_s expressed in terms of hours is 5.6 hrs. The product of P_{VRB} and $(t_f - t_s)$ is less than 500, and therefore, condition (3.9) is satisfied.

The results discussed in the foregoing paragraph are best explained by graphical means. The important point here is that we want to see if $S_c(t_m)$ is indeed equal to $S(t_s)$, as it is required as a necessary condition for an optimal solution. The following figure gives a good picture of the calculated results.

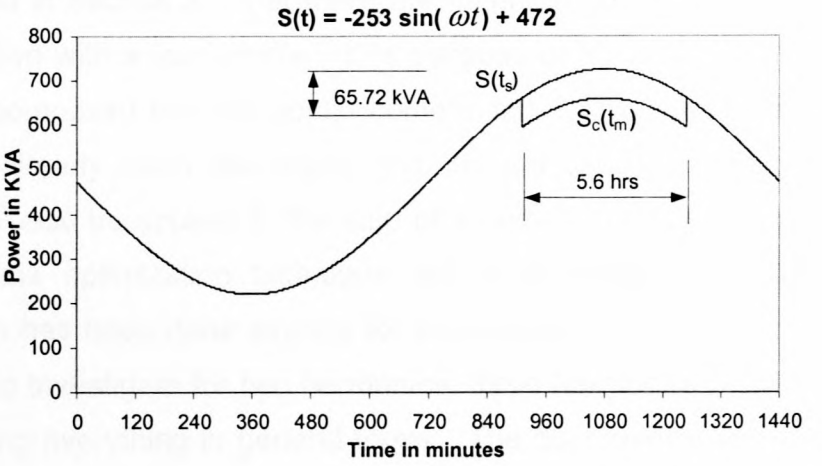

Figure 3.7 Preliminary results for an optimal solution simulated with Excel

As it is shown in figure 3.6, the simulated results tally with the analytical results. Furthermore, $S(t_s - \varepsilon) = S_c(t_m)$ as it is required for an optimal solution. However, it is necessary to emphasize that the results obtained in the foregoing discussion are not necessarily an optimal solution of a VRB in real life situation (i.e. when a peak shaving application is done on a daily load profile such as the one in figure 3.2). Instead, the strategy employed in getting these results is used to develop a method, which is applicable to a real load profile. The following section discusses the periodicity nature of a daily load profile.

3.5 EXPRESSING A LOAD PROFILE AS THE SUM OF n HARMONICS

It was stated in section 3.1 that there are inherent periodicity properties, which are associated with a load profile. It is because of this periodicity that a profile may be decomposed into sinusoidal components. The optimization technique, which has already been developed and applied to an elementary sinusoidal function, will also be applied to the sum of a certain number of harmonics. The validity of the optimization technique will be investigated inductively. The investigation has been done already for the fundamental harmonic, and what is left now is to investigate for two harmonics, three harmonics and then conclude by expressing everything in general terms. The decomposition of a load profile $S(t)$ may be expressed as a Fourier series, and its defining equation is as follows [14,16]:

$$S(t) = \frac{A_0}{2} + \sum_{n=1}^{\infty}[A_n \cos(n\omega t - \alpha_n) + B_n \sin(n\omega t - \beta_n)] \qquad \ldots (3.12)$$

where

A_0 = DC component of the signal (load profile in this case)

A_n and B_n = amplitudes of the harmonic components

α_n and β_n = phase angles that correspond to cosine and sine harmonics respectively.

ω = Angular frequency.

n = Positive integer

Although A_n and B_n represent the amplitudes of the harmonic components, but P_{ak} in equation (3.1) will still be used for convenience and consistency, where $k = 1, 2, 3, \ldots\ldots$. The main task here is to apply the optimizing strategy that has

already been developed, in a situation where the periodic signal is formed from n harmonics. The first thing is to assume that the signal (load profile) is expressed as a sum of two harmonics. Furthermore, this load profile is a signal whose period is 24 hours; hence, the corresponding number 2π will be used as a period throughout the discussion, unless otherwise specified.

3.6 REPRESENTING A LOAD PROFILE AS A SUM OF TWO HARMONICS

It is assumed that $h_1(t)$ and $h_2(t)$ represent the first (fundamental) and the second harmonics respectively. From equation (3.1) we may write these two harmonics as follows:

$$h_1(t) = P_{a1}\sin(t - \alpha_1) \qquad \ldots (3.13)$$

$$h_2(t) = P_{a2}\sin(2t - \alpha_2) \qquad \ldots (3.14)$$

Equations (3.13) and (3.14) have been extracted directly from equation (3.12), hence μ is missing in both of these equations. Now, the sum of $h_1(t)$ and $h_2(t)$ is represented by $S_2(t)$. Therefore,

$$S_2(t) = P_{a1}\sin(t - \alpha_1) + P_{a2}\sin(2t - \alpha_2) \qquad \ldots (3.15)$$

At this stage the validity of the optimization strategy when applied to equation (3.15) is investigated. The process is begun by first assigning arbitrary numerical values to the constants in equation (3.15). Now the constants are as follows: $P_{a1} = -300$, $\alpha_1 = 0$, $P_{a2} = -200$ and $\alpha_2 = \frac{\pi}{6}$. The sum $S_2(t)$, with all the constants substituted becomes

$$S_2(t) = -300\sin(t) - 200\sin(2t - \pi/6) \quad \ldots (3.16)$$

The following figure shows the graphs of $h_1(t)$, $h_2(t)$ and $S_2(t)$ drawn on the same system of axis.

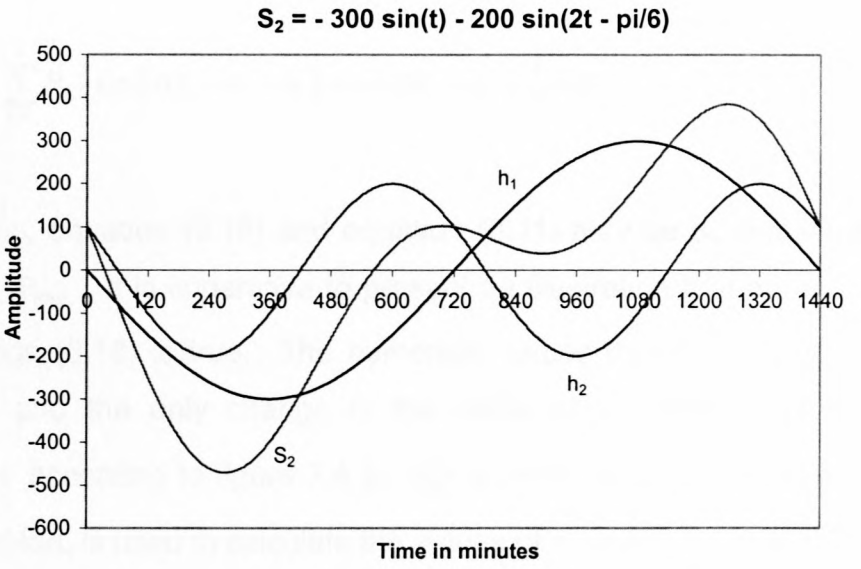

Figure 3.8 Sum of two harmonics with arbitrary constants

The curve represented by S_2 is viewed as a load model, and for that reason the procedures and techniques that have been developed so far are also applied to S_2. Rewriting equation (3.6) and label it as (3.17).

$$S(t_s) - S_c(t_s) = S(t_m) - S(t_s - \varepsilon) \quad \ldots (3.17)$$

Substituting equations (3.13) and (3.14) into equation (3.17) yields the following:

$$P_{a1}\sin(t_s - \alpha_1) + P_{a2}\sin(2t_s - \alpha_2) - \left[P_{a1}\sin(t_s - \alpha_1) + P_{a2}\sin(2t_s - \alpha_2) - \mathrm{P}_{VRB}\right] = P_{a1}\sin(t_m - \alpha_1) + P_{a2}\sin(2t_m - \alpha_2) - \left[P_{a1}\sin\left((t_s - \varepsilon) - \alpha_1\right) + P_{a2}\sin\left(2(t_s - \varepsilon) - \alpha_2\right)\right]$$

Simplification yields

$$P_{a1}\left[\sin\left((t_s-\varepsilon)-\alpha_1\right)-\sin\left(t_m-\alpha_1\right)\right]+P_{a2}\left[\sin\left(2(t_s-\varepsilon)-\alpha_2\right)-\sin\left(2t_m-\alpha_2\right)\right]+\mathrm{P}_{VRB}=0$$

In sigma notation,

$$\left\{\sum_{k=1}^{2}P_{ak}\left[\sin\left(k(t_s-\varepsilon)-\alpha_k\right)-\sin\left(kt_m-\alpha_k\right)\right]\right\}+\mathrm{P}_{VRB}=0 \qquad \ldots (3.18$$

Once again, equation (3.18) and equation (3.11) may be solved simultaneously for t_s and P_{VRB}. It is imperative to present an illustration that proves whether or not equation (3.18) is true. The numerical values used in equation (3.16) are repeated, and the only change is the value of t_m, which has shifted from $\frac{3\pi}{2}\approx 4.7124$ according to figure 3.4 to $\frac{1257\pi}{720}\approx 5.4847$ according to figure 3.8. In a similar fashion, is used to calculate the values of t_s and P_{VRB}. Maple® results are presented in tabular form. Moreover, the table below contains other values that are calculated from the known equation, such as equation (3.8)

Table 3.2 Optimal solution on the sum of two harmonics, S_2

	t_s	t_f	Δt
Radians	4.9524	5.9516	
Minutes	1135	1364	
Hours			3.817

In this particular problem there is more than one value for P_{VRB} suggested by Maple®. This is one of the cases whereby Maple® views P_{VRB} as a global

variable. However, a simulation with Excel® proves that $P_{VRB} = 104.1748$ kVA is an appropriate solution. The simulated results are shown in the following figure:

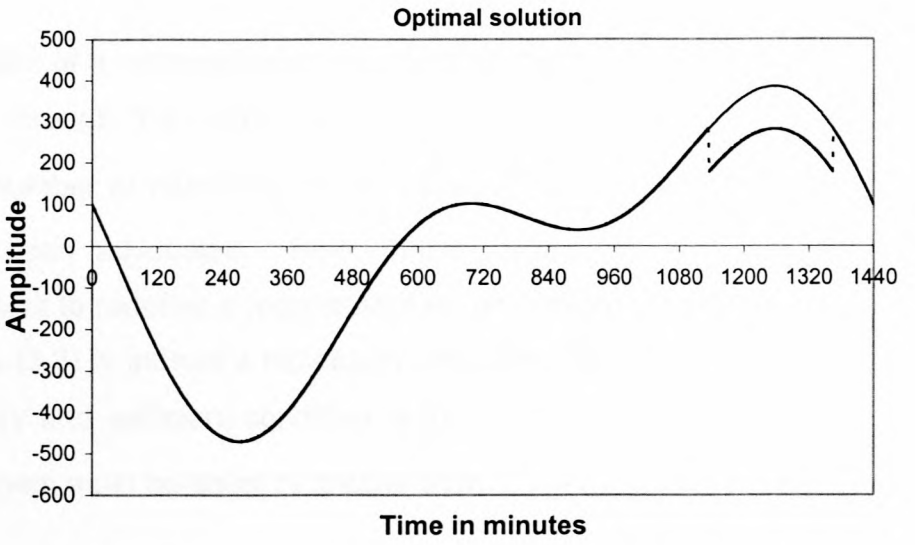

Figure 3.9 Simulated solution on the sum of two harmonics

The analytical results with Maple® together with the simulated results with Excel® prove the validity of our optimizing technique even if a signal is decomposed into two harmonics. If figure 3.9 were put in juxtaposition with figure 3.6, then one would observe that $S(t_s - \varepsilon)$ is indeed equal to $S_c(t_m)$, which is a necessary condition for an optimal solution. Another important observation about figure 3.9 is that the curve is not symmetrical about the point t_m. This suggests that the value $S(t_s)$ is not always equal to $S(t_f)$. So far the discussion has been focusing on the equality of $S(t_s - \varepsilon)$ and $S_c(t_m)$, and there is not much that has been said about the role of $S(t_f)$.

First and foremost, both $S(t_s)$ and $S(t_f)$ are lying on the original signal S_2. This means that they are technically exposed to the meter. Peak shaving in this particular case should be viewed as a strategy whereby an area covered by the

curve S and a line (L) joining $S(t_s)$ and $S(t_f)$ is cut off. Because of the capacity constraints or limitations for the VRB, equation (3.3) is seen as a necessary condition for an optimal solution.

In the case of a symmetrical profile such as the one in figure 3.6, L is expected to pass through the points $S(t_s-\varepsilon)$, $S_c(t_m)$ and $S(t_f+\varepsilon)$. But, the sum of a certain number of harmonics is not necessarily symmetrical about t_m, as it has already been advocated. Now, these paradoxical scenarios compelled the researchers to redefine a requirement for an optimal solution. In technical terms, equation (3.3) is indeed a necessary condition, but not a sufficient condition. A necessary and sufficient condition is that $S(t_s-\varepsilon)$ must be equal to $S_c(t_m)$ and both of them must be equal or greater than $S(t_f+\varepsilon)$. Mathematically,

$$\begin{cases} S(t_s-\varepsilon)=S_c(t_m) & \text{and} \\ \\ S(t_f+\varepsilon)\le S_c(t_m) \end{cases} \qquad \ldots (3.19)$$

The equation and inequality in (3.19) have been grouped together in order to emphasize their necessity and sufficiency.

It is imperative to investigate further the validity of our optimization technique, and consequently be able to put everything in general terms. The next section discusses a situation whereby a signal is decomposed into three harmonics.

3.7 REPRESENTING A LOAD PROFILE AS A SUM OF THREE HARMONICS

Let the first, second and third harmonics be defined respectively by

$h_1(t) = P_{a1}\sin(t-\alpha_1)$

$h_2(t) = P_{a2}\sin(2t-\alpha_2)$ and

$h_3(t) = P_{a3}\sin(3t-\alpha_3)$.

Therefore, the sum of h_1, h_2 and h_3, which is denoted by S_3 yields the following equation:

$$S_3(t) = P_{a1}\sin(t-\alpha_1) + P_{a2}\sin(2t-\alpha_2) + P_{a3}\sin(3t-\alpha_3) \quad \ldots (3.20)$$

From equation (3.6) and equation (3.20) we get

$$\begin{aligned}
&P_{a1}\sin(t_s-\alpha_1) + P_{a2}\sin(2t_s-\alpha_2) + P_{a3}\sin(3t_s-\alpha_3)\\
&-\left[P_{a1}\sin(t_s-\alpha_1) + P_{a2}\sin(2t_s-\alpha_2) + P_{a3}\sin(3t_s-\alpha_3) - \mathrm{P}_{VRB}\right]\\
&= P_{a1}\sin(t_m-\alpha_1) + P_{a2}\sin(2t_m-\alpha_2) + P_{a3}\sin(3t_m-\alpha_3)\\
&-\left[P_{a1}\sin\left((t_s-\varepsilon)-\alpha_1\right) + P_{a2}\sin\left((2t_s-\varepsilon)-\alpha_2\right) + P_{a3}\sin\left((3t_s-\varepsilon)-\alpha_3\right)\right]
\end{aligned}$$

Simplifying and transposing all the terms into the left hand side results into the following equation, expressed in sigma notation:

$$\left\{\sum_{k=1}^{3} P_{ak}\left[\sin\left(k(t_s-\varepsilon)-\alpha_k\right)-\sin\left(kt_m-\alpha_k\right)\right]\right\}+\mathrm{P}_{VRB}=0 \qquad \ldots (3.21)$$

Numerical arbitrary values are assigned to the constants in order to test if the optimizing strategy is valid in S_3. For convenience, graphical representations of h_1, h_2 and h_3 will be shown on the same system of axis, but the graph of S_3 will be drawn on a separate diagram. The assigned values to the constants are as follows: $P_{a1}=-300$, $P_{a2}=-250$, $P_{a3}=-200$, $\alpha_1=0$ and $\alpha_2=\alpha_3=\frac{\pi}{6}$. The analytical results with Maple® together with the simulated results with Excel® are given in the following table:

Table 3.3 Optimal solution on the sum of three harmonics S_3

	t_s	t_f	Δt	$S(t_s-\varepsilon)$	$S_c(t_m)$	$S(t_f+\varepsilon)$
Radians	5.4411	6.0781				
Minutes	1247	1393				
Hours			2.433			
kVA				440.0374	440.0374	439.9863

Before a comment on the above-tabulated results is made, it would be proper to present first the simulated results in the form of a graphic picture.

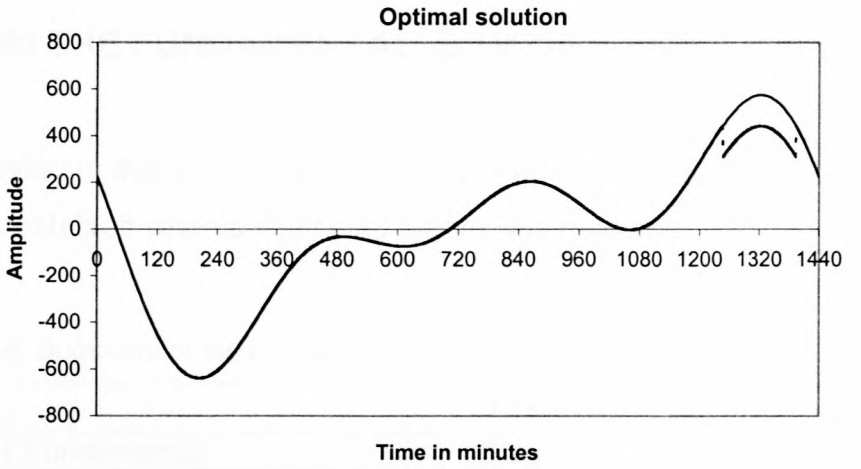

Figure 3.10 Simulated solution on the sum of three harmonics

The key point about these results is that they conform to the stipulated requirements and conditions. Briefly, it was mentioned in the previous sections of this chapter that the product of P_{VRB} and Δt should always be less than or equal to the energy capacity of the VRB, and in this particular case the VRB energy capacity is 500 kWh. In figure 3.10 we see that the maximum peak ($S_{\max}$) is equal to 573.498 kVA and $S_c(t_m)$ is equal to 440.0374 kVA, hence, the difference between these two values is 133. 46 kVA (i.e. P_{VRB}). Multiplying this value by Δt in table 3.3 yields 324.708 kWh, and for that reason equation (3.9) is satisfied. Furthermore, the necessary and sufficient condition for an optimal solution, which is given as (3.19) is also satisfied.

3.8 COMPARISON OF THE OPTIMAL SOLUTIONS OBTAINED FROM THE FUNDAMENTAL, SUM OF 2 AND 3 HARMONICS

The discussion in this section is begun by presenting a table, which summarizes key results obtained when a daily load profile was modeled by S_1, S_2 and S_3.

Table 3.4 Summary of the key results for fundamental, sum of 2 and 3 harmonics

	Δt /hrs	P_{VRB} /kVA
Fundamental	5.60	65.72
Sum of two harmonics	3.817	104.17
Sum of three harmonics	2.433	133.46

It is observed from table 3.4 that Δt decreases as P_{VRB} increases. On the other hand the corresponding P_{VRB} gets bigger and bigger with more harmonics. It is also noticed that none of these results violates the optimization conditions. The technique that has been used up to this far could be interpreted as a derivation of a mathematical model by induction. This argument is based upon the fact that the procedure was started with a simple sinusoidal wave (fundamental harmonic) up until the case where three harmonics were considered. It should be noted though that the magnitudes of the arbitrary constants used in the calculations do not affect the trend that we see in table 3.4 whatsoever. Now, it is essential at this point to put everything in a more generalized form. As a matter of convenience, equations (3.7), (3.18) and (3.21) are going to be rewritten without necessarily giving them new labels. For S_1, S_2 and S_3 we derived equations, which are respectively given below:

$$P_{a1}\left[\sin\left((t_s-\varepsilon)-\alpha_1\right)-\sin\left(t_m-\alpha_1\right)\right]+\mathrm{P}_{VRB}=0$$

$$\left\{\sum_{k=1}^{2}P_{ak}\left[\sin\left(k(t_s-\varepsilon)-\alpha_k\right)-\sin\left(kt_m-\alpha_k\right)\right]\right\}+\mathrm{P}_{VRB}=0$$

$$\left\{\sum_{k=1}^{3}P_{ak}\left[\sin\left(k(t_s-\varepsilon)-\alpha_k\right)-\sin\left(kt_m-\alpha_k\right)\right]\right\}+\mathrm{P}_{VRB}=0$$

From the above equations one may see that everything is the same except the summation number. Immediately from this observation, a general equation for n number of harmonics may be deduced and expressed as follows.

$$\left\{\sum_{k=1}^{n}Q_k\left[\sin\left(k(t_s-\varepsilon)-\alpha_k\right)-\sin\left(kt_m-\alpha_k\right)\right]\right\}+\mathrm{P}_{VRB}=0 \qquad \ldots (3.22)$$

Although the numerical calculations that were performed in the previous sections were based on the arbitrary values of the constants, the bottom line is that the derivation of equation (3.22) serves as a basis for the development of an optimization strategy in a real daily load profile, which is not necessarily a sinusoidal function. One of the most important aspects, which is a revelation from table 3.4 and equation (3.22) is that more harmonic components added together lead to a better optimal solution.

3.9 SUMMARY

In real life loads are subjected to a multitude of variations and the elementary sinusoidal curve suggested in figure 3.3 is merely a first-order approximation. However, noting that the load profile has a significant periodicity, as shown in figure 3.1, a logical representation would be obtained by employing a Fourier Transform. Since the Fourier series approximation consists of sinusoidal functions of varying frequencies, the optimization technique developed in this chapter can be expanded to a model that closely resembles a real-life load profile.

Chapter Four

4 MODELLING A DAILY LOAD PROFILE WITH A FAST FOURIER TRANSFORM ALGORITHM (FFT)

4.1 INTRODUCTION

The development of the optimization strategy in chapter three was based on the assumption that a load can be represented by a sinusoidal function. One of the common features of a sinusoidal function is that it is continuous at every point on the time domain. Moreover, a sinusoidal function is symmetrical about the point t_m. However, real-life loads profile such as the one in figure 3.2 consists of evenly spaced discrete points, and also, symmetry is not an inherent property. Now, a mathematical model, which can best approximate a load profile, is required. Since a load is periodic, it can be decomposed into a series of sine and cosine components of varying frequencies. It is therefore necessary to use a method to derive these components. Hence, the Fast Fourier Transform (FFT) algorithm has been chosen to address this problem. Describing some of the terms and concepts, which are prevalent in the FFT algorithm, begins the discussion in this chapter.

4.2 OVERVIEW OF TERMINILOGY USED IN FAST FOURIER TRANSFORM

A Fast Fourier Transform is widely used for many applications in the applied sciences, and for that reason it would be proper to present descriptions of those terms and concepts that are relevant to this thesis.

4.2.1 DISCRETE SIGNAL

A discrete signal is a signal, which consists of equally spaced distinct points. In this chapter, the signal of interest is a daily load profile whose discrete points are power values (measured in kVA) equally spaced at 30-minute intervals. The profile shown in figure 3.2 is redrawn just to illustrate the discreteness phenomenon.

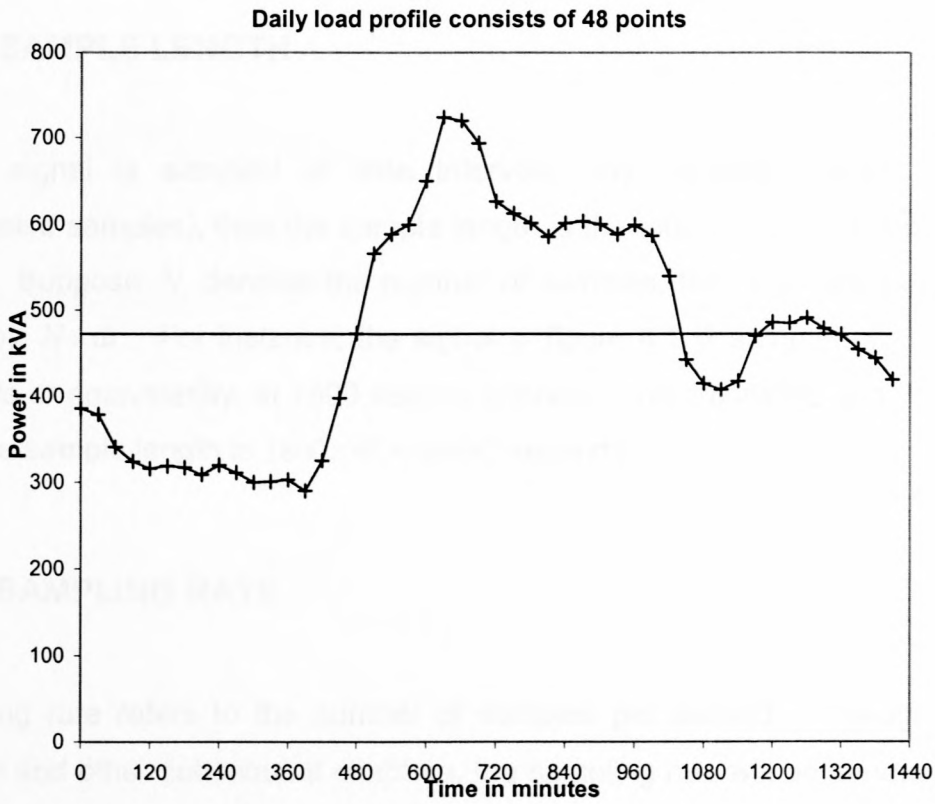

Figure 4.1 Power profile consisting of 48 discrete points

There are 48 discrete points forming a signal in figure 4.1, and the distance between two successive points is 30 minutes.

4.2.2 SAMPLED SIGNAL

A sampled signal refers to a portion or a certain number of discrete points, which have been extracted from the mother signal for the purposes of experimentation or analysis. In this particular case, the signal given in figure 4.1 is a sampled signal extracted from the one given in figure 3.1

4.2.3 SAMPLE LENGTH

If the signal is sampled at time intervals, say, dt (time interval between successive samples), then the sample length is the total duration of the sampled signal. Suppose N denotes the number of samples, then the sample length is given by $N \times dt$. For instance, the signal in figure 4.1 is sampled at 30-minute intervals or equivalently, at 1800 second intervals, and it consists of 48 samples, then the sample length is $1800 \times 48 = 86400$ seconds.

4.2.4 SAMPLING RATE

Sampling rate refers to the number of samples per second. Throughout this chapter and other subsequent chapters, the sampling rate will be denoted by f_s. The mathematical expression for the sample rate is as follows:

$$f_s = \frac{1}{dt} \qquad \ldots (4.1)$$

For instance, from section 4.2.3, the sampling rate would be $\frac{1}{1800} s^{-1} \approx 556\ \mu Hz$.

4.2.5 FREQUENCY SPECTRUM

When a proper Matlab® code is perfectly executed in order to extract the sine and cosine frequency components, then the displayed plot on the computer is called a frequency spectrum. The package may be commanded to display only the plot of the frequency amplitudes against the frequency domain, and this kind of a plot is called the amplitude spectrum. On the other hand, a plot of the phase angles against the frequency domain is called the phase spectrum.

4.2.6 SPECTRAL RESOLUTION

Spectral resolution is interpreted as the frequency difference between adjacent frequency components [14, 16]. In this thesis the spectral resolution will be denoted by f_r. The mathematical expression for the spectral resolution is as follows:

$$f_r = \frac{1}{N \times dt} \qquad \ldots (4.2)$$

4.2.7 NYQUIST FREQUENCY

Nyquist frequency refers to the highest frequency component of a sampled signal that can be correctly identified from the frequency spectrum [14, 16]. The FFT algorithm gives the amplitudes of the sine and cosine components of the signal over the frequency domain from 0 to the Nyquist frequency. In this thesis, Nyquist frequency is denoted by f_N and its mathematical representation is as follows:

$$f_N = \frac{f_s}{2} \qquad \ldots (4.3)$$

4.3 INTERPOLATION OF THE SIGNAL

One of the requirements for the FFT algorithm is that the number of samples of the signal must be equal to the power of 2 [14]. It was stated in section 4.2.3 that the number of samples is denoted by N, hence, the mathematical expression is as follows:

$$N = 2^n \qquad \ldots (4.4)$$

where n is a positive integer ($n = 1,2,3,.....$). It might have been noticed that the number of samples of the signal given in figure 4.1 is 48. According to the criterion in equation (4.4), the 48 samples have to be interpolated into 64 samples. The reason is that 64, being nearer to 48 can be expressed as 2^6. Deriving and expressing in general terms the coordinates of the 48 points, which are shown in figure 4.1, begin the process.

4.3.1 THE COORDINATES OF THE 48 DISCRETE POINTS

Without the loss of authenticity and generality pertaining to the signal in figure 4.1, researchers have adopted notations and symbols of their choice, mainly for the purposes of convenience and ease. In order to guard against misusing the well known symbol S for the apparent power and its measuring unit kVA, the following notation for the coordinates of a discrete point in figure 4.1 will be adopted: $(t;\varphi)$, where t and φ are the horizontal and vertical coordinates respectively. Now, the following table shows the derivation of the general term for t coordinates

Table 4.1 Horizontal coordinates of the 48 samples

t/min	Equivalent	Equivalent
0	30×0	$30\times(1-1)$
30	30×1	$30\times(2-1)$
60	30×2	$30\times(3-1)$
90	30×3	$30\times(4-1)$
:	:	:
1440	30×48	$30\times(49-1)$

From table 4.1 it can be deduced that the general term (t_k) for the t coordinates of the 48 points is expressed as follows:

$$t_k = 30\times(k-1) \qquad \ldots (4.5)$$

and

$$t_{(k+1)} = 30\times k \qquad \ldots (4.6)$$

where $k = 1,2,3,.....65$. In general terms, the coordinates of a particular point in figure 4.1 are given by $(30\times(k-1);\ \varphi_k)$, where φ is the power in kVA.

4.3.2 EQUATION OF A STRAIGHT LINE JOINING ANY TWO OF THE 48 POINTS

The coordinates of any two successive points, read from left to right in figure 4.1 are $(30\times(k-1);\ \varphi_k)$ and $(30\times k;\ \varphi_{(k+1)})$ respectively. Therefore, the general equation of a straight line joining these two points is given by:

$$\varphi - \varphi_k = \frac{\varphi_{(k+1)} - \varphi_k}{30 \times k - (30 \times (k-1))} \{t - (30 \times (k-1))\} \quad \ldots (4.7)$$

4.3.3 GENERATING 64 POINTS FROM 48 POINTS

In order to generate 64 discrete points, 64 must divide the sample length of the signal in figure 4.1, expressed in minutes. The calculation is as follows:

$$\frac{\text{Sample length}}{64} = \frac{1440}{64} = 22.5 \text{ minutes}$$

The number 22.5 is the distance between two successive points lying on the new signal that would be generated as a result of interpolation. The t coordinates of the new points, written as a row vector, are $[0\ 22.5\ 45\ 67.5\ 90\ \ldots\ldots\ldots 1440\ \text{min}]$. In a similar fashion as it was done in table 4.1 the general terms for these points will be denoted by t^*, and they are written as:

$$t_k^* = 22.5 \times (k-1) \quad \ldots (4.8)$$

and

$$t_{(k+1)}^* = 22.5 \times k \quad \ldots (4.9)$$

where $k = 1,2,3,\ldots\ldots\ldots 65$. It is observed that when the terms generated by the expression in equation (4.5) are compared to those generated in (4.8), then the terms represented by $90 \times (k-1)$ $(k = 1,2,3,\ldots\ldots 17)$ are common. Hence, these terms will remain unchanged in the t^* domain of the new signal with 64 points.

The t^* interval can be divided into 16 subintervals whose lower and upper bounds are the elements $90\times(k-1)$ where $k=1,2,3,.....17$. Now, these lower and upper bounds are respectively given in the following equations:

$$t_k^{**} = 90\times(k-1) \qquad \ldots (4.10)$$

and

$$t_{(k+1)}^{**} = 90\times k \qquad \ldots (4.11)$$

It is observed immediately from equations (4.10) and (4.11) that there are three points between t_k^{**} and $t_{(k+1)}^{**}$ that are not known yet. Moreover, the manner in which these points are located is same in all the 16 subintervals. An illustration as to how these three points lying between t_k^{**} and $t_{(k+1)}^{**}$ are determined will be given only for $k=1$.

Before the calculations are done, the discrete 48 points of the original signal in figure 4.1 are presented in the form of a row vector. The vector is as follows:

$\varphi = [386\ 379\ 341\ 324\ 316\ 319\ 317\ 309\ 320\ 311\ 300\ 301\ 303\ 290\ 325\ 398$
$473\ 565\ 588\ 599\ 650\ 724\ 720\ 694\ 626\ 612\ 601\ 585\ 601\ 603\ 600\ 588$
$599\ 586\ 539\ 443\ 415\ 408\ 418\ 470\ 486\ 485\ 491\ 479\ 472\ 455\ 445\ 420]$

From the discussion in section 4.3.1 and the above matrix, it is observed that φ_1 and φ_2 are 386 kVA and 379 kVA respectively. This means that the numerical coordinates $(30\times(k-1);\ \varphi_k)$ and $(30\times k;\ \varphi_{(k+1)})$ for $k=1$ are $(0;\ \varphi_1)$ and $(30;\ \varphi_2)$ or $(0\text{ min};\ 386\text{ kVA})$ and $(30\text{ min};\ 379\text{ kVA})$ respectively. Substituting these values into equation (4.7) yields

$$\varphi - 386 = \frac{379 - 386}{30 - 0}\{t - 0\} \qquad \ldots (4.12)$$

Simplifying,

$$\varphi = -\tfrac{7}{30}\, t + 386 \qquad \ldots (4.13)$$

The interval $\left(t_k^*;\, t_{(k+1)}^*\right)$ from (4.8) and (4.9) is contained in $\left(t_k;\, t_{(k+1)}\right)$, and therefore, at $k = 1$, $t^* = 22.5$. Setting $t = t^*$ and substituting into equation (4.13) will generate $\varphi = 380.75$. In a similar fashion, the remaining points could be constructed for all $k = 2,3,4,.....65$. It is imperative at this point to mention that the geometric and analytical procedures (which seemed rather laborious and tedious) that were employed in determining the 64 points cannot be presented in this thesis. Nevertheless, it was presupposed that the illustration given above would suffice for the general acceptance of the method, as discussed in all the subsections of section 4.3.

The next steps is to present all the generated 64 discrete points in the form of a row matrix, and then represent them in the form of a plot. Now, the row vector denoted by φ^* is as follows:

$$\begin{aligned}\varphi^* = [&386\ 380.75\ 360\ 336.75\ 324\ 318\ 317.5\ 318.5\\ &317\ 311\ 314.5\ 317.75\ 311\ 302.75\ 300.5\ 301.5\\ &303\ 293.25\ 307.5\ 343.25\ 398\ 454.25\ 519\ 570.75\\ &588\ 596.25\ 624.5\ 668.5\ 724\ 721\ 707\ 677\\ &626\ 615.5\ 606.5\ 597\ 585\ 597\ 602\ 602.25\\ &600\ 591\ 593.5\ 595.75\ 586\ 550.75\ 491\ 436\\ &415\ 409.75\ 413\ 431\ 470\ 482\ 485.5\ 486.5\\ &491\ 482\ 475.5\ 467.75\ 455\ 447.5\ 432.5\ 408.5]\end{aligned}$$

The Excel® plot of the above points is given below:

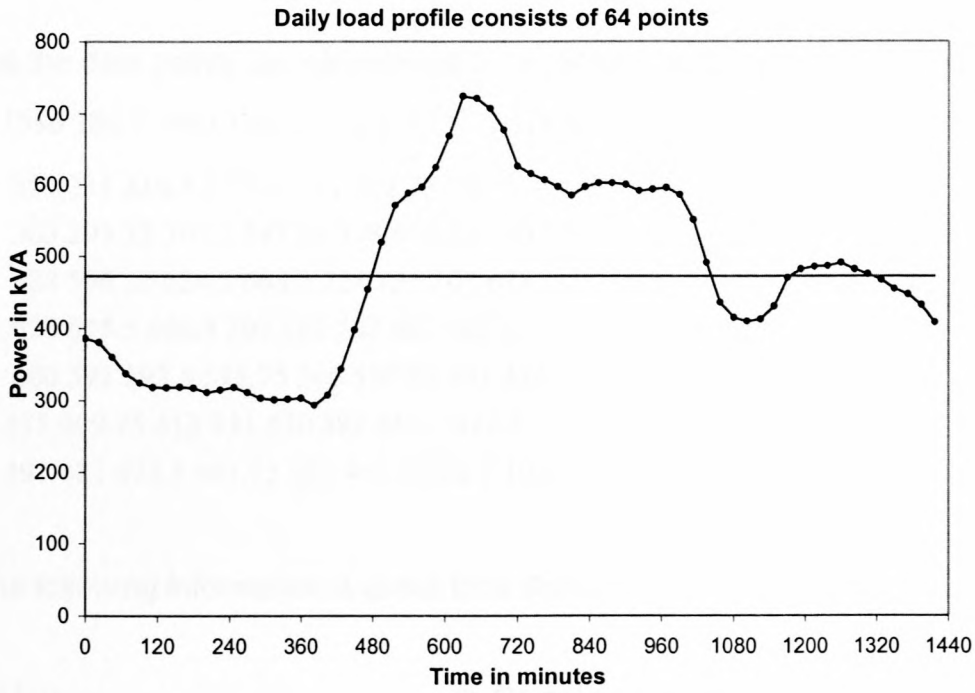

Figure 4.2 *Power profile consisting of 64 discrete points*

It is observed from figure 4.1 and figure 4.2 that the shapes of the profiles are congruent. This congruency allows the investigation to accommodate the exploration of the FFT algorithm. The next sections will focus on the verification of the optimization strategy developed in chapter 3 by using the FFT algorithm. As a reminder, the FFT algorithm is used because of the following reasons:

- The profile in figure 4.2 is a sampled signal, which has been extracted from the periodic signal shown in figure 3.1.
- The signal satisfies the requirement given in equation (4.4)
- All the 64 points in figure 4.2 are evenly spaced at 22.5 minutes.

4.4 MATLAB® CODE FOR THE EXTRACTION OF THE FREQUENCY COMPONENTS

% Let the data points be represented as a (64×1) matrix, which is denoted by X.

X = [386 380.75 360 336.75 324 318 317.5 318.5
317 311 314.5 317.75 311 302.75 300.5 301.5
303 293.25 307.5 343.25 398 454.25 519 570.75
588 596.25 624.5 668.5 724 721 707 677
626 615.5 606.5 597 585 597 602 602.25
600 591 593.5 595.75 586 550.75 491 436
415 409.75 413 431 470 482 485.5 486.5
491 482 475.5 467.75 455 447.5 432.5 408.5];

% The following information is about time domain:

$dt = 1350;$ % Sampling period.

$t = \text{linspace}\ (0, 63, 64);$ % Time domain.

$f_s = \frac{1}{dt};$ % Sampling rate.

$Ls = 86400;$ % Sample length.

% The following information is about frequency domain:

$f_r = \frac{1}{2 \times Ls};$ % Spectral resolution.

$f_n = \frac{f_s}{2};$ % Nyquist frequency.

$f = 0 : f_r : f_n - f_r;$ % Frequency domain.

$\mathrm{F} = \frac{\text{fft}\ (\mathrm{X})}{64};$

Figure (1)

plot (t, X)

figure (2)

stem $(f,\ \mathrm{abs(F)})$

figure (3)

stem $(f,\ \mathrm{angle(F)})$

% This is the end of the code.

All the three Matlab® plots are plots are given below:

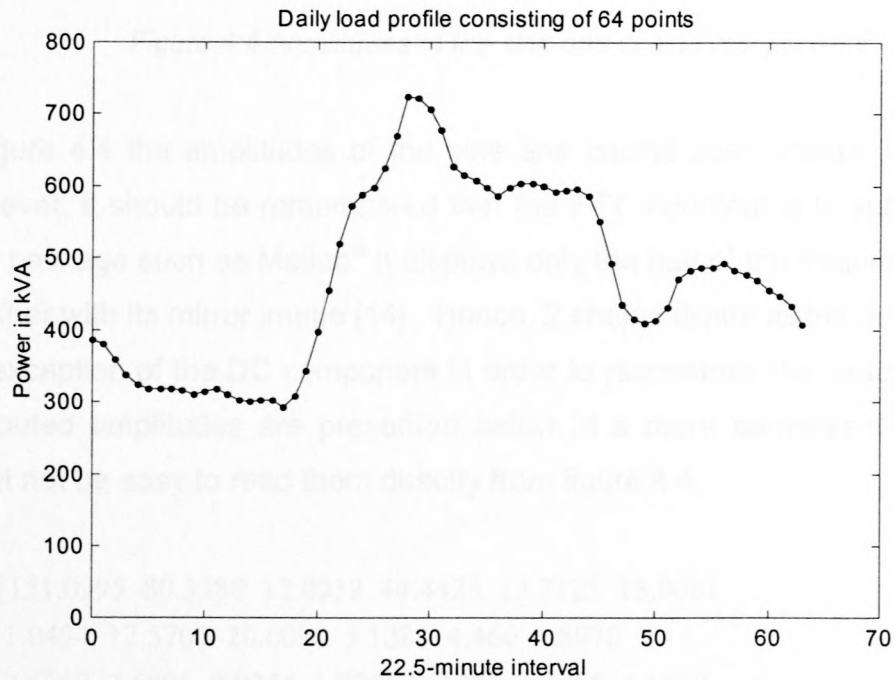

Figure 4.3 Power signal with 64 discrete points

The amplitude spectrum is given in the following figure:

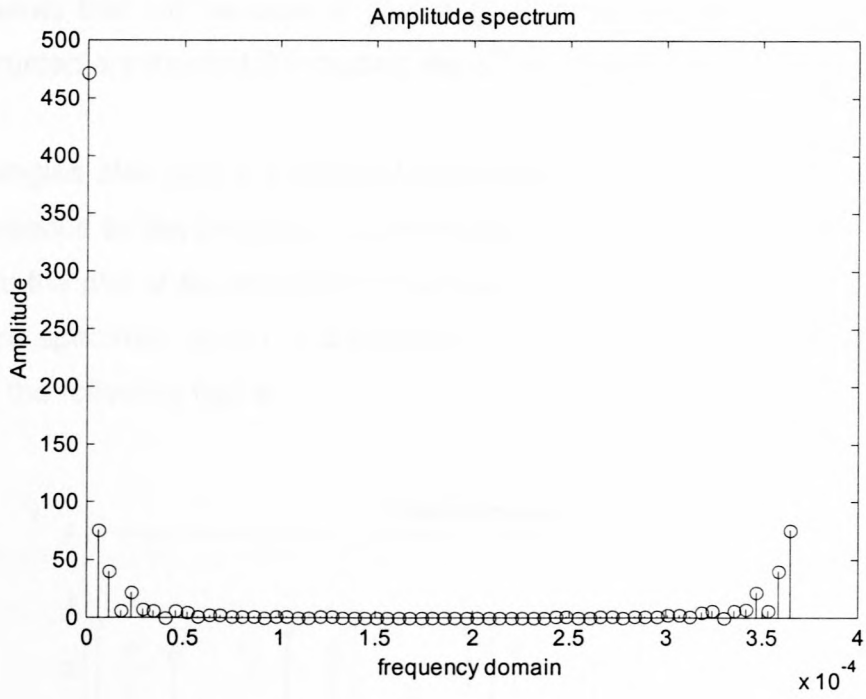

Figure 4.4 Amplitudes of the sine and cosine components

In figure 4.4 the amplitudes of the sine and cosine components are displayed. However, it should be remembered that the FFT algorithm is in such a way that on a package such as Matlab® it displays only the half of the frequency spectrum together with its mirror image [14]. Hence, 2 should divide all the amplitudes with the exception of the DC component in order to reconstruct the exact signal. The computed amplitudes are presented below in a more convenient way since it might not be easy to read them directly from figure 4.4.

A = [151.0995 80.3388 12.0939 44.4423 13.7122 13.0081
1.0494 12.5700 10.6090 3.1283 4.460 1.8970
2.6988 2.6001 0.9254 1.8745 2.1236 1.1555 1.1660
1.5435 1.2539 0.7711 0.6854 0.6594 1.1710 1.1669
0.6821 0.5632 1.1653 0.1401]

The magnitude of the DC component is 472.5078 and it is not given in the above row matrix. It is observed immediately from this vector that the frequency

components that will be able to give a good approximation when the signal is reconstructed are the first 6 including the 8^{th} and the 9^{th}.

Phase angles also play a significant role when a signal is reconstructed; hence, their presence in this discussion is inevitable. The plot of the phase spectrum is similar to the plot of the amplitude spectrum in the sense that it is only the half of the entire spectrum, which is displayed. The dispersion of the phase angles is given in the following figure:

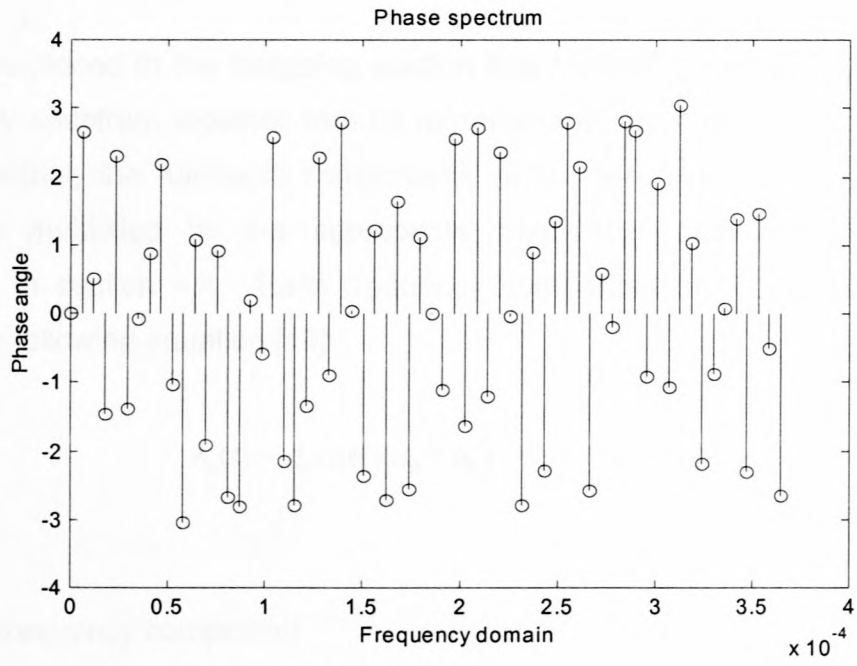

Figure 4.5 Phase angles of sine and cosine frequency components

The magnitudes of the phase angles measured in radians are summarized below as a row matrix:

$$\alpha = [2.6565\ \ 0.5007\ \ -1.4716\ \ 2.3083\ \ -13813\ \ -0.0790\ \ 0.8702$$
$$2.1899\ \ -1.0248\ \ -3.0428\ \ 1.0642\ \ -1.9163\ \ 0.9235\ \ -2.6793$$
$$-2.8136\ \ 0.2040\ \ -0.5869\ \ 2.5761\ \ -2.1405\ \ -2.7958\ \ -1.3556$$
$$2.2788\ \ -0.8895\ \ 2.7885\ \ 0.0297\ \ -2.3690\ \ 1.2019\ \ -2.7052$$
$$1.6412\ \ -2.5541\ \ 1.1061]$$

Once again, the phase angle corresponding to the DC component is 0 and it is not included in the above matrix. Thus, the FFT algorithm has managed to extract the useful information that are hidden between the discrete points. It is necessary to display this information in the form of graphs just before the optimization strategy developed in chapter 3 is further investigated.

4.5 DISPLAY OF THE FREQUENCY COMPONENTS EXTRACTED BY MEANS OF FFT ALGORITHM

It was mentioned in the foregoing section that Matlab® displays only half of the frequency spectrum together with its mirror image. In order to reconstruct the mother signal, the harmonic components, which are given by equation (3.12) must be multiplied by the appropriate frequency coefficients (amplitudes) obtained in section 4.4. Each frequency component may be constructed by using the following equation [14]:

$$h_n(t) = A_n \cos(n\omega_0 + \alpha_n) \tag{4.14}$$

where

h = frequency component

A = frequency coefficient

ω_0 = fundamental angular frequency

α = phase angle

t = time in radians

n = 1, 2, 3,....

The load profile given in figure 4.1 is a sampled signal extracted from a periodic signal, which repeats itself every 24 hours, as shown in figure 3.1. Now as a reminder, it was also given in table 3.1 that 24 hours corresponds to 2π, hence,

the fundamental angular frequency can be calculated from the following equation [16]:

$$\omega_0 = \frac{2\pi}{period} \tag{4.14}$$

It follows immediately from equation (4.14) that the fundamental angular frequency is 1, and therefore, the remaining frequencies will be multiples of 1.

For convenience, the plots for the 1st and 2nd, 4th and 8th as well as the 31st frequency component will be shown on separate figures. There is no particular reason for the selection of these components except that they will only serve as a proof for the validity of the FFT algorithm employed in this chapter.

4.5.1 PLOTS OF THE FIRST AND SECOND HARMONICS

Consider the following data for the plots: A_1 = 151.0995, ω_0 = 0, α_1 =2.6565, A_2 = 80.3388, α_2 = 0.5007. Substituting these values into equation (4.14) yields the following Excel® plots:

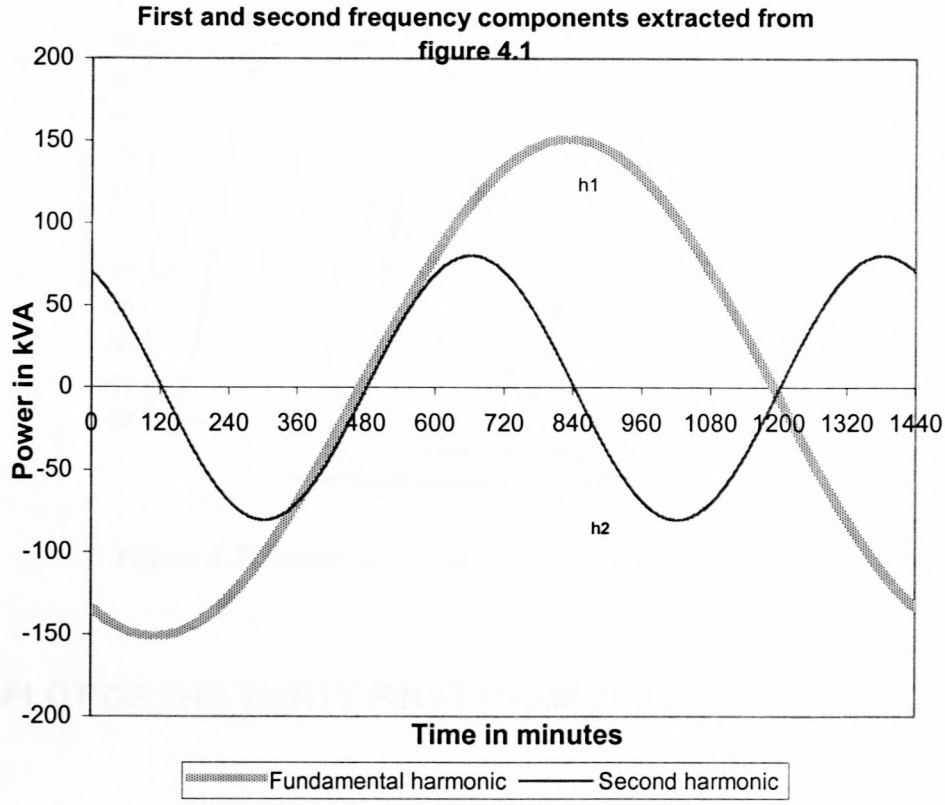

Figure 4.6 Fundamentlt and second frequency components

It should be noted that the DC component has not been considered in figure 4.6

4.5.2 PLOTS OF THE FOURTH AND EIGTH HARMONICS

Consider the following data for the plots: A_4 = 44.4423, α_4 = 2.3083 A_8 = 12.5700, α_8 = 2.1899. Substituting into equation (4.14) yields the following plots:

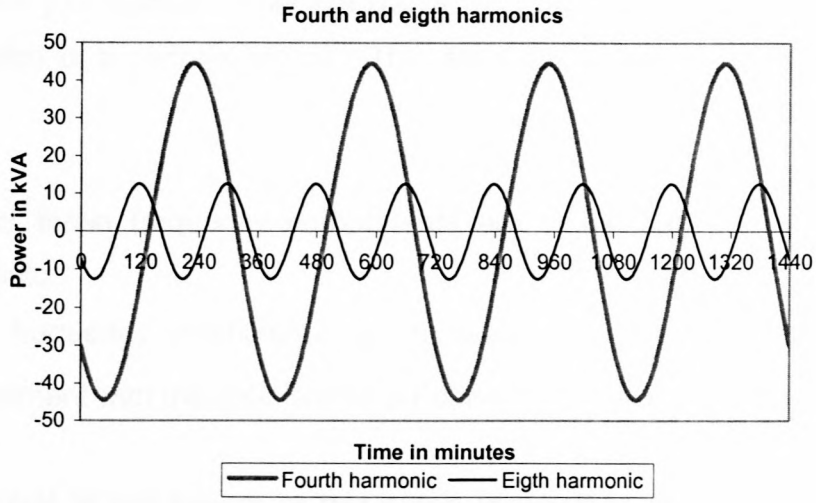

Figure 4.7 Fourth and eigth frequency components

4.5.3 PLOT OF THE THIRTY FIRST HARMONIC

Consider the following data for the plot: A_{31} = 0.1401 and α_{31} = 1.1061. Substituting into equation (4.14) yields the following plot:

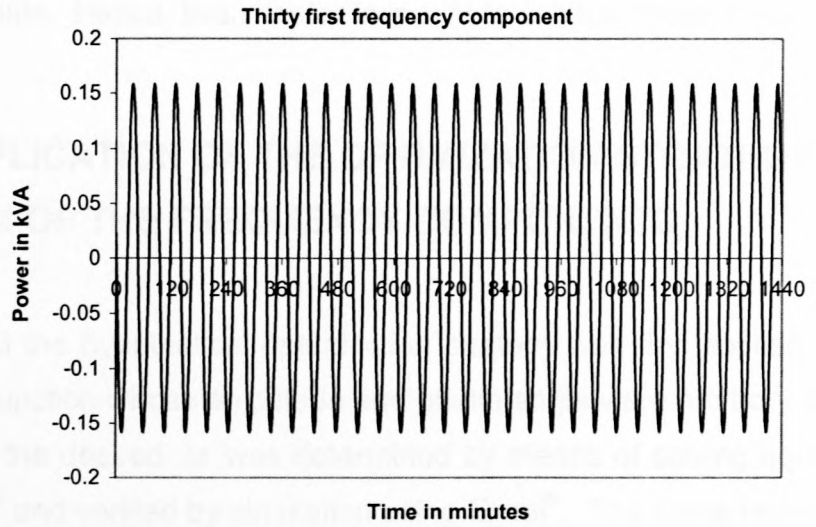

Figure 4.8 Thirty first frequency component

The frequency components that are shown in figures 4.6, 4.7 and 4.8 exhibit the characteristics of a periodic signal. This argument is based upon the following reasons:

- All of these frequency components are sinusoidal, and therefore also periodic.
- The frequency coefficients A_n decrease as n increases. This is in agreement with the definition of a Fourier series expansion [16].

However, what is not known at this stage is whether or not these frequency components will be able to give a good approximation when the mother signal is reconstructed. In the next sections the harmonics that have been created by the FFT algorithm are going to be added together in order to regenerate the mother signal as shown in figure 4.1. The procedures that were employed in chapter 3 in order to investigate the optimization strategy will be applied, exactly the same way, to the signal, which is going to be generated from a certain number of harmonics. The reason for doing this whole process is that the development of the optimization strategy was based on a number of assumptions that pertain to the load profile. Hence, this chapter is meant to validate those assumptions.

4.6 APPLICATION OF THE OPTIMIZATION STRATEGY ON THE SUM OF THE FREQUENCY COMPONENTS

In chapter 3 the hypothetical optimization strategy was first applied to a simple sinusoidal function whose amplitude and phase angle were arbitrary values. The solution for the desired Δt was determined by means of solving equation (3.22) with Maple® and verified by simulation using Excel®. The same technique will be used on the sum of two and three harmonics. In this section the optimization will be investigated exactly the same as it was done in chapter 3. Thus, the fundamental frequency will be the first to be considered followed by the sum of

two and three respectively. The final investigation will be made on the sum of all the frequency components.

4.6.1 OPTIMIZATION ON THE FUNDAMENTAL FREQUENCY COMPONENT

For convenience, some of the equations derived in chapter 3 will be rewritten. The solution may be found by solving equations (3.7) and (3.11) simultaneously. The equations are as follows:

$$P_{a1}\left[\sin\left((t_s-\varepsilon)-\alpha_1\right)-\sin\left(t_m-\alpha_1\right)\right]+\mathrm{P}_{VRB}=0$$

and

$$\mathrm{P}_{VRB}\times\left(t_m-t_s\right)\le\frac{250\pi}{12}$$

where

$P_{a1}=151.0995$, $\varepsilon=\frac{\pi}{720}$, $\alpha_1=2.6565$, $t_m=\frac{83\pi}{72}$ (see table 3.1 and figure 4.6 for the minute-radian conversion). Substituting into the above equations produces the solution tabulated below:

Table 4.2 Optimal solution on the fundamental harmonic

	t_s	t_f	Δt	$S\left(t_s-\varepsilon\right)$	$S_c\left(t_m\right)$	$S\left(t_f+\varepsilon\right)$	P_{VRB}
Radians	2.8972	4.3590					
Minutes	664	999					
Hours			5.58				
kVA				584.79	584.79	584.54	38.89

It is observed in table 4.2 that all the necessary and sufficient conditions (i.e. equations (3.11) and (3.19)) discussed in chapter 3 are satisfied. The discharge period obtained in chapter 3 when the fundamental harmonic was considered is almost the same as the one obtained when considering h_1 in figure 4.6. The only difference is in the P_{VRB} values, and the researchers believe that this difference is caused by the fact that the amplitudes in chapter three were arbitrary values. The plot in the following figure shows an Excel® simulated results.

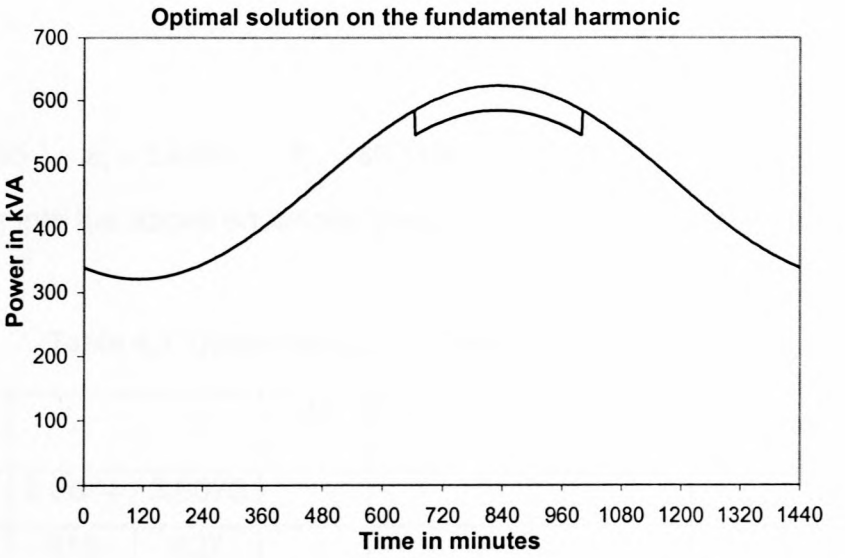

Figure 4.9 Optimal solution on the fundamental harmonic

Optimization on the sum of the first two frequency components will be investigated in the following subsection.

4.6.2 OPTIMIZATION ON THE SUM OF THE FIRST TWO HARMONICS

The equations that may be solved for an optimal solution when the first two frequency components are added together are as follows:

$$\left\{\sum_{k=1}^{2} P_{ak}\left[\sin\left(k(t_s-\varepsilon)-\alpha_k\right)-\sin\left(kt_m-\alpha_k\right)\right]\right\}+\mathrm{P}_{VRB}=0$$

and

$$\mathrm{P}_{VRB}\times\left(t_m-t_s\right)\leq\frac{250\pi}{12}$$

where

$P_{a1}=151.0995$, $\alpha_1=2.6565$, $P_{a2}=80.3388$, $\alpha_2=0.5007$, $t_m=\frac{179\pi}{180}$, $\varepsilon=\frac{\pi}{720}$.

Substituting into the above equations yields the solution tabulated below:

Table 4.3 Optimal solution on the sum of two harmonics

	t_s	t_f	Δt	$S\left(t_s-\varepsilon\right)$	$S_c\left(t_m\right)$	$S\left(t_f+\varepsilon\right)$	P_{VRB}
Radians	2.6834	3.6075					
Minutes	615	827					
Hours			3.533				
kVA				634.0060	634.0060	633.9159	42.80

Comparing the results in table 4.2 and table 4.3 it is observed that the value of P_{VRB} increases as Δt decreases. Although these results are not exactly the same as those obtained in chapter 3 for S_2, the important point is that there is a common trend (mentioned in the foregoing sentence) between the Δt and P_{VRB} values. The existence of this trend will be investigated further by optimizing on S_3 as it was done in chapter 3 and then conclude by considering the sum of all the frequency components. However, it is necessary to present the simulated

results for S_2 before going further with the investigation. The following figure shows an optimal solution for the sum of two harmonics:

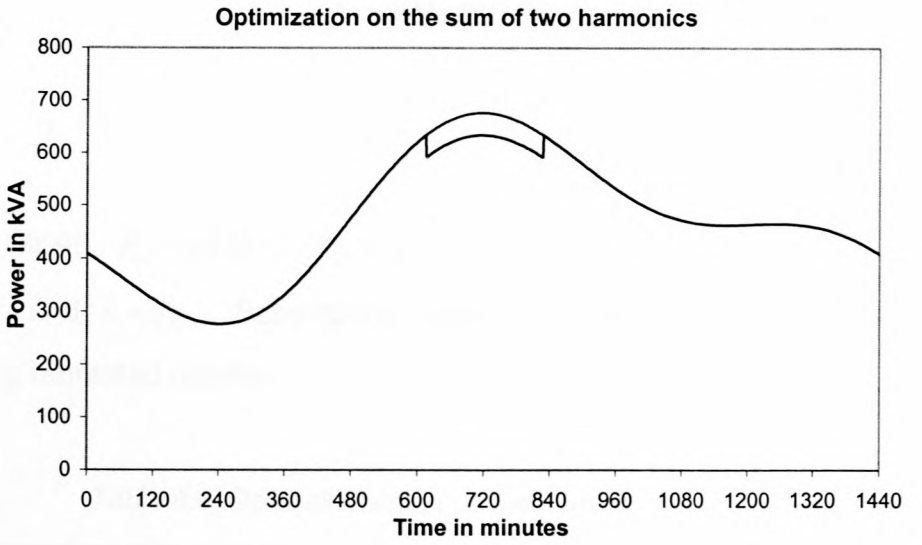

Figure 4.10 Optimal solution on the sum of two harmonics

Another important observation is that the signal in figure 4.10 has just started to approximate the mother signal shown in figure 4.2. This is an indication that the mother signal will be better approximated when the number of frequency components to be added is increased. The optimization on S_3 is investigated in the next subsection.

4.6.3 OPTIMIZATION ON THE SUM OF THREE HARMONICS

In order to determine an optimal solution with Maple®, the following equations must be solved:

$$\left\{\sum_{k=1}^{3} P_{ak}\left[\sin\left(k(t_s-\varepsilon)-\alpha_k\right)-\sin\left(kt_m-\alpha_k\right)\right]\right\}+\mathrm{P}_{VRB}=0$$

and

$$P_{VRB} \times (t_m - t_s) \leq \frac{250\pi}{12}$$

where

$P_{a1} = 151.0995$, $P_{a2} = 80.3388$, $P_{a3} = 44.4423$, $\alpha_1 = 2.6565$, $\alpha_2 = 0.5007$, $\alpha_3 = 2.3083$, $t_m = \frac{641\pi}{720}$ and $\varepsilon = \frac{\pi}{720}$. Substituting into the equations given above yields the following tabulated results:

Table 4.4 Optimall solution on the sum of three harmonics

	t_s	t_f	Δt	$S(t_s - \varepsilon)$	$S_c(t_m)$	$S(t_f + \varepsilon)$	P_{VRB}
Radians	2.4522	3.3641					
Minutes	562	771					
Hours			3.483				
kVA				620.7907	620.7907	620.7599	59.40

The analytical results shown in table 4.4 satisfy all the conditions for an optimal solution, which were discussed in chapter 3. It is imperative to conclude the optimization investigation with a case where the mother signal is reconstructed from all the frequency components that are generated by means of FFT. An optimal solution found from the actual load profile will form the basis for the economic implications that pertain to the use of the VRB in load leveling and peak-shaving applications. Before reconstructing the signal from all of its frequency components, it is necessary to present the graphical solution of the problem discussed in this subsection. The figure given below shows an Excel® simulated results when the sum of three harmonics is considered for optimization:

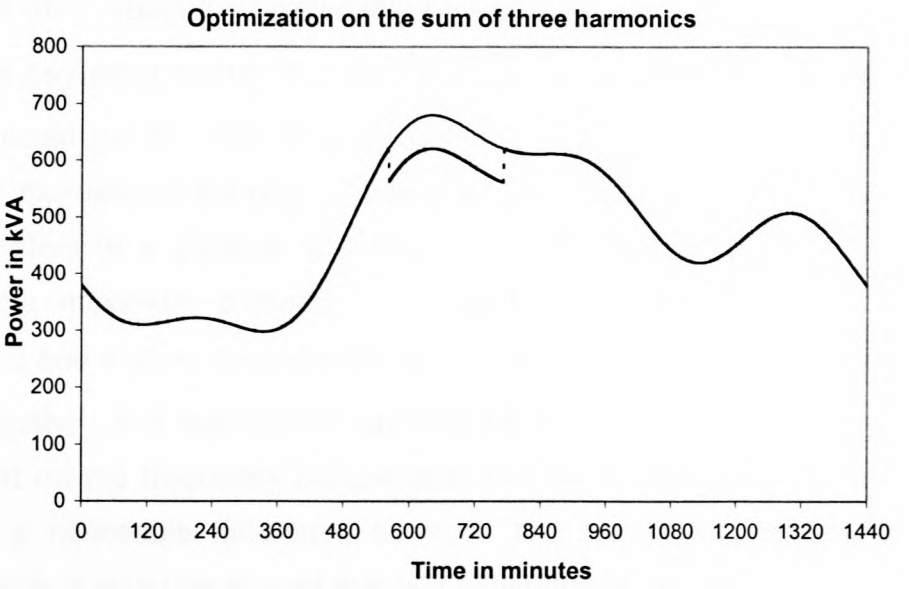

Figure 4.11 Optimal solution on the sum of three harmonics

It is evident from figure 4.11 that the consideration of more frequency components will give a much better approximation. To understand what has been discussed pertaining to the optimization strategy, it is vital to put the results obtained in chapter three together with the results obtained in this chapter. The results will be presented in a tabular form in order to enable one to see the common trends. The observation of these trends with regard to the changes in Δt and P_{VRB} will serve as an evidence and validation of the optimization technique.

Table 4.5 Comparison of the results for an optimal solution

No. of harmonics	Δt /hrs chapter 3	P_{VRB} /kVA chapter 3	Δt /hrs chapter 4	P_{VRB} /kVA chapter 4
Fundamental	5.60	65.72	5.58	38.89
Sum of two	3.82	104.17	3.53	42.80
Sum of three	2.43	133.46	3.48	59.40

A general trend about the relationship between Δt and P_{VRB} is observed in table 4.5. The key point is that P_{VRB} increases as Δt decreases. A better optimal solution could be obtained by sufficiently adding more frequency components that best approximate the original power signal. In this context, a better optimal solution refers to a situation whereby a VRB delivers more power in order to reduce the maximum demand quite significantly. The results obtained in chapters 3 and 4 show the increase of P_{VRB} as more frequency components are added together. It is important to remember that the results obtained in chapter 3 are based on the frequency components that were arbitrarily chosen. Hence, there is a noticeable difference between the results in chapters 3 and 4. Furthermore, it could be argued that this difference is caused by the fact that the arbitrary power signals in chapter 3 have different shapes and sizes to those presented in chapter 4.

Although the optimization technique was investigated only in the case of the fundamental, sum of two harmonics and sum of three harmonics respectively, it is imperative that all the frequency components generated by means of FFT are considered for the optimization. The optimization based on the sum of 31 frequency components according to the amplitude spectrum (figure 4.4) is presented in section 4.6.4.

4.6.4 OPTIMIZATION ON THE SUM OF ALL THE 31 HARMONICS

In the same manner as it was done in the foregoing subsections, row matrices A and α are used to reconstruct the signal. The graph representing the sum of 31 frequency components is given in the following figure:

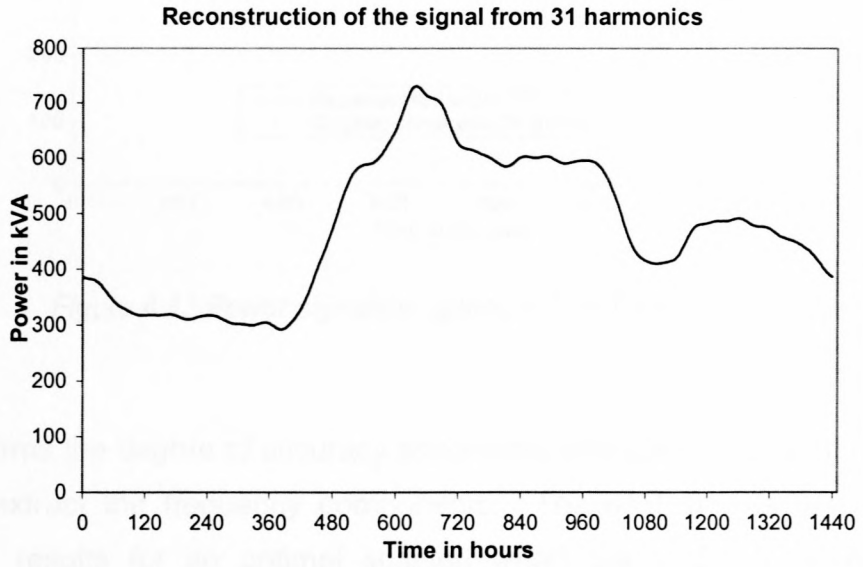

Figure 4.12 Approximation of the signal from 31 harmonics

The signal in figure 4.12 closely approximates the signal given in figure 4.2. Figure 4.13 shows these two signals drawn on the same system of axis.

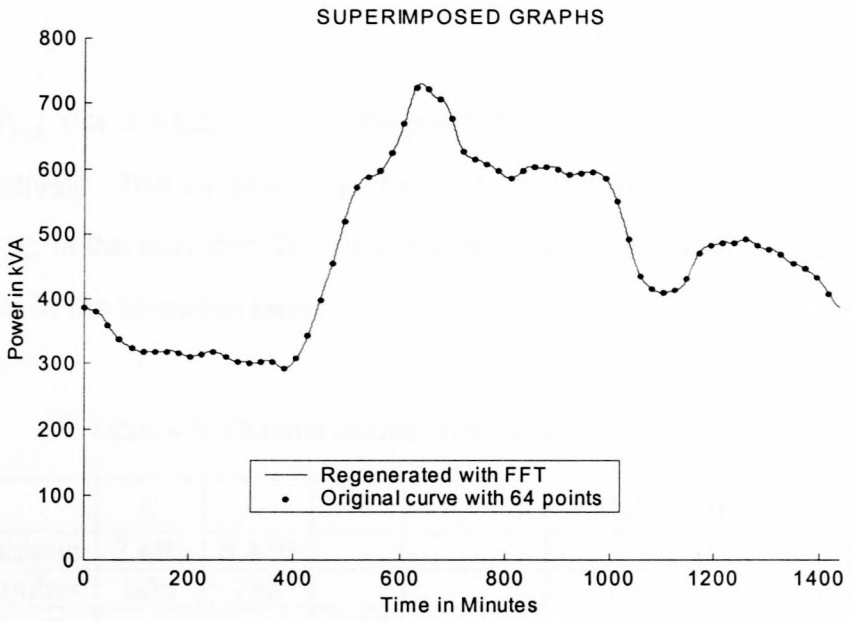

Figure 4.13 Power signals in figures 4.2 and 4.13 are superimposed

This confirms the degree of accuracy associated with the FFT algorithm that was used to extract the frequency components. The next step is to present the analytical results for an optimal solution when the profile in figure 4.12 is considered. The following equations for the value of Δt and P_{VRB} are used:

$$\left\{\sum_{k=1}^{31} P_{ak}\left[\sin\left(k(t_s-\varepsilon)-\alpha_k\right)-\sin\left(kt_m-\alpha_k\right)\right]\right\}+\mathrm{P}_{VRB}=0$$

and

$$\mathrm{P}_{VRB}\times\left(t_m-t_s\right)\leq\frac{250\pi}{12}$$

where

α_k and P_{VRB} (for $k = 1,2,3,.....31$) are given in section 4.4 as row matrices α and A respectively. The value of ε is the same as in the previous calculations. The value for t_m is the only one that has changed, and it is equal to $\frac{639\pi}{720}$. The results are shown in the following table;

Table 4.6 Optimal solution onr the sum of 31 harmonics

	t_s	t_f	Δt	$S(t_s - \varepsilon)$	$S_c(t_m)$	$S(t_f + \varepsilon)$	P_{VRB}
Radians	2.465	3.430					
Minutes	565	786					
Hours			3.68				
kVA				597.02	597.02	597.04	133.67

All the necessary and sufficient conditions that were discussed in chapter 3 are satisfied even when the profile is not a pure sinusoid curve. Before summarizing the key points in this chapter, it is necessary to present the simulated results in the form of an Excel® plot.

4.7 SUMMARY

The main focus in this chapter was on the validation of the model that was developed in chapter 3. The FFT algorithm employed was chosen because of its capability to decompose a signal into a series of sine and cosine functions, of which a sinusoidal function given in equation (3.1) formed the basis for the optimization technique. One of the greatest revelations in this chapter is that the developed optimization strategy can be extended to other energy storage technologies, as long as the power distribution is periodic. However, it is necessary to emphasize that load profiles may have different patterns depending on the customer's needs, meaning that the desired values for Δt and power released by any other energy storage system may also have different values. The question of whether or not there are any economic benefits associated with this strategy will be addressed in chapter 6.

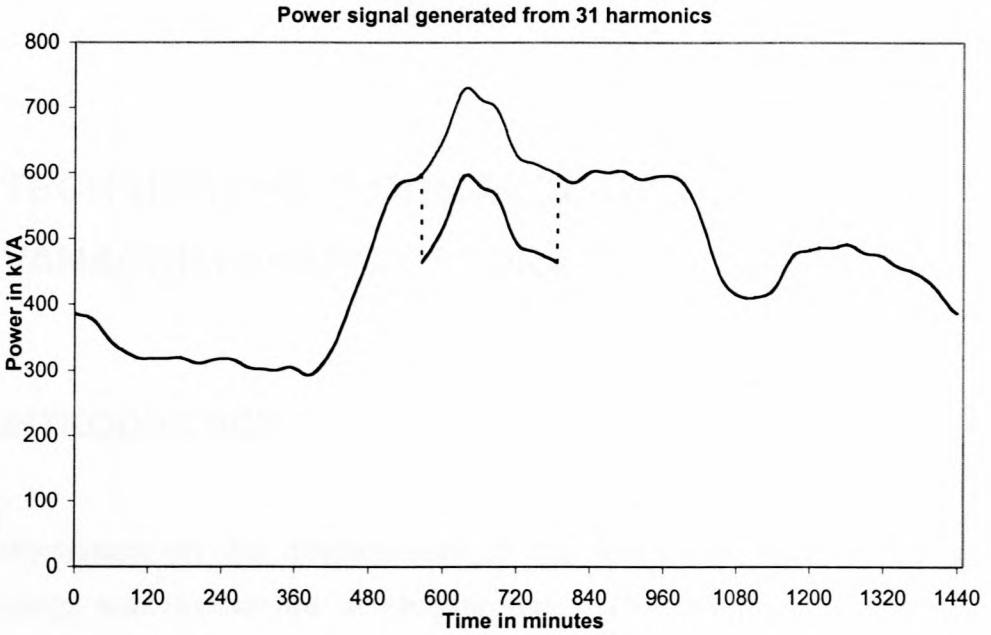

Figure 4.14 Optimization on the power signal generated with FFT

When the economic implications are discussed in chapter 6, it is going to be revealed that the 133.67 kVA savings shown in table 4.6 and figure 4.14 may increase by a significant amount. This increase normally results from a filtering process, which is associated with the maximum demand meter due to the moving average characteristics of the device. The average power demand is calculated over an interval of time that moves along with time. For instance, the meter, which is located in the engineering building averages the electricity distributed over a period of 30 minutes. It might have been noticed in figure 4.2 that the maximum peak was 724 kVA, whereas in figure 4.14 the maximum peak is 730.71 kVA. The reason for this difference is simple; first and foremost, it is known that 724 is the average value recorded by the meter over a period of 22.5 minutes, but 730.71 is a value at a particular point (minute). This is because of the FFT algorithm, which extracted all the information, which was hiding between two discrete points, 22.5 minutes apart. A detailed discussion on moving averages will be presented in chapter 6.

Chapter Five

5 TECHNICAL PERFORMANCE OF THE 250-kVA VANADIUM ENERGY STORAGE TECHNOLOGY

5.1 INTRODUCTION

The discussion on the development of the Vanadium Redox Battery (VRB) technology was exhausted in chapter two. The main focus was on 1 kW prototype VRB and 200 kW VRB that were developed in Australia and Japan respectively. The technical and economic implications surrounding the two VRB technologies were presented. However, the 250-kVA vanadium energy storage technology is the one, which was available for the researchers at the University of Stellenbosch. Moreover, the energy rating of the 250-kVA VRB was used as a constraint in the optimization technique discussed in chapter three and chapter four. Hence, this chapter presents the necessary information and experimental evidence that pertain to the performance of the 250-kVA VRB. In this chapter, the acronym VRB (without the power rating) will be used strictly for the 250-kVA vanadium energy storage system, unless otherwise specified.

5.2 ESTABLISHMENT OF THE VRB PROJECT IN SOUTH AFRICA

Quality and reliability are some of the major concerns for the majority of electricity utilities around the world, and Eskom (South African main utility) is no exception to the problem. In order to address this problem in a more cost-effective manner, Eskom suggested the VRB technology as an alternative for applications such as load leveling, uninterrupted power supply (UPS), etc. The

University of Stellenbosch got selected to investigate the performance of the VRB, hence, the project is named as the Stellenbosch VESS Trial [17]. The installation took place in the beginning of year 2001, and the research got underway in the same year. The whole idea behind the call for a research about the VRB was to investigate its technical performance before embarking on a rigorous research about its economic viability. The system was officially launched in October of 2001, and that is when the public demonstration of the VRB performance was done. The results obtained during the experimental investigations facilitated some of the research activities within the electrical and electronic engineering department at the University of Stellenbosch. One of the research activities is the modeling of a load profile when the utility grid is augmented with the VRB system. This modeling of the load is done solely for the economic benefit of both the utility and the customer. Some of the research work includes the development of the optimization techniques, of which one of these techniques has been already discussed in chapter three and chapter four.

5.3 SPECIFICATIONS AND DESIGN OF THE VRB SYSTEM

First and foremost, VRB technology is a flow battery, meaning that it is a DC power source. However, the system was connected in such a way that it delivers its DC power to a 3-phase AC load. It is for this reason that a bi-directional converter had to be introduced in order to complete the system. The dynamic power quality compensator (DPQC) is the converter that was used during the investigation. This DPQC is capable of converting DC power to AC power and vice versa. The power rating of the DPQC is the one that dictates the power rating of the entire VRB system.

The VRB system had been designed to complement the Eskom's evaluation of other energy storage technologies. Amongst other technologies are the ones that have been discussed in chapter two. It is necessary to mention that 380V

was the voltage level at which the 3-phase AC load (mentioned in the foregoing paragraph) had been connected for experimental purposes. Because of the possibility of unpredictable outages, the DPQC was connected between the load and the static switch[1]. The specifications of the VRB system are summarized in the following table [39]:

Table 5.1 Specifications of the VRB system

Parameter	Specification
Maximum DC current	400A
DC line voltage	700V (nominal)
DC voltage range	650V-850V
Rated power	250 kVA
AC output line	380V (3-phase)
Operational run-time	2 hours

5.4 SUB-SYSTEMS OF THE VRB SYSTEM

Before going further with the discussions, it is essential to present a block diagram, which illustrates the sub-systems of the VRB system. The following figure shows the general outline (configuration) of the system:

[1] Static switch isolates the Eskom's grid line from the load during outages.

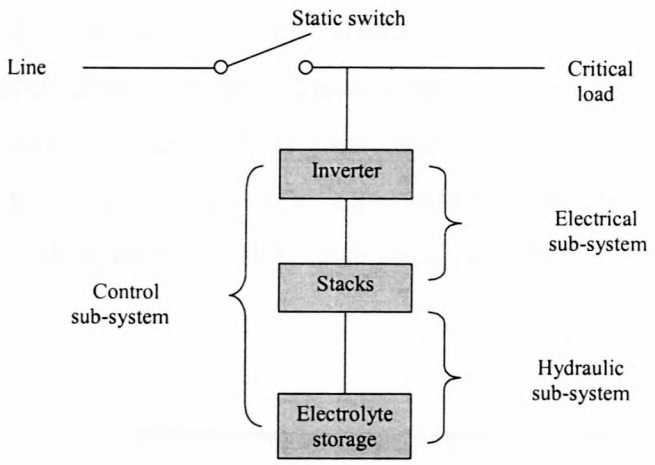

Figure 5.1 General outline of the VRB system

5.4.1 ELECTRICAL SUB-SYSTEM

This sub-system is made up of two major components. One is the DPQC, which dictates the power rating of the whole system, the other component is the group of six stacks, each stack consisting of 100 cells. The power rating of each stack is 42 kW. These stacks are connected in series in order to provide a nominal voltage ranging between 650V-850V as shown in table 5.1 [39].

5.4.2 HYDRAULIC SUB-SYSTEM

It has been already mentioned in chapter two that this department is responsible for the availability of energy. Increasing the volume of the electrolyte, which is stored in four separate tanks, could increase the energy capacity of the system. The components that form the hydraulic sub-system include electrolyte storage tanks, pumps, pipes, heat exchangers and control valve. The specifications of some of the key components of this sub-system will be presented later in this chapter.

5.5 CONFIGURATION OF THE VRB SYSTEM

Figure 5.2 shows the integration of the sub-systems. Amongst other components that complete the system are the six stacks and four electrolyte storage tanks. Moreover it has been seen in table 5.1 that the nominal DC voltage is 700 V. Therefore, this combination makes the system to be divided into two sub-systems, each operating at 350V DC as shown in the following figure:

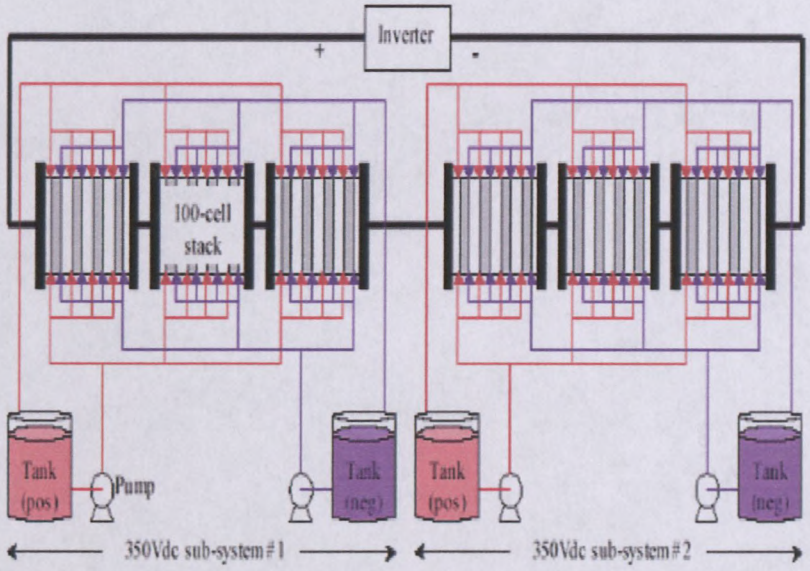

Figure 5.2 Two sub-systems of the VRB system [17]

The two electrolyte tanks in each sub-system are responsible for the oxidation half-reaction and reduction half-reaction respectively. The specifications pertaining to the contents of these storage tanks will be discussed later in the next sections. A photographic view of the tanks and other components of the electrolyte sub-system are presented in the following figure:

Figure 5.3 Hydraulic sub-system of the VRB

Some of the components that were mentioned in section 5.4.2 are clearly shown in figure 5.3. The blue pipes are the ones that transport the electrolyte from the tanks to the stacks.

A view of the stacks taken from an oblique angle is also shown in the figure given below:

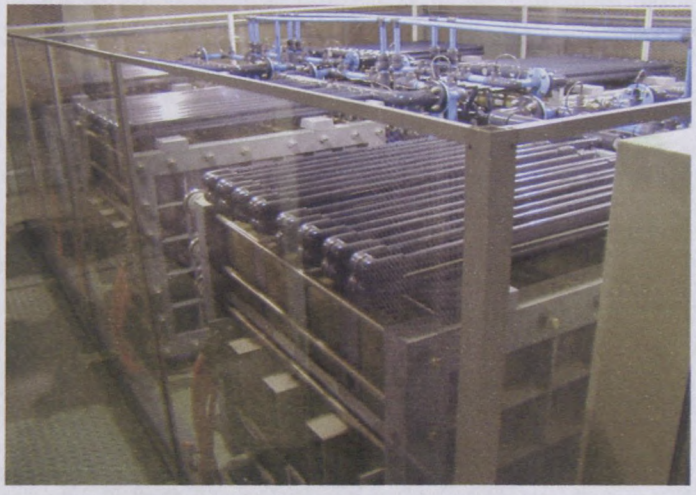

Figure 5.4 Electrical sub-system (stacks) of the VRB

It was stated in chapter two that the generation of the current to the external circuit occurs as a result of the ion exchange. The ion exchange mechanism takes place in the stacks shown in figure 5.4. The specifications of the major

components in figure 5.4 will be tabulated in the next sections. Recapitulating on what was mentioned in section 5.4.1, the DPQC is one of the major components that form the electrical sub-system, moreover, it dictates the power rating of the entire VRB system. Figure 5.5 shows the picture of the DPQC whose power rating is 250 kV

Figure 5.5 Photographic view of the 250 -kVA DPQC

A number of key components have been mentioned in the previous sections. When all of these components are connected together they form a system. Now, it is necessary at this stage to present a topological representation of the system. The topology will show the appropriate position of each of the components.

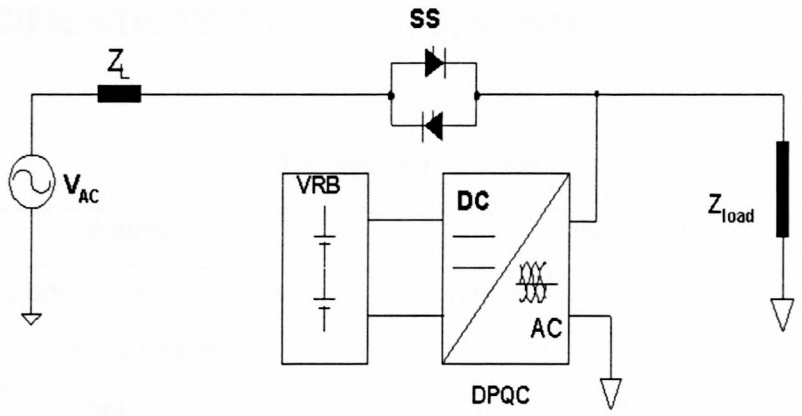

Figure 5.6 Topological representation of the VRB system

The position of the battery in figure 5.6 shows that if it is at full capacity, then it can feed the load on its own even if it is for a short period. In actual fact, it is reported that apart from load leveling and peak shaving, the augmentation of the AC power with a VRB system could be a solution to many problems such as momentary voltage dips [10, 17, 39].

5.6 SPECIFICATIONS OF THE VRB SYSTEM COMPONENTS

Table 5.2 Specification of each component

Element	Specification
Concentration of the electrolyte	1.6 M of V solution in 4.6 M of H_2SO_4
Ionic ratio	1:1 V^{4+} : V^{3+}
Volume of the electrolyte	42 m^3 total
Operating state of charge	20% - 80%
Tanks	4×2.5 m^3
Piping	UPVC
Pumps and motors	4 x centrifugal pump/2.2 kW
Heat exchangers	4 x 6 kW
Valving	Manual and motorized
Control VESS	Automated with manual
Stack power rating	42 kW
Number of stacks	6
Stack dimensions	1.2L x 0.9W x 1.1H (in meters)
Stack weight	1.400 kg

The components of the system shown in table 5.2 were obtained from different countries around the world. For instance, the vanadium electrolyte was provided by Highveld Corporation (South Africa). DPQC is an Eskom's own product (South Africa), whereas the stacks were purchased from Japan. The software involved in the system was provided by one of the Australian companies. One of the South African engineering companies was approached for the civil installation of the system.

5.7 DEMONSTRATION RESULTS OF THE VRB SYSTEM

As a new technology, the performance of the system had to be investigated in order to make good comparisons with other competing energy storage devices. The VRB technology is an electrochemical storage device, and therefore, amongst other issues the researchers were particularly interested in the coulombic and voltaic efficiencies.

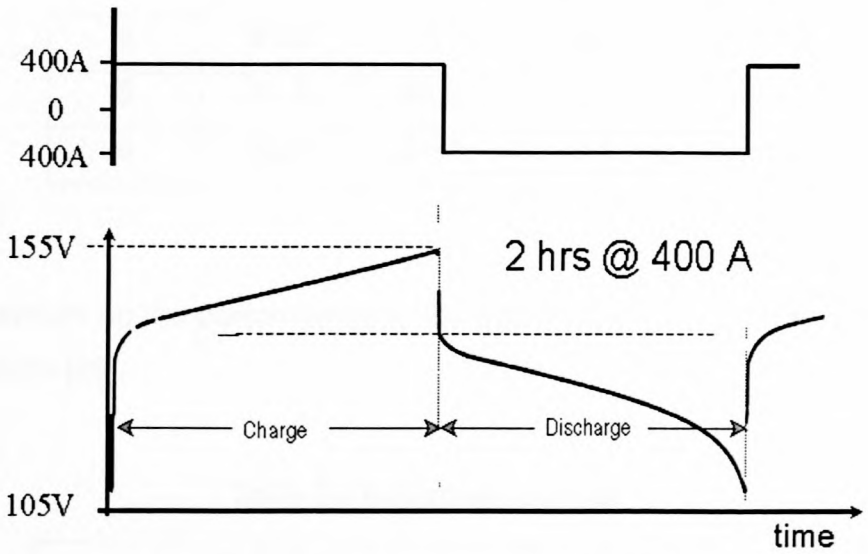

Figure 5.7 Charge - discharge profile for one stack [39]

Under normal circumstances, an ordinary secondary battery will always charge for longer periods than when it discharges. However, in the case of the VRB the discharge time depends on the amount of charge electrolyte supplied to the stacks. Figure 5.7 shows that this particular VRB was designed in such a way that it runs for 2 hours at full capacity. Moreover, it is observed from figure 5.7 that the charge period is the same as the discharge period (something contrary to what has been just said about secondary batteries). It is also argued that even if the run-time design was for 20 minutes for instance, then the curve behavior shown in figure 5.7 would still be the same [39]. The results in figure 5.7 were

obtained when the maximum DC operational current was kept at 400 A. The process of discharging at 400 A was repeated on three consecutive cycles and the following efficiencies corresponding to each stack were recorded [17]:

Table 5.3 Stack performance – efficiency values (%)

Stack	Cycle 1	Cycle 2	Cycle 3	Average
1	82.1	81.7	81.6	81.8
2	83.2	83.3	83.5	83.3
3	83.9	84.3	84.4	84.2
4	84.5	84.7	84.9	84.7
5	84.5	84.5	84.7	84.6
6	84.5	84.4	84.4	84.4

The key aspects on the performance of the 250-kVA VRB are summarized in the following table [39]:

Table 5.4 Performance results

Parameter	Performance
Battery	
Stack efficiency	82% - 85%
Battery DC efficiency	81% - 82%
Energy density	Ca 20 Wh/l
System	
Conversion efficiency	Ca 95%
Round trip	Ca 78
Pumping loss at max. power	10.2 kW (ca 5%)

Later in this thesis, the information given in table 5.4 will be compared against other energy storage devices.

The response of the VRB to the interruptions ranging from medium to longer time scale standby as well as shorter-time scale ride-through was investigated. The following figure shows the response of the VRB when subjected to a series of discharge and discharge demands:

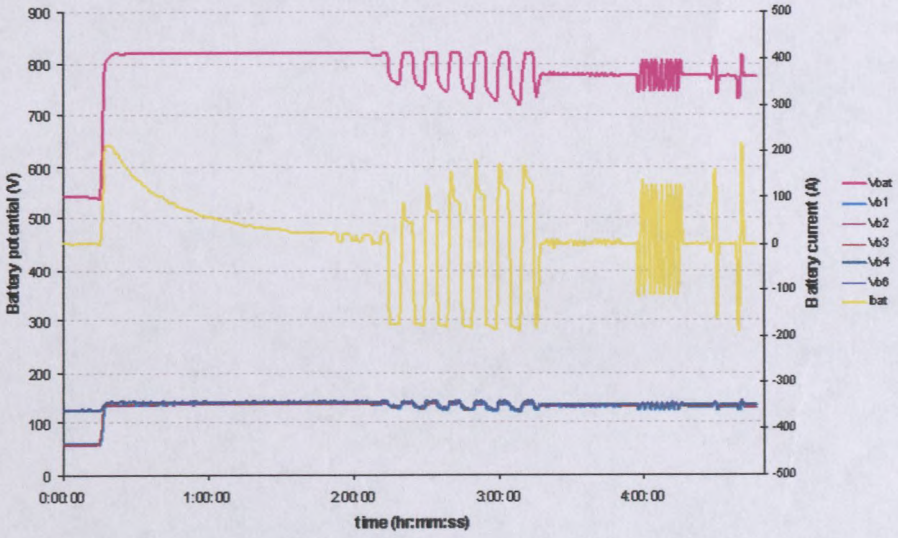

Figure 5.8 Medium-to-long time response

Figure 5.8 shows that the VRB is completely charged after a period of two hours. This is indicated by zero (yellow profile) DC current at $\Delta t = 2$ hours. It should be remembered that most of the energy storage devices, particularly batteries, do not exhibit this characteristic. In fact it was already mentioned in the previous paragraphs that long to recharge. The blue curve at the bottom shows the response in terms of DC potential of each of the six stacks when the discharge and charge demands last for a period of about 5 to 10 minutes. On top is the combination of all the stacks, and this is indicated by a red profile. This profile also shows that the stacks track each other quite harmoniously. It is also observed that the same pattern is found even if the discharge and charge demands last for seconds.

5.8 SUMMARY

This chapter focused on the technical credibility of the VRB. The specifications of the major components that complete the system were discussed. The performance results presented in this chapter give a preliminary proof that VRB is indeed one of the promising energy storage technologies.

The manner in which the system had responded to the discharge and charge demands of different time intervals increased the chances of being considered as a potential candidate for many applications. Nevertheless, the focal point in this thesis is on the peak shaving and load-leveling applications.

Chapter Six

6 INVESTIGATION INTO THE ECONOMIC BENEFITS OF 250 kVA VANADIUM STORAGE SYSTEM

6.1 INTRODUCTION

This chapter presents a discussion on the economic modeling of the 250-kVA vanadium energy storage system. The optimization strategy developed in chapters three and four will be used as the basis for the investigation about possible economic savings that the VRB may offer.

6.2 OVERVIEW OF TERMINOLOGY USED IN DEMAND SIDE MANAGEMENT

6.2.1 DEMAND

In this chapter demand is interpreted as the average of the electricity (electrical load) drawn by a particular customer (electricity consumer) over a specified time interval. Throughout the discussions, a 30-minute interval will be used as the period over which the electrical power is averaged, unless otherwise specified. Whenever the unity power factor is considered, kW and kVA will be used interchangeably as the unit measurements of the loads.

6.2.2 MAXIMUM DEMAND

The electricity supply through the meter is and continuous. The distribution can be monitored over seconds, minutes, days, weeks or months. As mentioned in section 6.2.1, the demand is associated with a 30-minute interval. In a month (with 30 days) there are 1440 30-minute intervals, therefore, the maximum demand is the highest (in terms of magnitude) of all these 30-minute demands. In other words, there must be one and only one maximum demand in a month under consideration.

6.2.3 ENERGY CONSUMPTION

As the electricity passes through the meter, the apparent (kVA), real power (kW) and reactive power (kVAr) values are being recorded. The product of power (kW) and time (e.g. one hour) is the energy consumption measured in kWh. However, the energy consumption in this section will be considered over a month.

6.2.4 BILLING PERIOD

Utilities and other electricity suppliers such as local municipalities normally have specified daily time intervals that are used to charge their customers for the electricity they consume. These intervals are usually chosen on the basis that there is a likelihood of peak occurrence. This particular type of an interval is called the billing period. In this chapter, a month will be considered as a billing period. However, the sub-interval [6:00 a.m.; 10:00 p.m.] will be used as a daily billing period for a time-of-use tariff.

6.3 TOTAL COST FOR POWER

6.3.1 MATHEMATICAL REPRESENTATION OF THE TOTAL COST FOR POWER

Utilities such as Eskom have standard electricity tariff structures that they use to charge their customers. At the customer point of connection there is a meter that continuously records (assuming no outages) the electricity supply. This measurement is normally observed on hourly, daily, weekly or monthly basis depending on the agreement terms between the utility and the customer. In actual fact, billing structures adopted by utilities and other private suppliers around the world are not the same and there are a number of reasons that could be attributed to such variations.

The load data used for the research were obtained from one of the metering points located in the engineering building (University of Stellenbosch). The Stellenbosch Local Municipality supplies the electricity distributed through this meter. Hence, the investigation in this thesis will be based on municipality tariffs. According to the billing structures of the municipality mentioned in the foregoing paragraph, the total cost for power depends on the maximum demand cost and the energy cost. The mathematical equation for the calculation of the total cost for power can be expressed as follows:

$$\text{Total cost for Power} = \text{Maximum demand cost} + \text{Energy Cost} \qquad \ldots(6.1)$$

The following municipality tariffs will be considered throughout the discussion:

Table 6.1 Stellenbosch Municipality tariffs

Unit quantity	Cost per unit
kVA (max.)	R54.39
kWhr	12.59 c

It was mentioned in section 6.2.3 that energy consumed by a customer is determined by calculating the total area covered by the power vs. time curve and the total duration of the supply. The energy cost can be mathematically expressed as follows:

$$E_c = \left[\sum_{k=1}^{n} \left(\mathrm{P}_k \times \Delta t \right) \right] \times \text{tariff} \qquad \ldots (6.2)$$

Where

E_c = Energy cost

P = Average real power (measured in kW) over kth time interval

Δt = Time interval (constant for all) in which the meter averages a load

n = Number of time intervals.

The maximum demand cost is expressed as follows:

$$\text{Maximum Demand Cost} = \mathrm{S}_{\max} \times \text{tariff} \qquad \ldots (6.3)$$

Where $\mathrm{S}_{\max}$ is the greatest of all apparent power values occurring within the billing period. The equations (6.2) and (6.3), equation (6.1) can be written as

$$\text{Total Cost for Power} = \left[\sum_{k=1}^{n} P_k \times \Delta t\right] \times \text{energy tariff} + S_{max} \times \text{power tariff} \quad \ldots (6.4)$$

The manner in which the electricity supply through a meter is averaged over Δt depends on how the meter is set. For instance, the meter located in the engineering building (University of Stellenbosch) is set to average the load over a period (Δt) of 30 minutes. The calculations in section 6.3.3 will be based on the 30-minute intervals, unless otherwise specified.

6.3.2 MOVING AVERAGES

The load profile shown in figure 4.1 will be used in this chapter to illustrate how the total cost for power is calculated. However, it is necessary to explain first the reason why this load profile is chosen. In figure 4.1 the maximum peak of 723.50 kVA occurred at 10:30 a.m. However, the penetration of the electricity through the meter is continuous, meaning that at each minute (seconds are ignored) there is a corresponding kVA value. If the electricity distribution were monitored on a one-minute demand basis, then there would be 30 distinct needles of different magnitudes occurring between 10:00 a.m. and 10:30 a.m. However, these needles are being filtered out (averaged) as the electricity passes through the meter. Assuming a thermal demand meter, it will display only the average of these 30 needles, hence, 723.50 kVA mentioned in the foregoing paragraph is also called the 30-minute moving average.

The load profile shown in figure 4.2 was obtained through an interpolation process. The primary reason for doing the interpolation was to increase the number of data points from 48 to 64 (FFT requirement). The interpolation in this context can be viewed as a process of extracting at least 16 of the needles that have been smoothened (filtered out) by the meter. The fact that the maximum peak in figure 4.2 is 724.00 kVA signifies that at a particular point (minute) within

the 30-minute interval, there existed (before filtering) a demand needle whose magnitude is 0.5 greater than the average. Furthermore, the maximum peak of the profile shown in figure 4.13 is 730.71 kVA. This is due to the fact that the FFT algorithm extracted all the 1440-minute peaks, of which the greatest 10:00 a.m. and 10:30 a.m. is 730.71 kVA, thus 7.21 kVA greater than the average.

The above discussion justifies the reason why the profile in figure 4.1 is chosen for the calculation of the total cost for power. The reason is that a meter records moving averages (over a specified minute interval), but not the instantaneous minute values.

6.3.3 CALCULATION OF THE TOTAL COST FOR POWER

The local municipality considers total energy consumed in a month as well as the maximum demand occurring in that particular month. The daily load profile shown in figure 4.1 was extracted from the October load data (2000). The number of 30-minute intervals is 1488 (i.e. 48 daily half-hour intervals times 31 days). In calculations for the total energy, only the first 2 and the last 2 real power values will be shown for illustration purposes. From equation (6.2) the total energy consumed in October can be calculated as follows:

$$\text{Total Energy} = \sum_{k=1}^{1488} \left(P_k \times \tfrac{h}{2}\right) \qquad \ldots (6.5)$$

where $\frac{h}{2}$ = 30 minutes. Expanding equation (6.5) yields

$$\text{Total Energy} = \left(P_1 \times \tfrac{h}{2}\right) + \left(P_2 \times \tfrac{h}{2}\right) + \ldots\ldots\ldots + \left(P_{1487} \times \tfrac{h}{2}\right) + \left(P_{1488} \times \tfrac{h}{2}\right) \qquad \ldots (6.6)$$

Substituting data values into equation (6.6) yields

$$\text{Toata Energy} = \tfrac{h}{2}(343.3 + 341 + ...+369.3 + 355.6)$$

$$= \tfrac{h}{2}(592977.11\ \text{kW})$$

$$= 296488.56\ \text{kWh} \qquad \ldots(6.7)$$

Therefore, the total energy consumed in October 2000 is 296488.65 kWh. From equation (6.2) and table 6.1 the energy cost (E_c) for October is

$$E_c = 296488.65 \times \text{R } 0.1259 \qquad \ldots (6.8)$$

Therefore, the energy cost is equal to R 37,327.92. The maximum demand of the month as shown in figure 4.1 is 723.50 kVA. Multiplying this maximum demand by the tariff (table 6.1) yields the maximum demand cost of R39, 351.17 for that month. Therefore, substituting the energy cost and the maximum demand cost into equation (6.1) yields the total cost for power of R 76,678.71. This is the amount that the university paid for the power consumption recorded at only one metering point. With a viable energy storage device this amount could have been reduced substantially. The next section will investigate the impact that the vanadium redox battery may have on the economic aspects.

6.4 ECONOMIC SAVINGS FROM THE VRB

In section 6.3.3 the total cost for power was calculated by considering figure 4.1 for both the maximum demand and the total energy. However, the optimization (peak-shaving) was done on the load regenerated with FFT as shown in figure 4.13. The reason why the maximum peaks of the profiles shown in figures 4.1 and 4.13 are not the same was explained in section 6.3.2. In order to avoid any possible biased results in the analysis, figure 4.13 will be used in this section.

6.4.1 CALCULATION OF THE TOTAL COST FOR POWER FROM THE PROFILE RECONSTRUCTED WITH FFT

The maximum demand of the profile shown in figure 4.13 is 730.712 kVA. Using the procedure described in section 6.3.3 and table 6.1, the maximum demand cost is R 39,743.43. The next step is to investigate the energy cost. It was mentioned in the above sections that the total energy consumed in a month is equal to the sum of all the rectangles that are enclosed by time intervals (Δt) of equal lengths and their corresponding kW values. In figure 4.13 (1 day-profile) there are 1440 minute-intervals, meaning that there are 44640 minute-intervals in 31 days. At this stage the known peak values corresponding to each minute-interval are for only one day (figure 4.13). This information is definitely not enough for the calculation of the total energy. In order to deal with this problem effectively an assumption is required. However, it is necessary first to form the basis of the assumption by considering one daily load profile, which consist of 1440 points. For convenience, the profile shown in figure 4.13 and the mean of all the 1440 peaks are drawn on the same system of axis.

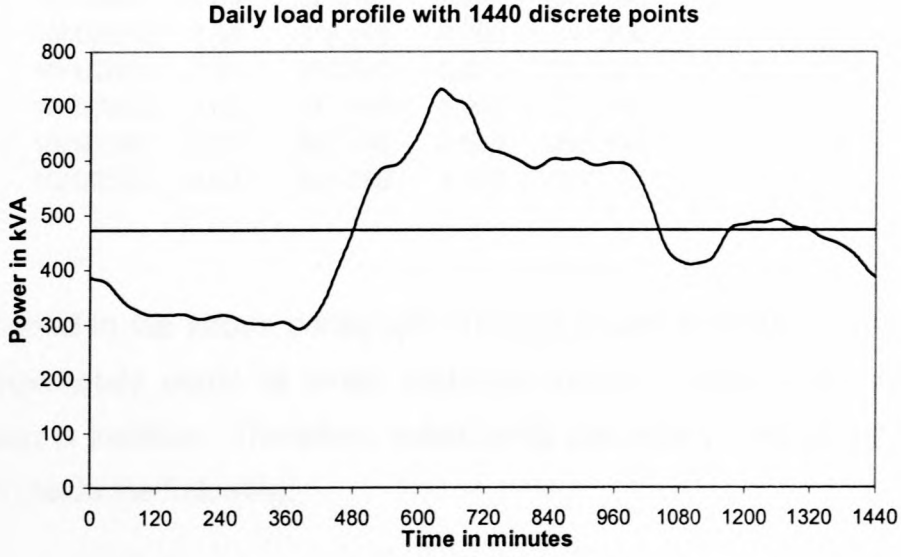

Figure 6.1 Daily load profile consisting of 1440 kVA values

The area enclosed by the curve and the 1440-minute interval as shown in figure 6.1 can be calculated as follows:

$$\text{Area} = (P_1 \times 1\,\text{min}) + (P_2 \times 1\,\text{min}) + \ldots\ldots\ldots + (P_{1439} \times 1\,\text{min}) + (P_{1440} \times 1\,\text{min}) \quad \ldots (6.9)$$

It is observed that the discrete points in figure 6.1 are measured in kVA whereas all the Ps in equation (6.9) are measured in kW. This means that a unity power factor has been suggested as the first assumption. In actual fact, the load data used for the analysis consist of kVA and kW values that are almost the same at each time interval. An extract from the original load data is provided below. The extract serves as a justification for the assumption.

Table 6.2 Load data extracted from October 2000

DATE	TIME	kW	kVAr	kVA	POWER FACTOR
10/1/2000	0:00	343.300	0.200	343.300	1.00
10/1/2000	0:30	341.000	2.800	341.011	1.00
10/1/2000	1:00	334.100	2.000	334.106	1.00
10/1/2000	1:30	323.100	5.200	323.142	1.00
10/1/2000	2:00	314.600	0.200	314.600	1.00
10/1/2000	2:30	302.500	0.800	302.501	1.00
10/1/2000	3:00	311.600	3.000	311.614	1.00
10/1/2000	3:30	296.100	4.500	296.134	1.00
10/1/2000	4:00	297.200	1.300	297.203	1.00

As mentioned in the above paragraph, the real power and the apparent power are approximately equal at every half-hour interval, hence, the unity factor assumption is justified. Therefore, substituting the peak values of the profile in figure 6.1 yields the following:

$$\text{Area} = (385.72 \times 1\,\text{min}) + (385.81 \times 1\,\text{min}) + \ldots.. + (386.80 \times 1\,\text{min}) + (386.28) \quad \ldots (6.10)$$

Therefore, the area enclosed by the curve in figure 6.1 is 681010.358 kWmin. In terms of kWh the area can be written as 11350.173 kWh.

It is necessary to determine the area directly from the original profile (figure 4.1), and then compare the two values. Since the domain consists of half-hour interval, the area can be determined as follows:

$$\text{Area} = \left(385.60 \times \tfrac{h}{2}\right) + \left(378.50 \times \tfrac{h}{2}\right) + ... + \left(445.11 \times \tfrac{h}{2}\right) + \left(419.90 \times \tfrac{h}{2}\right) \qquad \ldots (6.11)$$

The values (in kW) in the above equation are the first two and the last two of the 48 data points obtained from the original load profile. Simplifying on the right in equation (6.11) yields an area of 11337.655 kWh. This value is 12.518 kWh (i.e. 0.11% of 11350.173 kWh) less than the one obtained from equation (6.10). Recapitulating on the key points from the previous discussion is necessary before further assumptions are unfolded. It is known that the FFT algorithm generated the profile (figure 6.1) from the discrete points of the profile shown in figure 4.1. The 12.518 kWh difference came as a result of the moving average concept. Therefore, it can be assumed that the 0.11% (of the FFT profile) difference may be observed even in other remaining 30 daily load profiles, provided that the FFT algorithm is employed to all of them. Furthermore this assumption is also based upon the fact that the 30-minute moving average applies continually throughout the month. A general mathematical representation of the relationship between a monthly total energy (calculated from half-hour intervals) and its corresponding energy (calculated from the FFT profile) is required. The derivation of the expression is presented in the following paragraph.

Let E_D represents the energy of the day calculated from half-hour intervals. Again, let E_R represents the energy of the day whose profile is a reconstruction

with FFT algorithm. Therefore, the results obtained from equations (6.10) and (6.11) yield

$$E_R - 0.11\% \text{ of } E_R = E_D \quad \ldots (6.12)$$

Rearranging,

$$E_R - \frac{0.11 \times E_R}{100} = E_D \quad \ldots (6.13)$$

Rearranging further,

$$100E_R - 0.11E_R = E_D \times 100 \quad \ldots (6.14)$$

Solving for E_R,

$$E_R = \frac{100E_D}{100 - 0.11} \quad \ldots (6.15)$$

Simplifying,

$$E_R = \frac{100E_D}{99,89} \quad \ldots (6.16)$$

Equation (6.16) can be verified easily by substituting E_D = 11337.655 kWh. The calculated value of E_R is11350.173 kWh, which is exactly the same as the one, obtained from equation (6.10). The derivation of equation (6.16) leads to a general mathematical representation of the total monthly energy expressed in terms of FFT reconstructed profile.

$$\text{Total Energy for a month} = \sum_{k=1}^{N} E_{Rk} \quad \ldots (6.17)$$

Where N is the number of days in a month and k = 1, 2, 3,..... $N-1$, N.

Substituting equation (6.16) into equation (6.17) yields

$$\text{Total Energy for a month} = \frac{100}{99.89}\sum_{k=1}^{N} E_{Dk} \qquad \ldots (6.18)$$

Where

$$E_D = \frac{h}{2}\sum_{r=1}^{M} \mathrm{P}_r \qquad \ldots (6.19)$$

P is the power in kW, M is the number of half-hour intervals and r = 1, 2, 3,.....,48.

Substituting equation (6.19) into equation (6.18) yields

$$\text{Total Energy for a Month} = \frac{100\times h}{2\times 99.89}\sum_{k=1}^{N}\sum_{r=1}^{M} \mathrm{P}_{rk} \qquad \ldots (6.20)$$

Substituting P values (from October month) into equation (6.20) yields the total energy of 296815.05 kWh. This value is 326.49 kWh greater than the energy obtained from equation (6.7). The reason for this difference is that all the real power values at each minute of the month have been considered in equation (6.20), whereas in equation (6.7) only the 30-minute moving averages were considered. The foregoing discussion allows the recharging process of the VRB system to be modeled directly on the FFT generated profile (figure 6.1).

6.4.2 RECHARGING OF THE 250 kVA VANADIUM STORAGE SYSTEM

During the demand period there are some uncertainties about when the maximum peak is due to occur, its magnitude, duration and things of that kind. However, these variations do not normally concern the customers during the off-peak hours simply because the power supply is far below the average, as shown in figure 6.1. In this discussion the interval [10 p.m.; 6 a.m.] Will be used as an

off-peak period. This means that the VRB can be recharged at any time within this time interval. However, it is assumed that the VRB is charged for 8 hours starting from 10:00 p.m. to 6:00 a.m. It was mentioned in chapter two that one of the advantages of the VRB is that it does not deteriorate because of the deep discharge-charge cycles. Nevertheless, the duration of the cycles will be restricted by the energy capacity of the VRB.

In chapter four the peak-shaving using the 250 kVA VRB system was modeled on a single daily load profile. It was discovered that 133.67 kW delivered by the VRB over a period of 3.68 hours is an optimal solution. For simplicity and consistency, these values will be used throughout the investigation. On the other hand, the profile shown in figure 6.1 will be used as a representative of all the 31 daily load profiles.

It is assumed that the VRB is always at full capacity before it discharges. As a reminder, the energy rating of the VRB used for the research is 520 kWh. This means that if the VRB discharges 133.67 kVA for 3.68 hours ($\approx$ 492 kWh), then an amount of 28 kWh remains unused. In chapters 3 and 4, the discharge time interval was denoted by $\Delta t = t_f - t_s$. The remaining 28 kWh can be discharged at any rate just to shave any other possible peaks that are greater than the one corresponding to t_f. In this particular investigation the discharge rate of 3.6 kW per hour (delivering-- 10 kW for 2.75 hrs) is arbitrarily chosen.

Whenever the VRB undergoes the discharge-charge processes, there are losses ($I^2 R$) associated with the resistive components. In order to minimize these losses, the battery has to be charged at a low rate. In this discussion, the VRB recharges by drawing a constant power of 65 kW over a period of 8 hours. The Excel® plot that shows the discharge-charge processes is given in the following figure:

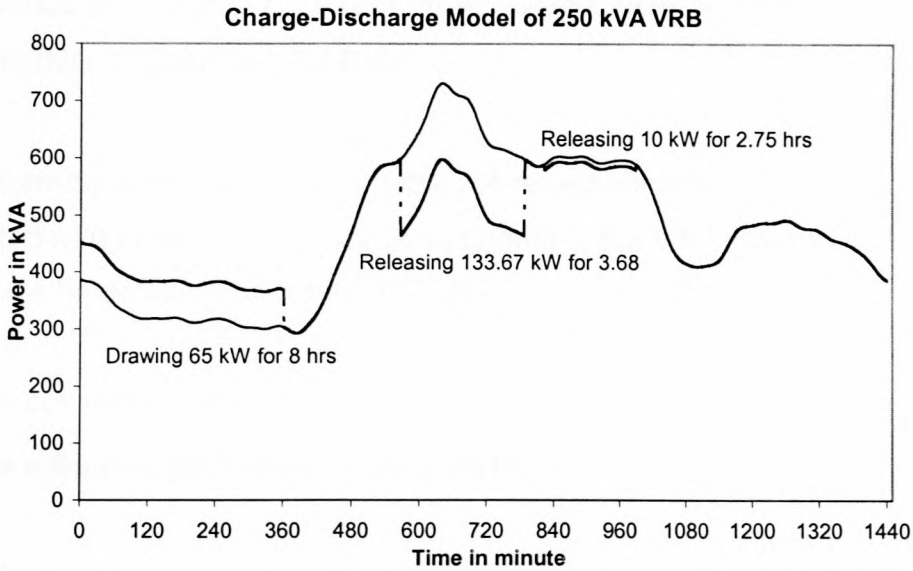

Figure 6.2 Discharge-charge Model on a Daily load Profile

There are uncertainties about the day in which the greatest maximum demand of the month is due to occurs. Therefore, it is necessary that the discharge-charge technique shown in figure 6.2 is employed everyday except for the weekends. The discharge-charge processes of the VRB may affect the total cost for power in many ways. The efficiency (ratio of output to input) of the VRB needs to be considered in the calculations. There are costs associated with the power used for charging the VRB if the customer uses a straight tariff. However, electrical power is normally bought at a lower price if the customer is on the time-of-use (TOU) tariff. Therefore, it is necessary to consider both scenarios (i.e. straight and TOU tariffs) when calculating the total cost for power.

6.4.3 CALCULATION OF THE TOTAL COST FOR POWER WHEN USING STRAIGHT TARIFF

The performance results shown in table 5.4 reflect efficiencies that are associated with some of the major components of the VRB system. Let these efficiencies be defined as follows [17, 39]:

η_c = conversion efficiency = 90%

η_B = efficiency (DC) of the battery = 81%

From equation (6.20) the total energy for the month before the VRB is connected is 296815.05 kWh. Assuming that the VRB is charged for 22 days (month minus weekends) at a constant rate as shown in figure 6.2, the new total energy (ignoring the impact of pea-shaving on the results) is as follows:

$$\text{Total Monthly Energy} = 296815.05\ \text{kWh} + 22 \times \left(\frac{65\ \text{kW} \times 8\ \text{hrs}}{\eta_c \times \eta_B} \right) \quad \ldots (6.21)$$

Substituting the values for η_c and η_B into equation (6.21) yields the following:

$$\text{Total Monthly Energy} = 296815.05\ \text{kWh} + 22 \times \left(\frac{65\ \text{kW} \times 8\ \text{hrs}}{0.90 \times 0.81} \right) \quad \ldots (6.22)$$

Simplifying,

$$\text{Total Monthly Energy} = 296815.05\ \text{kWh} + 15692.73\ \text{kWh} \quad \ldots (6.23)$$

Therefore,

$$\text{Total Monthly Energy} = 312\ 507\ 78\ \text{kWh} \quad \ldots (6.24)$$

Energy savings resulting from peak-shaving (figure 6.2) can be calculated as follows:

$$\text{Energy savings} = 22 \times (133,67\ \text{kWh} \times 3.68\ \text{hrs} \times (0.90 \times 0.81)) + 22 \times (10\ \text{kW} \times\ 2.75\ \text{hrs} \times (0.90 \times 0.81)) \quad \ldots (6.25)$$

Simplifying,

$$\text{Energy savings} = 8330.23\ \text{kWh} \quad \ldots (6.26)$$

Therefore, subtracting equation (6.25) from equation (6.23) yields the total monthly energy consumption of

$$\text{Total Monthly Energy Consumption} = 304\ 177\ 55\ \text{kWh} \quad \ldots (6.27)$$

The monthly energy cost is

$$\text{Monthly Energy Cost} = \text{Energy consumption} \times \text{Tariff} \quad \ldots (6.28)$$

Substituting the tariff from table 6.1 and equation (6.26) into equation (6.27) yields

$$\text{Monthly Energy Cost} = 304\ 177\ 55\ \text{kWh} \times \text{R}\ 0.1259 \quad \ldots (6.29)$$

Therefore,

$$\text{Monthly Energy Cost} = \text{R}\ 38,295.95 \quad \ldots (6.30)$$

Assuming that the maximum peak in figure 6.2 is the greatest maximum demand of the month, therefore, the maximum demand cost is

$$\text{Maximum Demand cost} = \text{Maximum Demand} \times \text{Tariff} \quad \ldots (6.31)$$

Substituting the maximum demand left after peak-shaving (figure 6.2) and the tariff given in table 6.1 into equation (6.29) yields

$$\text{Maximum Demand cost} = (730.712 - 133.67\ \text{kW}) \times \text{R}54.39 \quad \ldots (6.32)$$

Therefore,

$$\text{Maximum Demand cost} = \text{R } 32{,}473.11 \quad \ldots (6.33)$$

At this stage it is necessary to emphasize that all the calculations in the foregoing were based on the profile given in figure 6.2. The important point is that this profile is an FFT generated power signal, and for that reason the 30-minute moving average characteristics were not taken into consideration in the above calculations. It is known from the derivation of equation (6.20) that the monthly energy given in equation (6.26) is 326.49 kWh greater than when the moving averages are considered. Therefore, the actual energy consumption recorded by the demand meter is 303 851 06 kWh. Hence, the energy cost is R 38,254.85. Furthermore, the maximum demand before the VRB when moving averages are considered is 723.50 kW (figure 4.1). Therefore, the actual maximum demand cost is R 32,080.85. The total cost for power is as follows:

$$\text{Total Cost for Power} = \text{R } 70{,}335.70 \quad \ldots (6.34)$$

The total costs for power calculated when using and without using the VRB are summarized in the following table:

Table 6.3 Electricity bill for one metering point

Monthly Cost	Without VRB	With VRB
Energy cost	R 37,327.92	R 38,295.95
Max. demand cost	R 39,351.17	R 32,473.11
Total cost for power	R 76,678.71	R 70,335.70

Table 6.3 shows that the VRB offers monthly savings of about R 6,343.01 (or 8.27%) when used for peak-shaving and load-leveling applications.

6.4.4 CALCULATION OF THE TOTAL COST FOR POWER WHEN USING TIME-OF-USE TARIFF

Time-of-Use (TOU) tariffs are most suitable for large customers who are able to manage their energy consumption and maximum demand according to the utility's specified time schedule [36]. The cost of energy is dependent on the time of consumption. Time periods are defined as off-peak, standard and peak-time periods. The tariff is designed in such a way that it encourages customers to shift their load out of peak hours and to operate at maximum capacity during off-peak hours, taking advantage of the low energy price.

In the light of the above it is evident that a VRB owner who qualifies for the TOU tariff could score more simply because the power drawn from the grid during off-peak hours to charge the VRB is paid for at a lower cost. The researchers do acknowledge the fact that electricity charges change on a regular basis. However, for illustration purposes the TOU tariffs published on Eskom website (www.eskom.co.za/tariffs) at the time this thesis was written (i.e. November 2002) will be used. The energy charge for TOU is 9,04c/kWh. The new energy cost is derived as follows:

From equation (6.23) the energy cost incurred because of the VRB charge cycles is

$$\text{Energy cost for charging VRB} = 15692.73 \text{ kWh} \times \text{R } 0.0904 \quad \ldots (6.35)$$

Therefore,

$$\text{Energy cost for charging VRB} = \text{R } 1{,}418.23 \quad \ldots (6.36)$$

Subtracting equation (6.26) from the first energy component in equation (6.23), and multiply the result by the straight tariff (R 0.1259) yields R 36,320.24. Adding this value to equation (6.36) yields

$$\text{Total Monthly Energy Cost} = \text{R } 37{,}738.47 \quad \ldots (6.37)$$

From equations (6.30) and (6.37) the monthly energy saving is 1.46% if the VRB owner is in TOU tariff structure.

The above discussion indicates that the VRB is capable of offering some economic benefits in peak-shaving and load-leveling applications. The benefits could be more than the ones shown in this chapter. This argument is based upon the fact that all the calculations were based on certain assumptions. These assumptions are briefly summarized as follows:

- The modeling of discharge-charge cycles is based on one daily load profile. This is the profile that has the maximum demand of the month.
- Chances that certain profiles could have lower peaks are not taken into consideration. The duration and time of occurrence of these peaks is also not considered.
- The influence of weather conditions on the pattern of each daily load profile in a month is not considered.

o Public holidays that are normally treated as weekends by utilities are also not considered.

Under normal circumstances, the above factors may have significant changes (in favour or against the customer) on the results obtained in this discussion. A monthly load profile that shows variations amongst the daily load profiles is presented below:

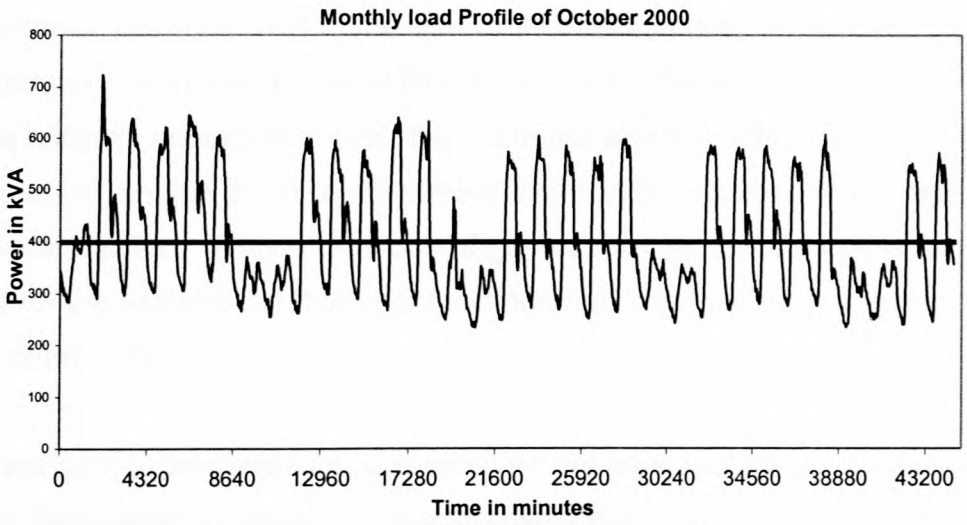

Figure 6.3 Monthly Power supply for October 2000

It is clearly shown in figure 6.3 that the daily maximum peaks are not the same. The exclusion of the weekends in the analysis is also justified, as it is observed that they peak far below average. The differences in terms of peak occurrence and duration might not be easily observed in figure 6.3; however, the data analysis proves the existence of such differences. Certain profiles that exhibit these differences are given in appendix A.

Although all the differences and variations existing amongst certain parameters in the load profiles are fully acknowledged, the results obtained in this section form the basis of the discussions presented in the next sections.

6.5 BREAK-EVEN POINT ANALYSIS

The discussions based on the technical credibility of the vanadium storage devices, starting from the prototypes in Australia and Japan up to the installation at the University of Stellenbosch were presented in chapters two and five. The economic implications based on the optimization strategy, which was developed in chapters three and four were presented in the previous sections of this chapter. Table 6.3 shows savings that the customer may benefit from the utilization of 250 kVA VRB. The aim of this section is to investigate the capital cost (expressed in Rands per kWh) of the VRB. The knowledge of this capital cost is critically important to both the customer and the VRB dealer in the sense that it would enable them to determine if the VRB is economically feasible for commercialization. Without the loss of generality, calculations in this section are based on the assumption that cost functions and other relevant parameters have linear characteristics.

The approach to this problem is to consider the total cost for power as a function of time (expressed in years). There are two major cost functions that have been identified. One is the total cost for power when there is no VRB connected, and the other is the total cost for power when the VRB is connected. Seven years is used as the time in which the VRB is evaluated. The graphical representation of the cost functions is given in the following figure:

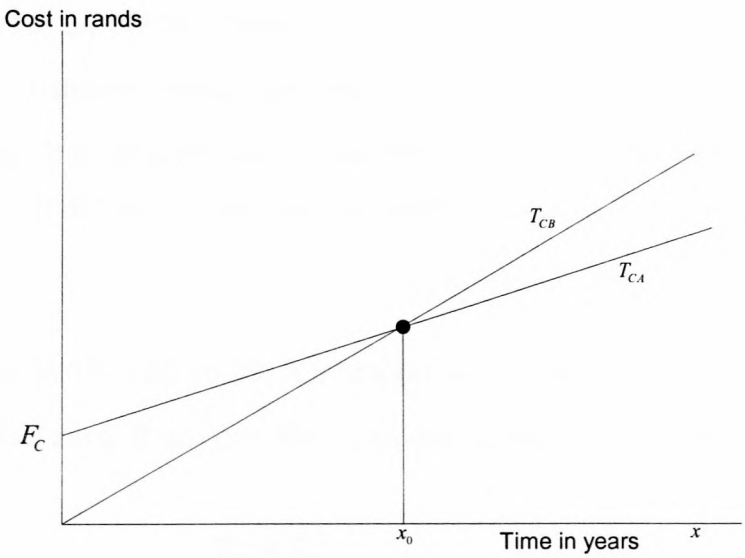

Figure 6.4 Graphical representation of the cost functions

The quantities in the above figure are defined as follows:

T_{CB} = total cost for power before VRB

T_{CA} = total cost for power after the use of VRB

F_C = capital cost for the VRB installation

x = time for VRB economic evaluation

x_0 = time, arbitrarily chosen for a break-even point

From figure 6.4 the cost functions can be mathematically expressed as follows:

$$T_{CB}(x) = G_1 \times x \qquad \ldots (6.38)$$

$$T_{CA}(x) = G_2 \times x + F_C \qquad \ldots (6.39)$$

Where G_1 is the total cost for power per year before the VRB and G_2 is the total cost for power per year after the of VRB. The important issue here is that before

the time reaches x_0, the customer runs the VRB technology at negative profit. However, the customer would be expected to gain profit after x_0. In this discussion only the straight-tariff scenario is considered, meaning that the optimal solution that led to the savings given in table 6.3 is the one taken into consideration.

From equations (6.38) and (6.39) it is assumed that at x_0 both the loss and the profit are equal to zero, therefore, the following condition must hold:

$$T_{CB} = T_{CA} \qquad \ldots (6.40)$$

or,

$$G_1 \times x_0 = G_2 \times x_0 + F_C \qquad \ldots (6.41)$$

Rearranging,

$$F_C = x_0 (G_1 - G_2) \qquad \ldots (6.42)$$

The capital cost expressed in South African Rand per kWh, or simply R/kWh is investigated under the following assumption. The calculations are performed under the assumption that the discharge-charge cycles shown in figure 6.2 hold throughout the year. The evaluation periods of 5 years and 7 years are arbitrarily chosen in this analysis.

From table 6.3,

G_1 = R 76, 678.71 × 12 months = R 920,144.52 per year

G_2 = R 70,335.70 × 12 months = R 844,028.40 per year

Substituting these values into equation (6.42) and letting $x_0 = 5$ years yields

$$F_c = 5 \text{ years} \times (\text{R } 920{,}144.52 \text{ per year} - \text{R } 844{,}028.40 \text{ per year}) \quad \ldots (6.43)$$

Therefore,

$$F_c = \text{R } 380{,}580.60 \quad \ldots (6.44)$$

The cost of the technology expressed in R/kWh is determined as follows:

$$\text{Cost of the technology} = \frac{F_c}{\text{Energy capacity of the VRB}} \quad \ldots (6.45)$$

Substituting equation (6.44) and the energy capacity of 520 kWh ([7,39]) into equation (6.45) yields

$$\text{Cost of the technology} = \frac{\text{R } 380{,}580.60}{520 \text{ kWh}} \quad \ldots (6.46)$$

Simplifying,

$$\text{Cost of the technology} = 732 \text{ R/kWh} \quad \ldots (6.47)$$

This is approximately equal to $ 73/kWh in year 2002. It should be noted though that this value is definitely not a true reflection of what would be expected under normal circumstances. Firstly, there is a significant difference between this value and the ones presented in table 2.1. The reason is that the value of F_c in equation 6.44 is based on the values of G_1 and G_2 that were obtained from an optimization technique. Under normal circumstances the value of F_c could be even 5 times greater than the one in equation 6.44. In this analysis all the components that normally constitute the installation cost of any energy storage technology have been ignored. The researchers find it very difficult to estimate the value of F_c for the VRB technology since it is still at the developmental

stages. Some of the components that need to be considered in the analysis of this nature include [27]:

Initial Fixed Costs

- Cost of the storage unit itself
- Shipping and Insurance
- Site preparation, foundation, control house
- Electric controls, protection
- Construction permit, survey,inspection fees, etc.

Initial Variable Cost

- Legal and fees for emissions permit (if applicable)

Annual Fixed Costs

- Property taxes
- Annual mechanical and electrical inspection

Annual Variable Costs

- Maintenance

Clearly, the inclusion of the above components in the calculations would yield the value of F_c, which is far above the one given in equation 6.44. Furthermore, the values in table 2.1 are inclusive – this means that the energy cost is for the whole system [27]. It is clear that for each battery system, the cost of the power electronic converting equipment is included.

Having considered all the assumptions, possible errors and limitations in the foregoing analysis, the fact of the matter is that the 250 kVA VRB should not cost more than 73 $/kWh when evaluated over 5 years. The same conclusion applies to the where the evaluation period is 7 years whose calculation is briefly outlined in the following paragraph.

In a similar fashion, the capital cost calculated over the evaluation period of 7 years is

$$\text{Capital Cost} = 1025 \text{ R/kWh} \quad \ldots (6.48)$$

It was stated before that any customer considering a VRB as an energy storage device for cost reduction applications would be definitely interested in the break-even point in terms of costs and time. It is acknowledged that the results in equations (6.47) and (6.48) were obtained based on a number of assumptions. However, it is believed that these results suffice the illustration pertaining to the economic feasibility of the VRB. It is also necessary to emphasize that reasonable improvement on the optimization and costs of the VRB can be achieved if the following points are taken into consideration:

- In this chapter the economic analysis is based on the optimal results that were obtained from the modeling of one daily load profile. However, under normal circumstances daily load profiles do not have similar pattern. The discrepancies amongst daily load profiles are clearly shown in appendix A.
- The VRB can reduce the maximum demand on the profile more substantially by delivering more than 133.67 kW, depending upon the pattern of the profile.
- The time-of-use tariff structure can improve the results quite significantly due to the fact that power would be bought at a lower cost during the recharge of the VRB.
- Upgrading the power rating of the DPQC may also improve the economic results.

In the light of the above discussion it is not possible at this stage to conclude whether or not the VRB technology is economically viable, particularly in comparison with other energy storage technologies.

The next section focuses on the time value of money. The purpose is to highlight just a few of the money matters that the customer would need to be aware of before embarking on the VRB investment.

6.6 PRESENT WORTH ANALYSIS

The aim of this section is to investigate the relationship between the amount of money at present and its corresponding value in future. For instance, it is observed from the previous section that the customer would have to invest at a capital cost of about R 532,812.84, provided the evaluation is done over 7 years. If a customer borrows this amount from a moneylender, then both parties need to know how much this amount at present is worth t years later (t is the number of years). The relationship between money at present and in future is based on the present worth factor (PWF) or simply P; the relationship is mathematically expressed as follows [13,21,26,41]:

$$\text{Value today of X dollars/rands t years ahead} = X \times P^t \qquad \ldots (6.49)$$

Willis H. Lee uses a PWF of 0.952 in the studies about the economic evaluation of distributed generation units [26]. Although utilities around the world may use different PWF values, the one advocated by Willis is adopted in this discussion.

The equivalent value of R 532,812.84 seven years later can be calculated as follows:

$$\text{Equivalent value of R 532,812.84} = \text{R 532,812.84} \times (0.952)^7 \qquad \ldots (6.50)$$

Therefore,

Equivalent value = R 377,601.16 ... (6.51)

What transpires from the result in equation (6.51) is that the value of money decreases with time. However, the moneylender would be interested to get a repayment, which is not less than what they have invested in the form of borrowing a customer. In many cases a customer is borrowed money on the agreement that the money would be compounded at a certain rate over specified time intervals (it may be compounded quarterly, monthly or yearly). This type of problem could be interpreted as a situation where R 532,812.84 is discounted to a value of R 377,601.16. Hence, an interest rate would be required to balance the two figures.

6.7 SUMMARY

This chapter focused on the economic assessment of the vanadium redox energy storage system whose energy and power ratings are 520 kWh and 250 kVA respectively. The potential savings that the 250 kVA VRB can offer were investigated based on the electricity billing structures, which are used Stellenbosch Municipality. A number of mathematical expressions representing relationships between parameters were presented. However, assumptions with regard to these assumptions were made due to the lack of information about specific values that could be assigned to those parameters. The reason for the lack of information about specific figures could be attributed to the fact that VRB is still at the developmental stages. Nevertheless, the information presented in this chapter may be used as the basis for further studies on models that evaluate the economic credibility of an energy storage device. It is hoped that all the necessary information would be available for researchers as soon as the VRB gets commercialized.

Chapter Seven

7 CONCLUSION

7.1 SUMMARY OF WORK PRESENTED IN THIS THESIS

An overview of some of the commercialized energy storage devices that are currently available is presented in chapter two. The discussion on each storage device focuses on the technical operation, economic implications, advantages and some potential drawbacks. An in-depth discussion on the development of vanadium redox flow batteries, starting with the prototypes that were developed in Australia and Japan, is also presented in chapter two. The installation of the 250-kVA vanadium redox battery at the University of Stellenbosch is reviewed in chapter two, and a detailed discussion is presented in chapter five. This chapter concludes with a summary, highlighting key aspects that make the VRB a promising energy storage device.

Chapter three discusses the development of a mathematical model that can be used to determine an optimal solution when the 250 kVA VRB is used for peak-shaving and load-leveling. The theme of chapter three is the modeling of a daily load profile using a sinusoidal function. Chapter three also highlights that Maple® can be used to solve the derived equation for an optimal solution. The graphical representation of the results that are simulated with Excel® is discussed in chapter three. This chapter concludes with a summary, emphasizing the necessity of the model that closely resembles a real-life load profile since a sinusoidal function is just a first oder approximation.

An overview of some of the terminology used in spectral analysis is presented in chapter four. The Fast Fourier Transform algorithm is used to validate the model

developed in chapter three. A daily load power profile consisting of 48 evenly spaced discrete points is interpolated into a profile that consists of 64 points (FFT requirement). The FFT algorithm is performed on Matlab® package to extract the amplitudes and phase angles of all the frequency components. The Excel® package is used to reconstruct the power signal from all the frequency components displayed as an FFT spectrum. This chapter concludes with a summary, emphasizing that the developed optimization strategy is suitable not only for the vanadium redox flow battery, but for any energy storage device.

The installation of 250 kVA Vanadium Redox Energy Storage at the University of Stellenbosch is discussed in chapter five. The design and specifications of all the system components are presented. The topological representation and photographic pictures of the VRB system are also presented. The performance results of the 250 kVA VRB obtained during the public demonstration in October 2001 are presented in this chapter. This chapter concludes with a summary emphasizing the future prospects of the VRB as a promising energy storage device, particularly for peak-shaving and load-leveling applications.

An overview of the terminology used in demand side management is presented in chapter six. The calculation of the total cost for power is done on a power load without the VRB, as well as on the load when the VRB is used. The results obtained are used to determine if the VRB is indeed a commercial candidate. A single daily load profile is used as a representative of all the daily profiles in a month. The economic implications that pertain to the discharge-charge processes of the VRB are also presented in this chapter. The derivation of a break-even point formula and the numerical calculation based on the estimated values are presented. This chapter concludes with a summary, focusing on the economic feasibility of the VRB in an energy storage application.

It has been observed that most of the utilities and some of the local authorities that supply electricity use demand meters with moving average characteristics.

This means that the discrete power values, either in kVA or kW, recorded by the meter are the moving averages with time over a specified interval, which is usually a 30-minute or 15-minute interval. It is evident that the information about the instantaneous power values at each minute, second, microsecond, etc. is not known. Hence, the FFT algorithm can be better utilized to model power profiles in general due to its capabilities to reveal that hidden information.

7.2 FUTURE WORK

Some of the work in this thesis may be used as the basis for further research on other topics. Some of the research topics are as follows:

- Models that predict the time and duration at which a daily maximum power peak occurs. Factors that influence the load demand need to be investigated. For instance, a maximum peak may occur as early as 10:00 a.m. for several hours during the winter periods, whereas in summer the peak may occur at 2:00 p.m. for only 2 hours.

- Standard economic models that assess the commercial viability of newly developed energy storage technologies need to be developed.

- Using the analysis presented in this thesis, an optimal real time controller, based on DSP technology could be developed.

REFERENCES

1. Akira Shibata, Kanji Sato, "Development of Vanadium Redox Flow Battery for Electricity Storage", Power Engineering Journal, June 1999.

2. Anderson M.D., Chin H. Lo, "Economic Dispatch and Optimal Sizing of Battery Energy Storage Systems in Utility Load-Leveling Operations", IEEE Transactions on Energy Conversion, Vol. 14, No. 3, September 1999.

3. Anderson M.D., Dodd S. Carr, "Battery Energy Storage Technologies", Proceedings of the IEEE, Vol. 81, No. 3, March 1993.

4. Anderson M.D., Jungst R.G., Alt J.T., "Assessment of Utility Side Cost Savings from Battery Energy Storage", IEEE Transactions on Power Systems, Vol. 12, No. 3, August 1997.

5. Anderson M.D., Raymond M.K., Ronald C. Reckrodt, "Economic Models for Battery Energy Storage: Improvements for existing methods", IEEE Transactions on Energy Conversion, Vol. 5, No. 4, December 1990.

6. Bantley W.F., Heacock D.K., "Battery Management Considerations for Multichemistry Systems", IEEE AES Systems Magazine, May 1996.

7. Brtolozzi M., "Development of Redox Flow Batteries: A Historical Bibliography", Journal of Power Sources, ELSEVIER, 27, p. 219-234, 1989.

8. Carl Johan Rydh, "Environmental Assessment of Vanadium Redox and Lead-Acid Batteries for Stationary Energy Storage", Journal of Power Sources, ELSEVIER, 80, p. 21-29, 1999.

9. Chengi Kuo, "Business Fundamentals for Engineers", McGRAW-HILL Book Company Europe, England, 1992.

10. Clive D.S. Tuck, "Modern Battery Technology", Ellis Horwood Ltd, England, 1991.

11. Conway B.E., "Electrochemical Supercapacitors: Scientific Fundamentals and Technological Applications", Kluwer Academic / Plenum Publishers, New York 1999.

12. Crompton T.R., "Battery Reference Book", Butterworth-Heinemann Ltd, Oxford, 1995.

13. Donovan Young, "Modern Engineering Economy", John Wiley & Sons,INC., Canada, 1993.

14. Duane H. and Bruce L., "The Student Edition of MATLAB: Version 5 User's Guide", The Math Works Inc., New Jersey, 1997.

15. Edward J. Friedman, George E. Mouchahoir, Oscar G. Farah, Robert P. Ouellette, Paul N. Cheremisinaff, "Electrotechnology: Stationary Lead-Acid Battery Aplications and Performance", ANN Arbor Science Publishers INC, Ann Arbor, 1980.

16. Glyn James, David Burley, Phil Dyke, John Searl, Nigel Steele, Jerry Wright, "Advanced Modern Engineering Mathematics", Addison-Wesley Publishing Company, Wokingham, 1993.

17. Hawkins J.M., Robbins T.P., "A field trial of a Vanadium Energy Storage System", Telepower Australia Pty Ltd, INTELEC ^{R} 01, 2001.

18. Henry Oman, "Applications and Advances: News from the 1996 Battery Conference", IEEE AES Systems Magazine, May 1996.

19. Ignacio J. Ramirez-Rosado, "Demand Side Management Modelling to Evaluate Economical and Technical Improvements in Electric Distribution Systems", Departamento de Ingenieria Electrica e Informatica Maria de Luna 3, 50015 Zaragoza, Spain.

20. Jerry Mader, "Commercialization of Advanced Batteries", IEEE AES Systems Magazine, July 1996.

21. John A. White, Marvin H. Agee, Kenneth E. Case, "Principles of Engineering Economic Analysis", John Wiley & Sons, Canada, 1989.

22. John E. Freund, "Mathematical Statistics", Prentice/Hall International, INC., London, 1972.

23. Jones C. R., Mulholland H., "Fundamentals of statistics", Plenum Press, London, 1968.

24. Kottick D., Blau M., Edelstein D., "Battery Energy Storage for Frequency Regulation in an Island Power System", IEEE Transactions on Energy Conversions, Vol. 8, No. 3, September 1993.

25. Kyung-Hee Jung, Hoyong Kim, Daeseok Rho, "Determination of the Installation site and Optimal Capacity of the Battery Energy Storage System for Load Leveling", IEEE Transactions on energy Conversion, vol. 11, No. 1, March 1996.

26. Lee Willis H., Gary Huff R., Timotyy S. Yau, "Demand-Side Management Impact on the Transmission and Distribution System", IEEE Transactions on Power Systems, Vol. 5. No. 2, May 1990.
27. Lee Willis H., Walter G. Scott, "Distributed Power Generation: Planning and Evaluation", Marcel Dekker INc, New York, 2000.

28. Maly D.K., Kwan K.S., "Optimal battery Energy Storage System Charge Scheduling with dynamic programming", IEE proc-Sci. Meas. Technol., Vol. 142, No. 6, November 1995.

29. Maria Skyllas-Kazacos, Kasherman D.R. Hong, "Characteristics and performance of 1 kW UNSW Vanadium Redox Battery", Journal of Power Sources, ELSEVIER, 35, p. 399-404, 1991.

30. Masato N., Masatoshi S., Setsu Y., Kanji S., Hiroko K., Akira N., Ken N., "Vanadium Redox Flow Battery with Resources Saving Recycle Ability I. Production of Electrolytic Solution for Vanadium Redox Flow Battery from Boiler Soot", Denki Kaguku, 66, No. 6, 1998.

31. Michal J. Riezenman, "Metal Fuel Cells", IEEE SPECTRUM, June 2001.

32. Paulo F. Ribeiro, Brain K. Johnson, Mariesa L. Crow, Aysen Arsoy, Yilu Liu, "Energy Storage Systems for Advanced Power Applications", Procedings of the IEEE, Vol. 89, No. 12, December 2001.

33. Prabhakara F.S., Robert L. Smith, Ray P. Stratford, "Industrial and Commercial Power Systems Handbook", McGRAW-HILL, New York, 1996.

34. Roy Nicolaides, Noel Walkington, "MAPLE A Comprehensive Introduction", Cambridge University Press, Cambridge, 1996.

35. Smith G, "Storage Batteries", Third Edition, Pitman Ltd., London, 1980

36. Surtees R., "Demand-side electricity management in South Africa",Journal of Energy in South Africa, May 1998.

37. Tada M., Sakamoto T., Mori N., Mizunzmi K., Shigematsu T., "Development of Redox Flow Battery for Utility Load Leveling", IFAC Energy Systems, Management and Economics, Tokyo, Japan, 1989

38. Tatsuhiko Sakamoto, Norihiro Mori, Mineya Kuno, Kazuhito Mizunami, Toshio Shigematsu, "Development of Redox Flow Battery", Sumitomo Electric Technical Review, Number 28, January 1989.

39. Timothy C. Hesterberg, Alex D. Papalexopoulos, "A Regression-Based Approach to Short-Term System Load Forecasting", IEEE Transactions on Power Systems, Vol. 5, No. 4, November 1990.

40. Tuck Clive, D.S., "Modern Battery Technology", Elli, New York, 1991.

41. Tung AU, Thomas P. AU, "Engineering Economics for Investment Analysis", ALLYN AND BACON, INC., Boston, 1983.

42. Zink, J.C., "Who Says You Can't Store Electricity?" Power Engineering, March 1997, pp.21-25.

Appendix A

In each month of the year there is a daily load profile that has the greatest maximum demand of that particular month. The pattern of each profile is influenced by a number of factors. These factors include weather conditions, appliences, seasons and things of that kind. This appendix presents the daily load profiles,which contain the greatest maximum demands of their corresponding month.

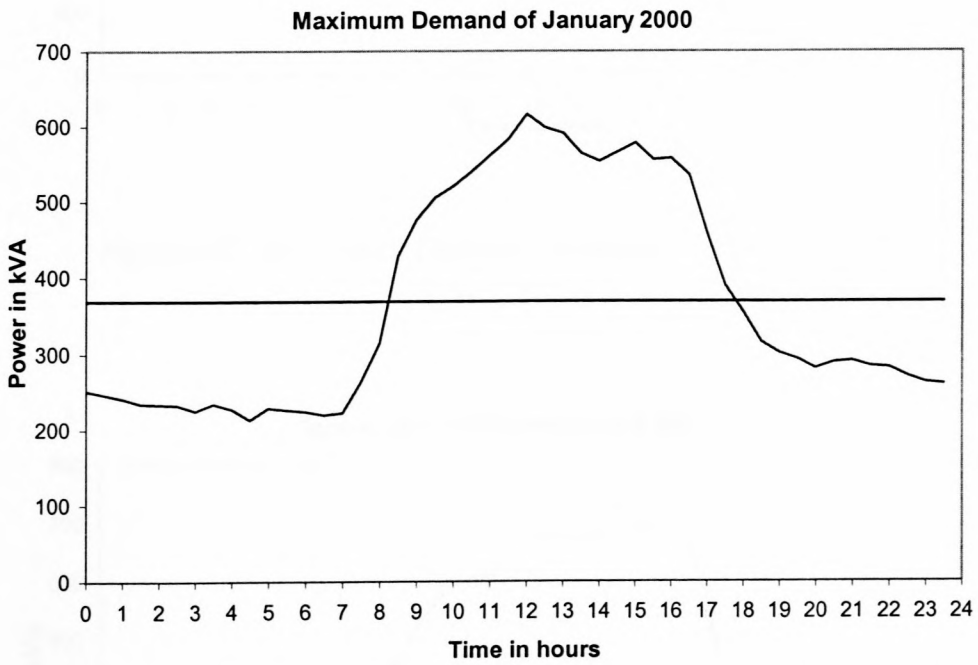

Figure A1 Maximum Demand occurred in January 2000

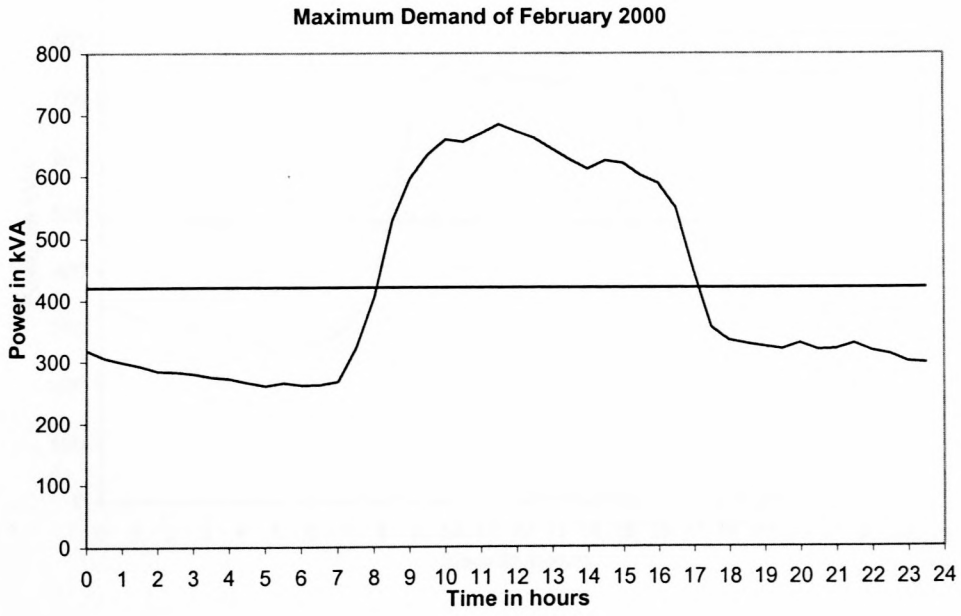

Figure A2 Maximum Demand occurred in February 2000

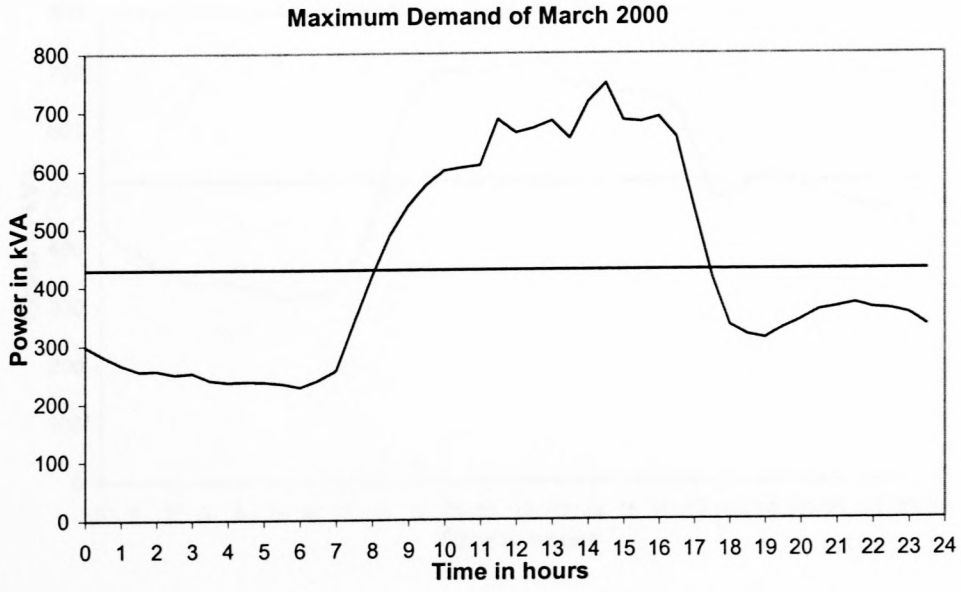

Figure A3 Maximum Demand occurred in March 2000

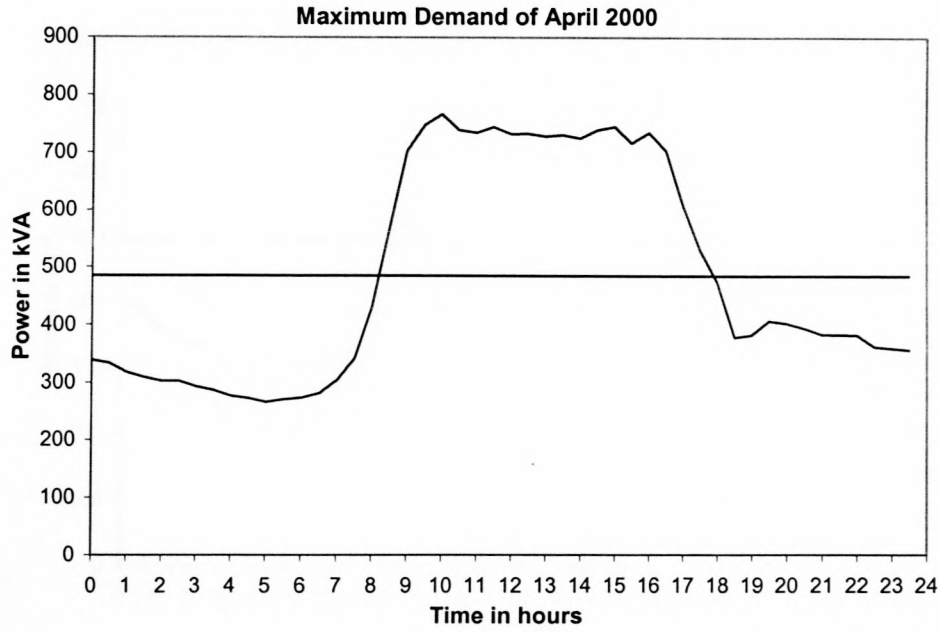

Figure A4 Maximum Demand occurred in April 2000

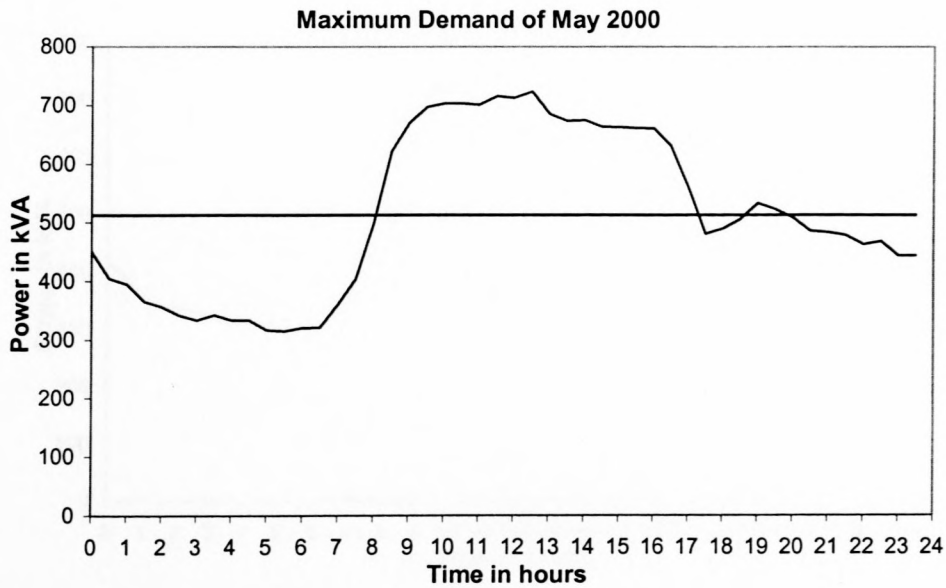

Figure A5 Maximum Demand occurred in May 2000

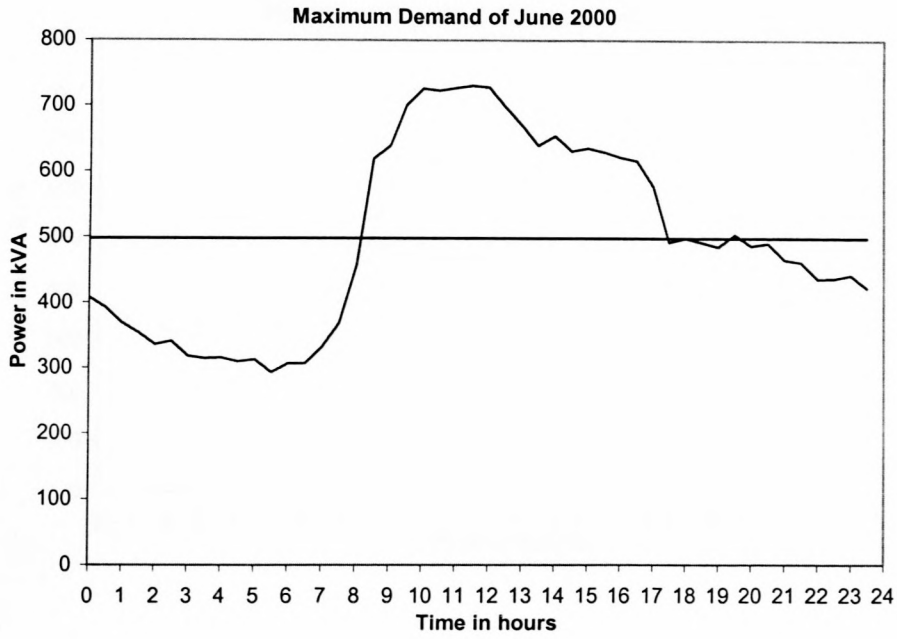

Figure A6 Maximum Demand occurred in June 2000

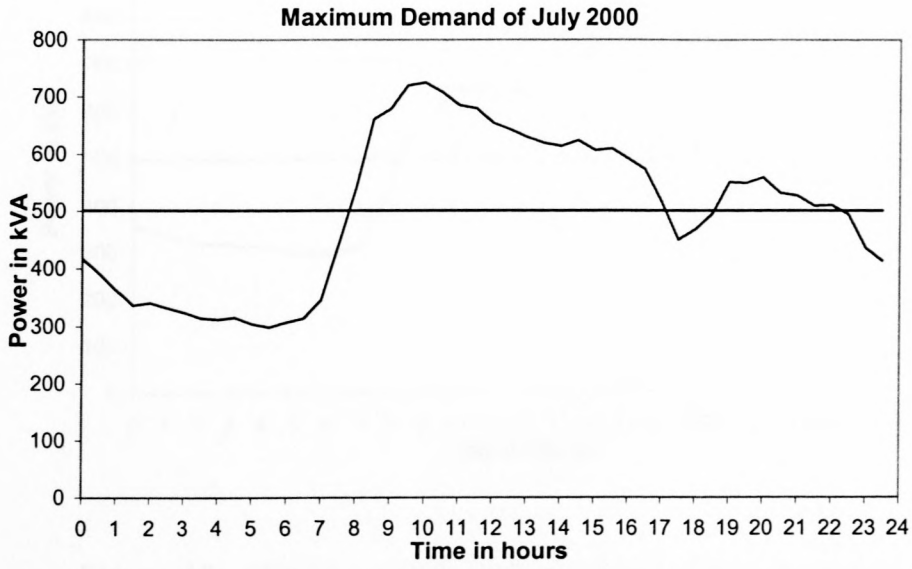

Figure A7 Maximum Demand occurred in July 2000

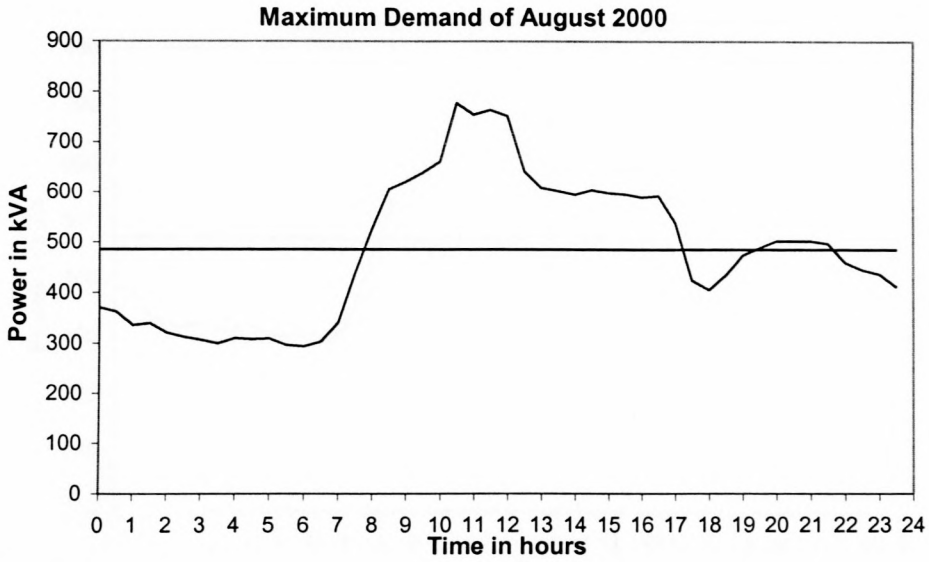

Figure A8 Maximum Demand occurred in August 2000

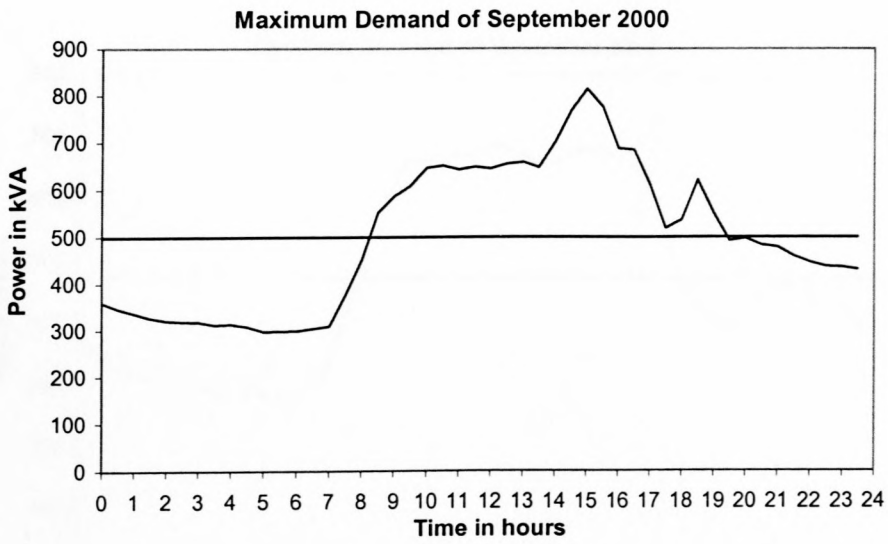

Figure A9 Maximum Demand occurred in September 2000

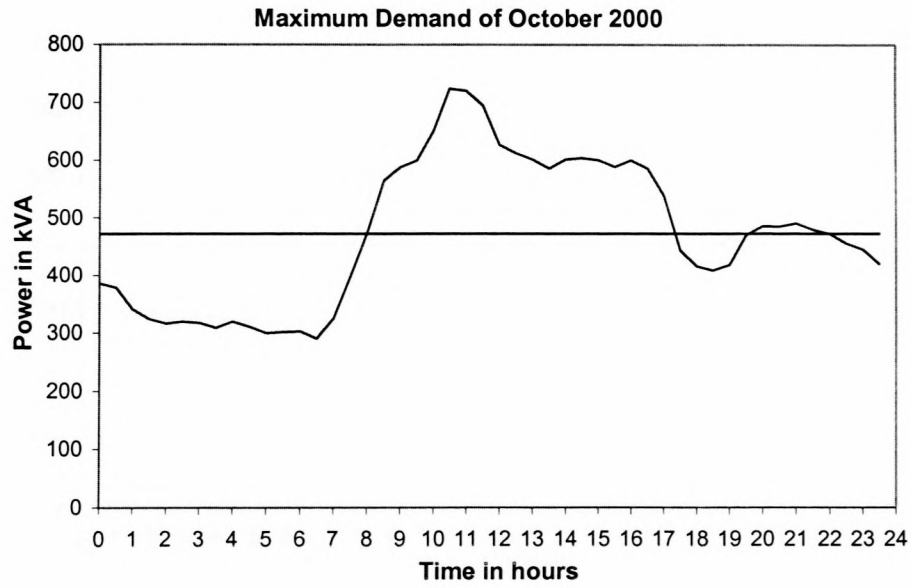

Figure A10 Maximum Demand occurred in October 2000

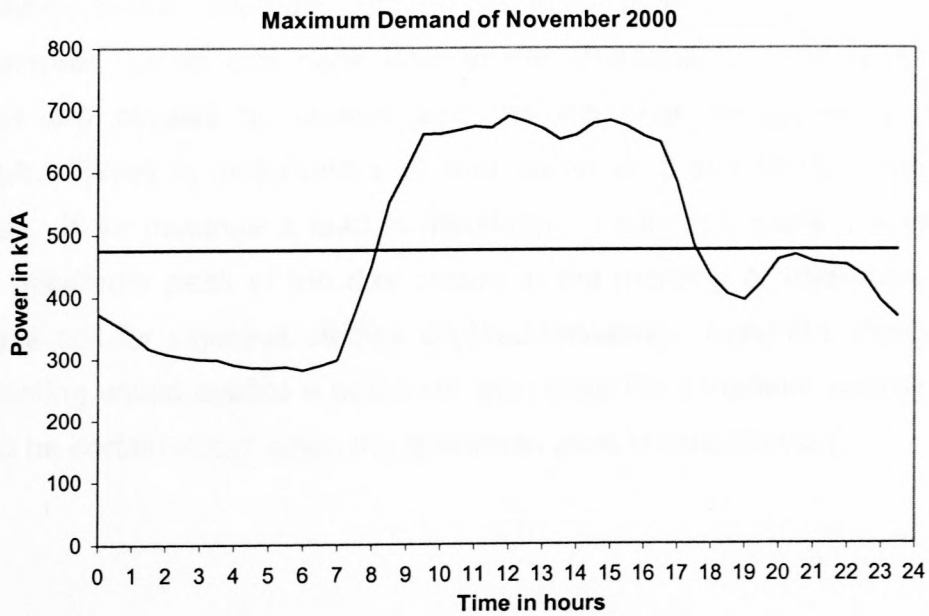

Figure A11 Maximum Demand occurred in November 2000

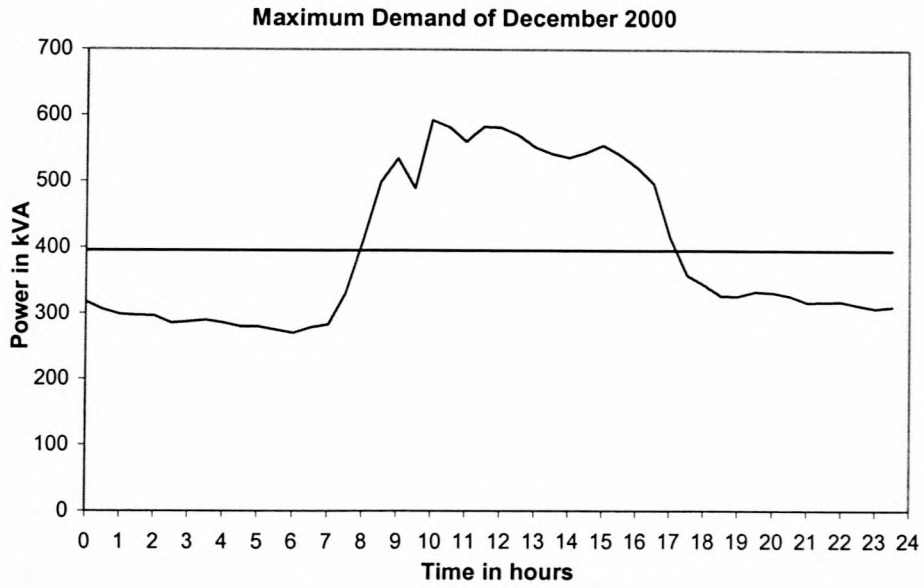

Figure A12 Maximum Demand occurred in December 2000

It is observed that a maximum demand can occur as early as 10:00 a.m. (figure A10), whereas others can peak later in the afternoon at 15:00 p.m. These variations are caused by factors such as the ones mentioned in the first paragraph. What is unfortunate is that some of these factors con not be controlled. If for instance a load is monitored in summer, there is a possibility that the maximum peak of the day occurs in the morning or afternoon. These challenges call for vigorous studies on load-focasting. Accurate algorithms for load-focasting would enable a customer who uses the vanadium energy storage device to be certain about when the maximum peak is due to occur.